Winter 12-15-2014

Isotope Harvesting at Heavy-Ion Fragmentation Facilities

Tara Elise Mastren
Washington University in St. Louis

WASHINGTON UNIVERSITY IN ST. LOUIS

Department of Chemistry

Dissertation Examination Committee:
Suzanne E. Lapi, Co-Chair
Lee G. Sobotka, Co-Chair
John R. Bleeke
Robert Charity
Richard Laforest
Demetrios G. Sarantities

Isotope Harvesting at Heavy-Ion Fragmentation Facilities

by
Tara Mastren

A dissertation presented to the
Graduate School of Arts & Sciences
of Washington University in
partial fulfillment of the
requirements for the degree
of Doctor of Philosophy

December 2014

Saint Louis, Missouri

Table of Contents

List of Figures

List of Tables

Acknowledgements

I would like to thank my advisors Dr. Suzanne E. Lapi and Dr. Lee G. Sobotka for their continual support and guidance over the past four years. I would especially like to thank Dr. Suzanne E. Lapi for her generous financial support and for providing me with a project that allowed me to grow in many ways. She gave me the freedom to think independently, which helped mold me into the scientist I am today. I would also like to thank Dr. Lee G. Sobotka for taking the time to personally work with me and for helping me to learn the basics of nuclear and radiochemistry. Without your support I would have never made it to this point.

I would also like to thank Dr. Demetrios G. Sarantites for his instruction in the nuclear and radiochemistry courses. These courses gave me valuable tools that I needed to perform the work discussed in this dissertation. I am also grateful for the opportunity to have served as a TA in these courses as it provided me with valuable experience and reinforced the information from both courses.

In addition I would like to thank Dr. John Bleeke for being a part of my yearly committee. Your suggestions have been very helpful towards the progression of my research. I would also like to thank Dr. Demetrios G. Sarantites, Dr. John Bleeke, Dr. Robert Charity, and Dr. Richard Laforest for serving on my defense committee.

I would like to thank Dr. Graham Peaslee and his group at Hope College for their expertise in designing the water target station used in this work. In addition I would like to thank Dr. David J. Morrissey and the many people at the National Superconducting Cyclotron Laboratory for their assistance with the experiments we conducted over the past few years. The collaboration on this project with these groups has been very beneficial and I owe so much to them for their support.

I owe special thanks to the undergraduates Shaun Loveless and Elizabeth Bollinger whom I have mentored over the past couple of years. They both went above and beyond expectation with their help on this project. Their assistance was instrumental in my success.

The Lapi group has provided me with lots of emotional and scientific support over the last three years. I would like to specifically thank Dr. Bernadette V. Marquez, Dr. Vernal Richards, Mr. Alex Zheleznyak, Dr. Jennifer Burkemper, Dr. Nilantha Bandara, Dr. Brian Wright, Tom Voller, Deborah Sultan, and Paul Eisenbeis for their help in teaching me different laboratory skills and techniques. I would additionally like to thank Kyle Brown from Dr. Sobotka's group for his help setting up and performing the final experiment at the NSCL.

In addition to the Lapi group I would also like to thank Bill and Pat Margenau in the cyclotron facility and Amanda Klass and the small animal imaging facility for all their help. Additionally I would like to thank Katherine Andel for her assistance with all my administrative needs.

I would also like to thank my family for their support over the last four years. I would especially like to thank my grandmother. Her emotional support gave me the strength to continue when times were rough.

Finally I would like to thank my friends Tayo Ikotun, Bernadette Marquez, Michelle Harris, Maiko Kume, Morgan Murphey, Ben England, and Rathna Hok for their friendship and support during these last few years. They provided me with many outlets to relax, laugh, and enjoy life, which made my graduate experience one of the most special times in my life. I am very grateful to have met you all.

ABSTRACT OF THE DISSERTATION

Isotope Harvesting at Heavy-Ion Fragmentation Facilities

By

Tara Mastren

Doctor of Philosophy in Chemistry

Washington University in St. Louis, 2014

Dr. Suzanne E. Lapi, Co-Chair

Dr. Lee G. Sobotka, Co-Chair

Isotope harvesting from heavy-ion fragmentation facilities is a potential source of isotopes of interest for applications research. With the upgrade of the National Superconducting Cyclotron Laboratory (NSCL) to the Facility for Rare Isotope Beams (FRIB) usable quantities of many isotopes of interest will be produced and available for harvest from an aqueous beam dump. If available, these isotopes would be of interest to a broad range of applications such as medicine, geology, and stockpile stewardship. Preliminary experiments were performed at the NSCL in order to determine the feasibility of isotope harvesting at (FRIB).

A water target station that consisted of a 100 mL beam dump was designed and built to collect secondary beams at the NSCL. This target station could be controlled remotely from outside of the experimental vault allowing for multiple collections with minimal exposure to radioactivity. Three secondary beam collections were made with the water target station: a ^{24}Na beam, an analyzed ^{67}Cu beam, and an unanalyzed ^{67}Cu beam.

To test the durability of the target station, a 73% pure 85 MeV/u ^{24}Na secondary beam was stopped and collected in the beam dump. Multiple collections were made with currents up to 2 x 10^6 particles per second without visible radiolytic damage to the target cell. The station operated without any observed release of radiolytic gases, spills, or loss of radioactive liquids.

The water target station was then used collect a 77% pure 76 MeV/u ^{67}Cu secondary beam. ^{67}Cu was separated from the other secondary beam contaminants with an average recovery of 88 ± 3 % and used to radiolabel an antibody. The radiochemical yield of ^{67}Cu-NOTA-Bz-NCS-Trastuzumab was >95%.

To better mimic the conditions that would be present in the beam dump at FRIB an unanalyzed beam was collected. This secondary beam was 2.6% pure and contained many contaminants most of which are located in period four of the periodic table. ^{67}Cu was separated from the beam contaminants with an average recovery of 74 ± 4% and a radiochemical purity of >99%. The purified ^{67}Cu was then used to radiolabel NOTA conjugated Panitumumab antibodies and injected into HCT-116 tumor bearing mice via tail vein injection. A five day biodistribution profile was obtained and the tumor uptake of ^{67}Cu-NOTA-Bz-NCS-Panitumumab was measured to be 12.5 ± 0.7 % ID/g.

Chapter 1

Introduction

Nuclear Chemistry and its Applications in Medicine

Radioisotopes have been very important for the advancement of cancer imaging and treatment. Single Photon Emission Computed Tomography (SPECT) and Positron Emission Tomography (PET), which detect administered radiotracers in the body, have become routine imaging modalities in cancer assessment.[1-3] Additionally, advancements in radiotherapy now involve targeting cancers with therapeutic radioisotopes so that the radiation treatment is delivered directly to the tumor, reducing radioactive exposure to healthy cells.[7,8] The nuclear properties, availability, and chemistry of the radioisotopes all have to be considered when designing tracers for the above techniques.

Nuclear Chemistry

Nuclear Decay (β^+, β^-, and γ)

The chart of the nuclides, a map of all known nuclei with the number of protons (Z) displayed on the ordinate and neutron number (N) on the abscissa, is shown in **Figure 1-1**. Understanding of this playfield of nuclear science requires understanding a suppressed third axis – mass. The minimum mass as a function of mass number, A= Z+N, forms a mass valley populated by the stable isotopes. Isobars (A = constant) not at the bottom of the valley are on the (mass) valley walls and beta decay (via the isobar conserving weak interaction) to the stable nuclei at the valley bottom. Isotopes on the left side of stability (North-West on the diagonal isobar) are proton rich and decay by electron capture (ε) and/or positron emission (β^+). Isotopes on the right side of stability (South-East) are neutron rich and decay by electron emission (β^-).

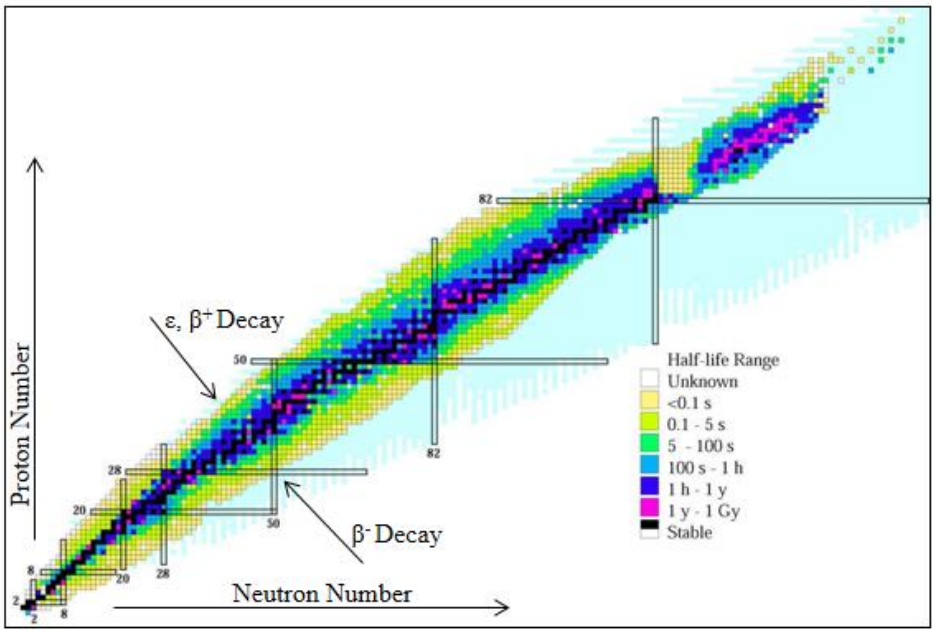

Figure 1-1. Chart of the Nuclides.[4]

Positron emission happens when a proton within the nucleus (indicated by the quotes in Equation (1)) of an atom is converted into a neutron by the emission of a positron and a neutrino (**Equation 1**) thus keeping the mass number the same and decreasing the atomic number by 1. An example of an isotope that undergoes positron decay is ^{18}F (**Equation 2**). The emitted positron thermalizes by electrostatic interactions with electrons, typically traveling 1-3mm before annihilating with an electron creating two 511 keV photons travelling at approximately 180º from each other (**Figure 1-2**). The Q-value makes the equations energy balanced and is the energy equivalent of the mass difference of the left and right sides of the arrow. For positron decay to occur, the atomic mass difference must be at least 1.022 MeV otherwise the decay will occur via electron capture which is discussed below. Note that the Q-value has the opposite sign

$$\text{“p”} \longrightarrow \text{“n”} + \beta^+ + \nu + Q \qquad (1)$$

$$^{18}\text{F} \longrightarrow {}^{18}\text{O}^- + \beta^+ + \nu + Q \qquad (2)$$

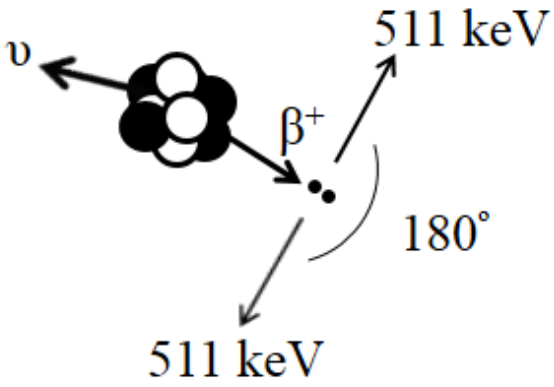

Figure 1-2. Positron decay and the resulting annihilation with an electron creating two 511 keV gamma rays approximately 180º apart.

convention as reaction enthalpies and is always provided on a unit basis rather than per mole of conversions. In spontaneous decays, the Q-value is always positive. Electron capture, which competes with positron decay, converts a proton into a neutron by capturing an inner-shell electron (**Equation 3**) also keeping the mass number the same, decreasing the atomic number by 1 and emitting a neutrino. An example of an isotope that undergoes electron capture is ^{49}V (**Equation 4**).

$$\textbf{“p”} + e^- \longrightarrow \textbf{“n”} + \nu + Q \qquad \textbf{(3)}$$

$$^{49}V^+ + e^- \longrightarrow {}^{49}Ti + \nu + Q \qquad \textbf{(4)}$$

β^- decay occurs when a neutron within the nucleus of an atom is converted into a proton by the emission of an electron and an antineutrino (**Equation 5**) thus keeping the mass number the same and increasing the atomic number by 1. As the neutron is more massive than the proton plus an electron, the decay represented in **Equation 5** without the quotes does occur

spontaneously with a $Q_n = 0.78$ MeV. An example of an isotope relevant for medicine that undergoes β^- decay is ^{99}Mo (**Equation 6**).

$$\text{“n”} \longrightarrow \text{“p”} + \beta^- + \bar{\nu} + Q \quad \textbf{(5)}$$

$$^{99}\text{Mo} \longrightarrow {}^{99m}\text{Tc} + \beta^- + \bar{\nu} + Q \quad \textbf{(6)}$$

When isotopes undergo the different types of β decay, they often decay to an excited state in the daughter nucleus. When this happens the nucleus decays to the ground state by the emission of one or several photons of discrete energy (γ decay) or by the emission of an orbital electron, which is called an internal-conversion electron.[10] This is the case in the above decay in **Equation 6** where ^{99}Mo decays to an excited state in ^{99}Tc, ^{99m}Tc, which after emission of an internal-conversion electron, with a kinetic energy of 2.2 keV minus the binding energy of the electron thereby decaying to another excited state in ^{99}Tc, then decays to the ground state, ^{99g}Tc, usually by emitting a 140.5 keV gamma ray. The atomic and mass numbers (Z and A) of the decaying atom remains unchanged in γ decay.

The decay properties for a specific radioisotope can be shown through a decay scheme. Decay schemes provide information on the type of decay, branching ratios to the different energy levels in the daughter nucleus, and the intensity and occurrence of the gamma rays from the

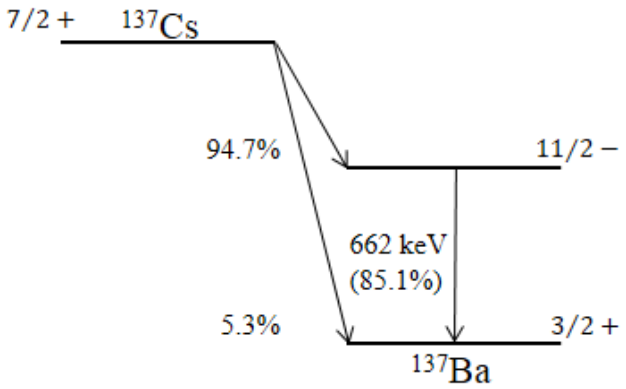

Figure 1-3. The ^{137}Cs decay scheme.[4] In this case, photon emission from the state populated 95% of the time in beta decay, decays to the ground state 85.1% of the time by the emission of a photon, the remainder of the deexcitations within the daughter ^{137}Ba are by the internal-conversion process.

excited states, populated by the beta decay of the parent atom, to the ground state of the daughter.[10,11] An example decay scheme is shown for ^{137}Cs in **Figure 1-3**.[4]

Positron Emission Tomography (PET)

Positron Emission Tomography (PET) is a common imaging modality used for diagnostic imaging in oncology, cardiology and neurology. PET takes advantage of the approximate collinearity of the annihilation photons resulting from β^+ decay. In a PET scanner, scintillation crystals are positioned in a ring around the patient. The event is detected through the coincidence detection of the two 511keV photons that are detected at the same time and across the ring. Algorithms are then used to reconstruct an image from the intersection of the lines from different decays (**Figure 1-4**).

The two main factors that limit the resolution of this method are non-collinearity, resulting from non-zero momentum from the positron-electron pair before the annihilation, and that the annihilation point is remote from that of the original radioactive decay. Since β^+ decay is a three-body final state as shown in Equations (1) and (2), the energy of an emitted positron is not discrete but rather a spectrum of energies. The positron energy distribution is therefore usually characterized by either $E(\beta^+_{mean})$ or $E(\beta^+_{max})$ with the mean positron energy about one third of the maximum energy for light nuclei. The $E(\beta^+_{max})$ limits the resolution of this imaging modality because higher energy positrons travel further in the tissue before reaching thermal energies where the probability of annihilation with an e^- is maximal. Algorithms have been created to decrease the effect from these factors and improve the overall resolution.[12,13]

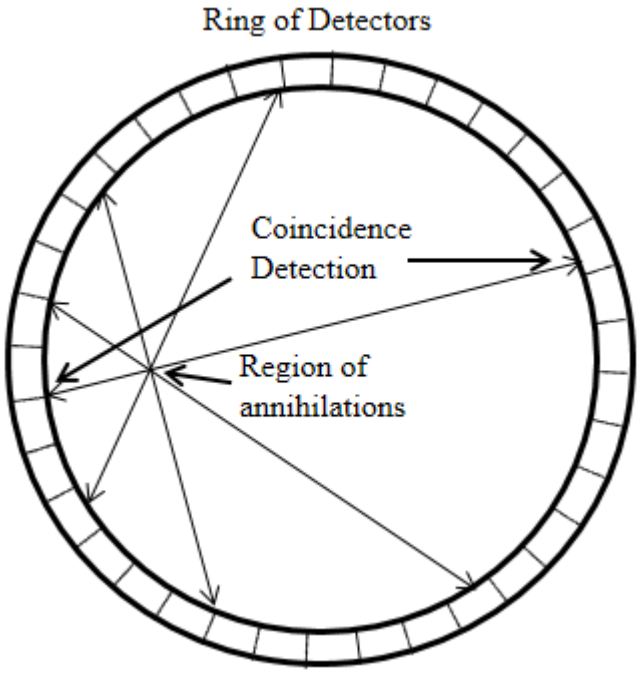

Figure 1-4. Schematic of Positron Emission Tomography (PET).

The most common PET radiopharmaceutical is [^{18}F]FDG (2-[^{18}F]Fluoro-2-deoxyglucose) (**Figure 1-5 A)** and has been used in cancer detection for more than twenty-five years.[14] As a glucose derivative [^{18}F]FDG's mechanism of action is through the glycolytic pathway. Unlike glucose (**Figure 1-5 B**), once [^{18}F]FDG is taken up by the cells and converted into 2-[^{18}F]fluoro-2-deoxyglucose-6-phosphate it cannot undergo further catabolism due to the lack of oxygen at the C-2 carbon thus it becomes trapped inside the cell.[14,15] Due to the high glycolytic rate of

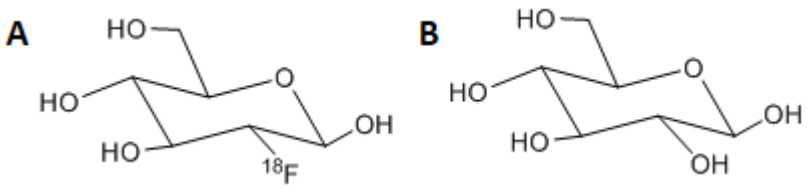

Figure 1-5. Structures of **A** 2-[^{18}F]Fluoro-2-deoxyglucose and **B** Glucose. The C-2 carbon (counting from the internal ether O) is bonded to the positron emitting radionuclide ^{18}F.

cancer cells, [^{18}F]FDG accumulation is typically higher in cancer cells than normal cells which makes it an optimal imaging agent for cancer detection based on metabolic function.

Single Photon Emission Computed Tomography (SPECT)

Single Photon Emission Computed Tomography (SPECT) is the most common nuclear medicine imaging modality. Radionuclides that are good for SPECT imaging typically decay with the emission of a low-energy gamma ray (~140 keV). In SPECT imaging one or more scintillation cameras rotate around the patient taking multiple two-dimensional projections that are then compiled to make a three-dimensional image with the use of algorithms taking advantage of the isotropic emission pattern of γ rays from nuclei existing under normal conditions (e.g. not employing ultra-low T and high magnetic fields) (**Figure 1-6**).

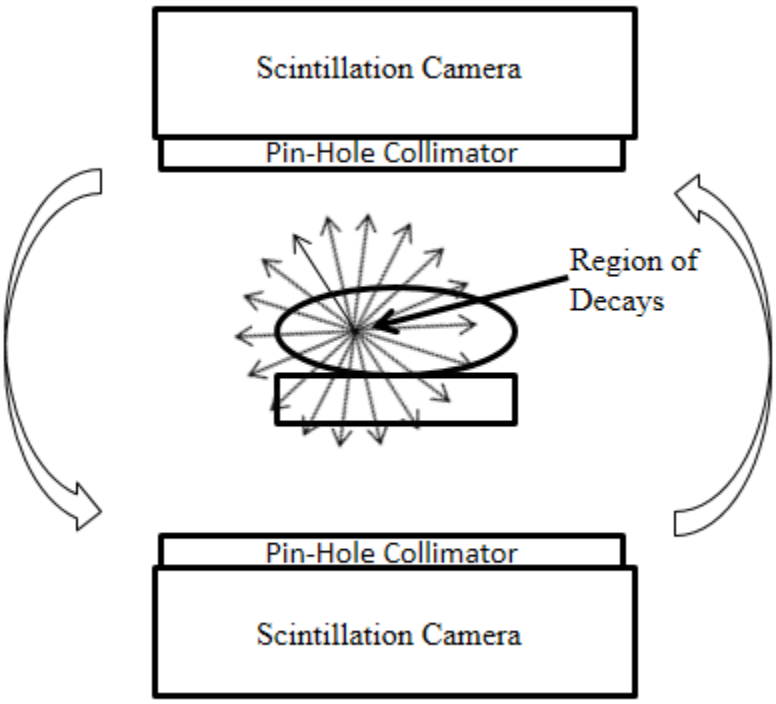

Figure 1-6. Schematic of Single Photon Emission Computed Tomography (SPECT).

A limitation of SPECT imaging is the need for collimators in order to determine the angle of incidence. These collimators reject photons that are outside a very small angular window. Because of this limitation, a larger amount of activity must be injected in order to achieve an image which is a major disadvantage as compared to the higher sensitivity of PET imaging.[12,13]

^{99m}Tc is the most widely used radionuclide in nuclear medicine and SPECT imaging has been optimized to accommodate the 140.5 keV gamma ray resulting from the decay of ^{99m}Tc as described earlier. One of the most common scans involving ^{99m}Tc is a bone scan which employs the radiopharmaceutical ^{99m}Tc-diphosphonate. Increased ^{99m}Tc-diphosphonate uptake can signify diseases such as certain types of bone metastases, osteomyelitis and arthritis, where decreased uptake signifies lytic lesions or tumor necrosis.[16]

Properties of Important Isotopes Presented in this Work

The isotopes and their decay properties discussed in this work are listed in Table 1. ^{64}Cu, ^{68}Ga, and ^{55}Co were made at Washington University School of Medicine.[17] ^{24}Na and ^{67}Cu were obtained from the National Superconducting Cyclotron Laboratory (NSCL) at Michigan State University.[18] The remaining isotopes listed in the table are side products.

Table 1-1. Properties of isotopes discussed

Isotope	Half-Life	Decay	β_{max}(MeV)	Associated Gammas (keV)
^{24}Na	14.97h	β^-	1.39	1369, 2754
^{55}Co	17.53h	β^+ (76%), ε (24%)	1.50	931, 477, 1408
^{57}Co	271.8d	ε (100%)		122, 136
^{57}Ni	35.6h	β^+ (43.6%), ε (56.4%)	0.865	1378, 127, 1919
^{64}Cu	12.7h	β^+ (17.6%), ε (43.9%), β^- (38.5)	β^+(0.653), β^-(0.579)	1346
^{67}Cu	2.58d	β^-	0.562	185, 93.3, 91.3
^{68}Ga	1.13h	β^+ (88.9%), ε (11.1%)	1.90	1077
Data was obtained from the National Nuclear Data Center, Brookhaven National Laboratory, Upton, NY. Website: http://www.nndc.bnl.gov/chart/chartNuc.jsp[4]				

Imaging and Therapeutic Applications of Radioisotopes

As discussed above, the gamma rays emitted from the decaying atom (either from the nucleus or annihilation photons) can be used for PET or SPECT imaging depending on the type of decay. In order to be useful for imaging, these isotopes need to be delivered to the target of interest, for example cancer cells. This requires different chemistries to incorporate the radioisotope onto a targeting probe (i.e. small molecules, antibodies, peptides, or nanoparticles). For radiometals this can be achieved by conjugating the probe with a chelate that has a high affinity for the isotope of interest. In this work we will discuss two chelators with high affinity for copper and cobalt.

In addition to imaging, radioactive decay can be employed for use in cancer therapy. β^- particles are of considerable interest for cancer therapy due to the increased linear energy transfer (LET) to the tissue being irradiated compared to gamma irradiation. Positrons have similar linear energy transfer to β^-, however this decay mode is not of interest for therapy for two reasons: the accompanying 511 keV gamma rays and the competition with electron capture. Beta particles travel about 1-3 mm in tissue effectively depositing all of their energy in a small distance causing damage to the nearby cells. To achieve this therapeutic effect, the radioisotopes must be delivered very close to the targeted tissue. An example of a therapeutic isotope often used in medicine is ^{90}Y with Q = 2.28 MeV, average β^- energy of 0.937 MeV, and an average range of 2.5mm in tissue.[19,20]

Antibodies for use in Cancer Imaging and Therapy

One class of molecular probes used for both cancer imaging and therapy is antibodies. Antibodies by themselves can be therapeutic and several are FDA approved for therapy.[21] Radiolabeling these antibodies with a therapeutic isotope can increase the therapeutic dose

delivered to the target tissue.[22-24] The incorporation of radiometal isotopes onto the antibody of interest is typically achieved by the use of chelators that are conjugated onto the antibody. Two popular chelates conjugated onto antibodies for radiometal incorporation are DOTA (1,4,7,10-tetraazacyclododecane-1,4,7,10-tetraacetic acid) and NOTA (1,4,7-triazacyclononane-N,N',N''-triacetic acid) (**Figure 1-7A, B**). The conjugation is typically achieved through an NCS group that is incorporated onto the chelate. The NCS group reacts with exposed lysine groups on the antibody (**Figure 1-7C**). Both NOTA and DOTA chelates can be used to incorporate radioactive copper and cobalt atoms, however, NOTA has been shown to lead to more stable copper conjugates than DOTA.[25,26]

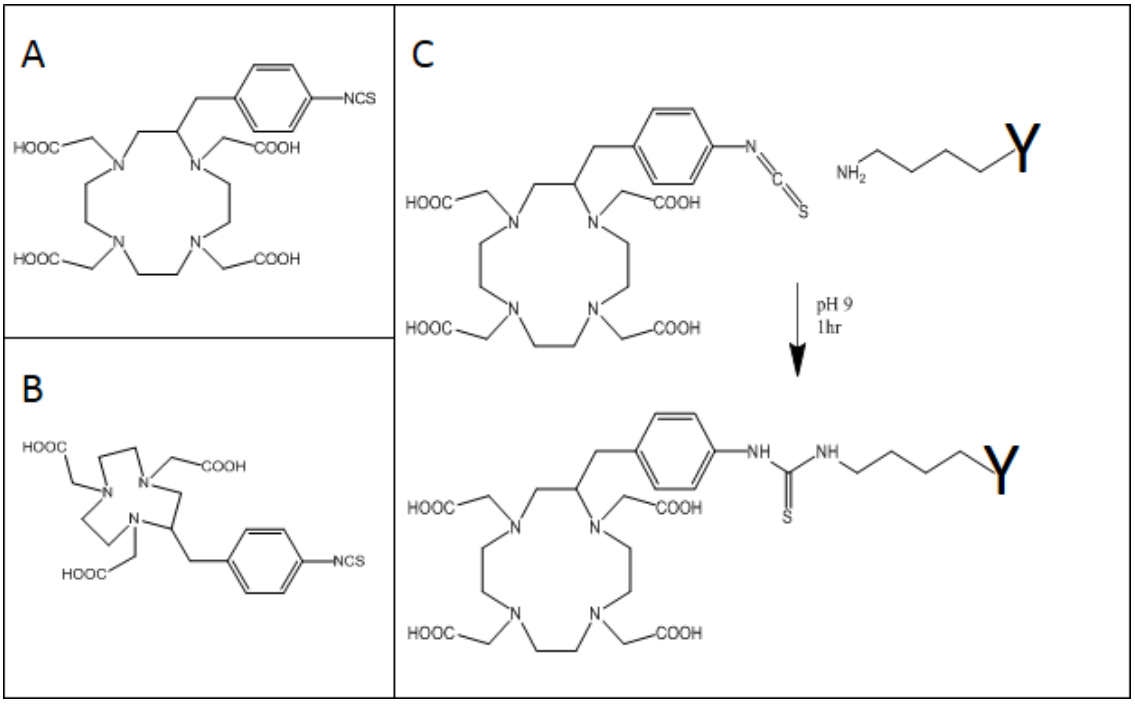

Figure 1-7. **A** DOTA-bz-NCS, **B** NOTA-bz-NCS, and **C** Conjugation of DOTA-bz-NCS to lysine residue on an antibody (Y).

Once an antibody is radiolabeled it can be injected into tumor bearing mice for preclinical studies or into patients for clinical assessment. Following this, tumor accumulation can be

determined through imaging (both preclinical and clinical) and/or biodistribution (preclinical, **Figure 1-8**). Tumor imaging using PET or SPECT gives a picture of where the radioisotope goes in the body and helps determine the time at which the best tumor to non-target contrast can be achieved. Standard uptake values (SUV) are used to quantify the amount of the radioisotope that was delivered to the tumor or other non-target organs by taking the activity measured through PET or SPECT imaging and dividing by the total injected dose per body weight. Biodistribution data is obtained by sacrificing the mice and performing a dissection to determine the radioactivity uptake by different organs. This information is typically provided as %ID/g (% Injected Dose per gram). With these two methods, radiotracers can be developed that lead to the highest tumor uptake with the smallest achievable dose to non-target tissues.

Figure 1-8. Purified radioisotope is added to a NOTA conjugated antibody to produce a radiopharmaceutical and that is then injected into tumor bearing mice. After some predetermined amount of time (usually 3-5 days for antibodies) animals are sacrificed, dissected and their organs and tumors are measured for radioactivity.

Heavy Ion Fragmentation Facilities

At several nuclear-physics research facilities, heavy-ion beams are generated and are used to bombard light element targets, like berylium or carbon, to produce secondary radioactive ion beams (usually by fragmentation reactions). These secondary beams can be used to study nuclear reactions involving reactants outside of the beta-stable region (higher up on the mass

valley walls as discussed earlier). These secondary reactions inform on the structure of nuclei with unusal n/p combinations, structure that, can dictate how elements are made in the first place - nucleosynthesis. Typically the end user is interested in one radioactive ion that was produced in the first reaction and the other isotope products created go to waste. Finding methods to "harvest" these unused isotopes is of considerable interest for applied research in medicine, stockpile stewardship, geology, and astrophysics.

National Superconducting Cyclotron Laboratory

The National Superconducting Cyclotron Laboratory (NSCL) is a heavy-ion fragmentation facility located at Michigan State University (MSU). Two cyclotrons in series, a K500 and a K1200, are used to accelerate heavy ions that are fragmented using a berylium target. (The K number is the collection of constants that, if there were no other limitations, would be the maximum proton energy.) An illustration of the fragmentation process is shown in **Figure 1-9**. After fragmentation, the isotopes are passed through the A1900 fragment separator[27] which selects the isotope of interest to an end user by employing two pairs of dipole magnets with an interviening wedge absorber that reduces the energy of the ions differently depending on their atomic number. Several quadrupole focusing magnets are also employed in the A1900 to achieve

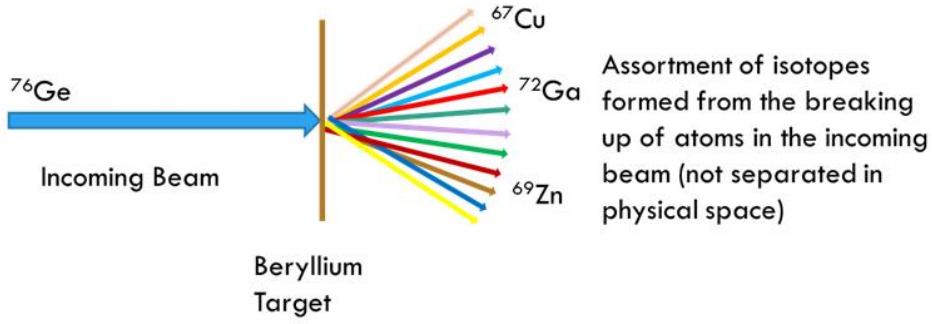

Figure 1-9. Illustration of heavy ion beam fragmentation. Note that isotopes created are not separated in physical space and can only be separated in the A1900 by magnetic rigidity.

high transmission of the desired ion. The secondary beam is then sent to one of many vaults for nuclear-physics research. **Figure 1-10** shows a schematic of the NSCL. A code called LISE++ can be used to simulate the primary fragmentation reaction and to detemine the optimal parameters for the magnets and wedge absorber to select the desired beam with maximal purity and to assess the contaminants in the beam.[28]

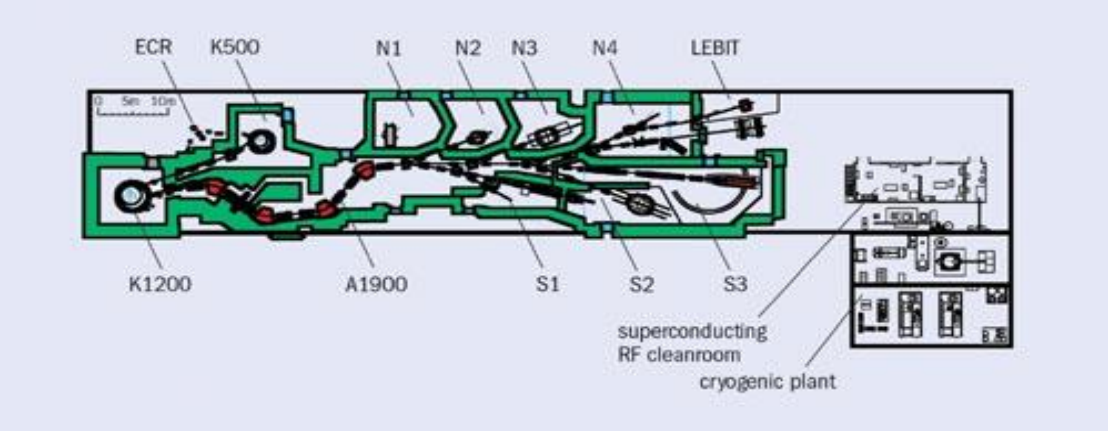

Figure 1-10. Schematic of the NSCL located at Michigan State University[9]

Upgrade to the Facility for Rare Isotope Beams

The NSCL is currently undergoing an upgrade to become the Facility for Rare Isotope Beams (FRIB) (**Figure 1-11**). FRIB will replace the two cyclotrons currently in operation at the NSCL with a linear accelerator. The new facility will be able to increase the energy of the heavy-ion beams available along with increasing the current by three orders of magnitude.[29] With the capability to fragment one thousand times more ions, an aqueous beam dump will be employed to collect the isotopes that are not wanted for the end user's experiments. This dramatically increases the potential for harvesting and has piqued the interest of several communities.

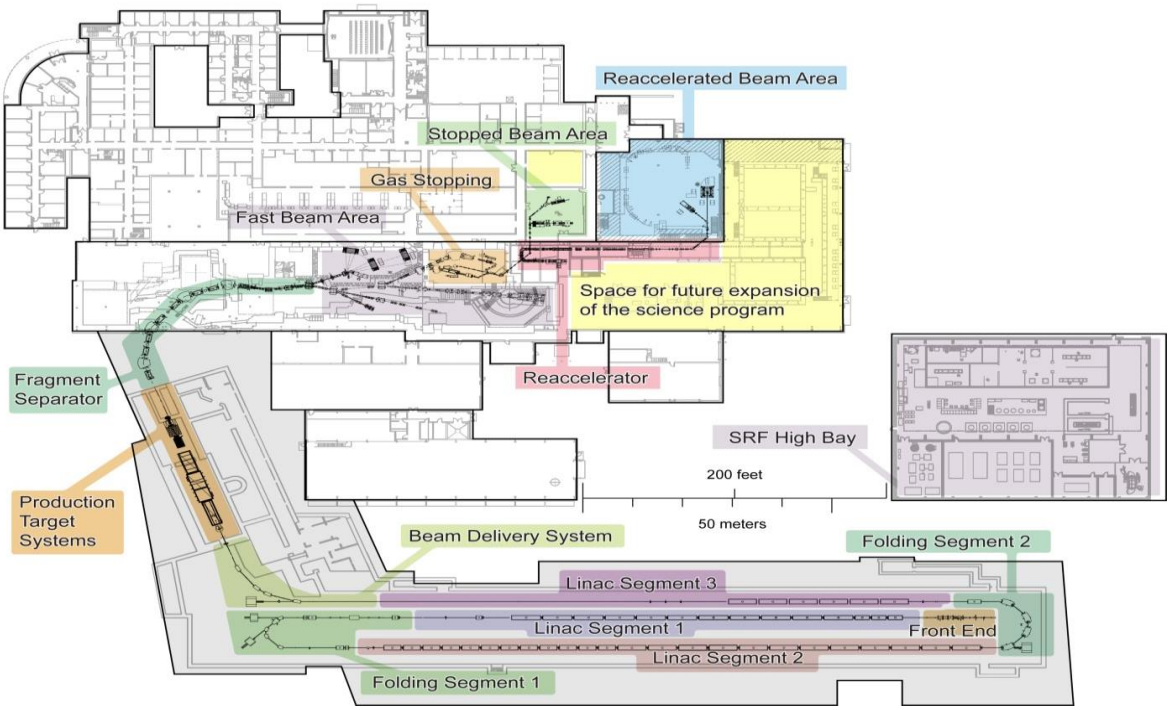

Figure 1-11. Schematic of the Facility for Rare Isotope Beams at Michigan State University[6]

Harvesting Isotopes of Interest from an Aqueous Beam Dump at FRIB

Many isotopes of interest will be available in usable quantities for harvest from the aqueous beam dump at FRIB.[30] A committee of users from the isotope community was formed to generate an initial list of isotopes of interest for a large range of scientific applications (**Table 1-2**). As part of this thesis work, proof-of-principal experiments were performed in order to develop strategies for the online harvesting of isotopes from the aqueous beam dump at FRIB so that optimal accomodation for harvesting can be made during the construction of the new facility. In order to perform these proof-of-principal experiments, a mock beam dump was designed and built to collect secondary radioisotope beams at the NSCL. Additionally, separation strategies were developed to determine feasibility, purity, and efficiency of separating

the isotopes of interest from the other activities in the aqueous beam dump. Preliminary experiments designed to address some of these concepts will be discussed in this thesis.

Table 1-2. Isotopes of interest for isotope harvesting.

Isotope	Decay Mode	Half-Life	Application
^{32}Si	β^-	162y	Tracer; geology, botany
^{44}Ti	ε	59.2y	Medicine, astrophysics, Nuclear Structure
^{48}V	β^+,ε	15.98d	Stockpile Stewardship, Medicine
^{67}Cu	β^-	2.6d	Medicine
^{85}Kr	β^-	10.76y	Astrophysics, Stockpile Stewardship
^{147}Eu-^{154}Eu		24d-37y	Stockpile Stewardship
^{211}Rn	α	14.6h	Medicine
^{225}Ra	β^-	14.9d	Medicine, Electric Dipole Moment
^{225}Ac	α	10.0d	Medicine

Radioisotope Production Using Small Medical Cyclotrons

The use of low-energy cyclotrons to produce isotopes at medical facilities has been increasing, largely due to the FDA approval of [^{18}F]FDG as previously discussed. These cyclotrons usually accelerate protons (some also accelerate deuterons and/or alpha particles) and typically range in proton energy from 11-30 MeV. A cyclotron works by accelerating charged protons, for example H^+ or H^-, using an AC modulated electric field and a single large dipole magnet (schematic shown in **Figure 1-12**). In the classical (as developed by E. Lawrence in the early 1930's) cyclotron there are two dees in which the ions are shielded from the electric field when they travel through them. Once a proton exits the inner edge of the dee it was traveling in, an accelerating electric field is sensed across the gap (between the dees) causing the proton to accelerate across the gap.[10,31] The protons travel in a circular path characteristic of a charged

particle moving in a constant magnetic field, imposed by the dipole. As the ions increase in speed, the circular path increases in diameter and a spiral trajectory results. (One can view a cyclotron as a linear accelerator made efficient in space and energy by the reuse, on each turn, of the same set of accelerating gaps. Higher energy cyclotrons often have 3 or more dees.) The engineering of the acceleration scheme for a cyclotron is simple compared to the initiation and extraction aspects. The latter is made much easier by using H^- rather than H^+. H^- ions are accelerated through a thin carbon stipper foil, which strips the H^- of its two electrons creating H^+. This change in charge causes the path to arc outwards and be directed towards an external target for isotope production at an efficiency of nearly 100%. H^+ ions are deflected by use of an electrostatic channel that steers the ions out of the cyclotron often with an efficiency less than 75%. The beam that is lost using H^+ deflection causes nuclear reactions making the internal cyclotron parts radioactive.[11,32]

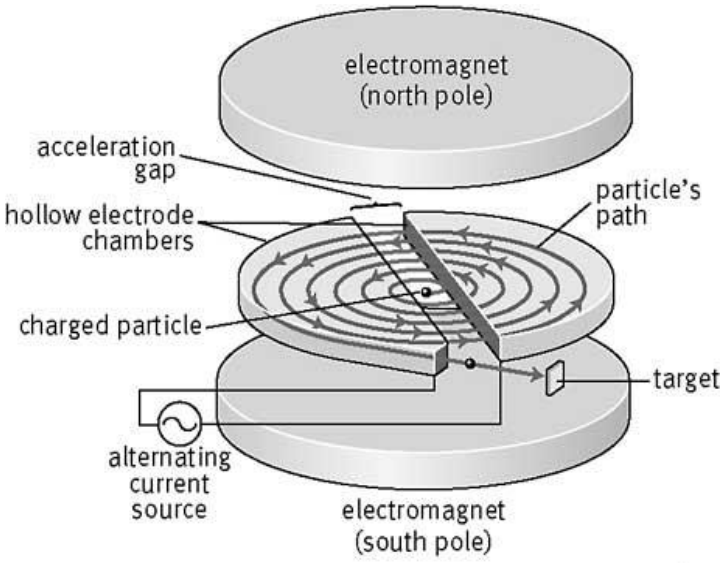

Figure 1-12. Schematic of a cyclotron[5]

Nuclear Reactions (p,n) and (p,α)

Several proton induced nuclear reactions are attainable at low energies (11-30 MeV). During most low-energy nuclear reactions the proton combines with the target nucleus to create a compound nucleus. This compound nucleus is highly excited and deexcites by evaporating particles, usually neutrons but sometimes protons or alpha particles and even more rarely larger nuclei, and leaves behind a new isotope. For example a 15MeV proton combines with a ^{58}Ni atom forming a compound nucleus of ^{59}Cu that then evaporates an alpha particle to become ^{55}Co (**Figure 1-13**). As in decay, the mass difference between reactants and products is the Q-value, but it can be of either sign for reactions. The Q-value is most conveniently calculated by subtracting the mass excess, Δ = (Actual mass in atomic mass units – A)*c^2, of the products from the reactants (**Equation 7**). (Mass excesses can be used as neither neutrons nor protons are being created, they are just being rearranged – this is no different than a reaction enthalpy where the masses of the atoms do not need to be considered as they just redistributed). The Q-value for the reaction above creating ^{55}Co is -1.33 MeV. This sign means that the mass of the products is more than that of the reactants thus there is an absolute minimum proton energy below which the reaction probability is zero.

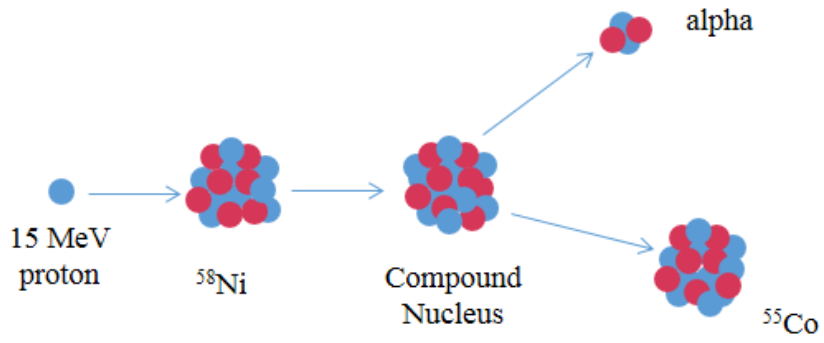

Figure 1-13. Illustration of the nuclear reaction ^{58}Ni(p,α)^{55}Co.

$$\mathbf{p + A \longrightarrow \alpha + B} \qquad \mathbf{or} \qquad \mathbf{A(p,\alpha)B} \qquad \mathbf{with} \quad \mathbf{Q = \Delta_p + \Delta_A - \Delta_\alpha - \Delta_B} \qquad \mathbf{(7)}$$

Another important factor to consider in reactions between charged particles is the Coloumb barrier. Because the proton and the target atom are both positively charged, the proton must overcome the Coulomb barrier (V_C) approximately given by Equation 8 where Z_1 is the atomic number of the incoming atom (1 for proton initiated reactions), Z_2 is the atomic number of the target nucleus, and R_1 and R_2 are the radii of the incoming and target nuclei respectively. In **Equation 8**, V_C is in MeV when R is in fm.[10,11] The larger the Coulomb barrier, the more energy must be provided for the reaction to occur with significant probability. The energy required to overcome the Coulomb barrier for ^{58}Ni(p,α)^{55}Co is 5.52 MeV. The threshold energy of the reaction (the amount of energy required for the reaction to occur) is the higher of the two energies: the negative of the Q-value (a thermodynamic threshold) and the Coulomb barrier (a kinetic threshold).

$$\mathbf{V_C = \frac{1.44 * Z_1 * Z_2}{R_1 + R_2}} \qquad \mathbf{(8)}$$

The probability of a nuclear reaction occuring is called a cross section, a quantity with the dimensions of area. Typically the units are given in millibarns where 1 millibarn = 1 x 10^{-27}cm^2. Plotting the cross section vs incident particle energy yields an excitation function (**Figure 1-14**). This functional dependence along with the thickness of the target can be used to estimate the yield of a reaction (**Equation 9**) where R is rate per second, N is the number of target atoms per cm^2, σ is the cross section in cm^2, and ϕ is the particle flux, which in this case is the number of protons per second. If the target is sufficiently thick so that the energy of the projectile drops as it proceeds though the target, the yield can be estimated summing (or integrating) the rate over an imagined stack of (L) thin targets each with N_i atoms per unit area and a cross section σ_i appropriate to the energy of the projectile when it arrives at that target slice. For bombardments

that are long compared to the half-life of the isotope being produced, saturation is achieved resulting from the decay rate of the produced radioactivity rising to match the production rate. In the work presented here I will discuss the use of small medical cyclotrons to produce ^{55}Co via the ^{58}Ni(p,α)^{55}Co reaction.

$$\mathbf{R = N\sigma\phi = \sum_{i=1}^{L}(N_i\sigma_i\phi)} \quad \textbf{(9)}$$

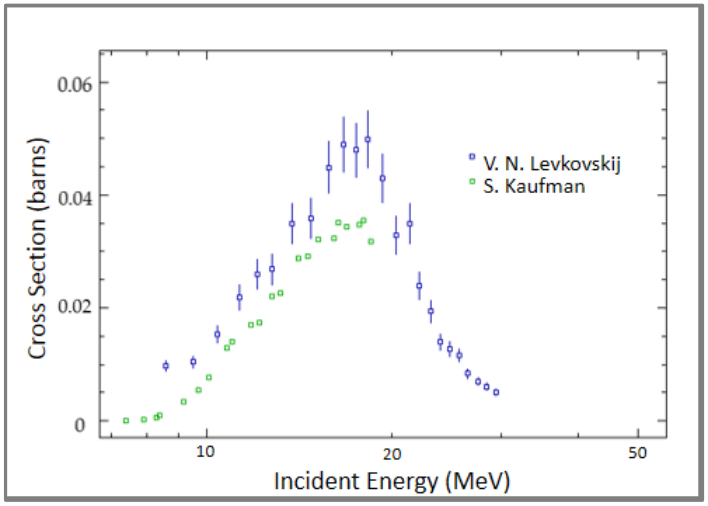

Figure 1-14. Excitation functions for the ^{58}Ni(p,α)^{55}Co reaction.[4]

This thesis will discuss the first attempts and "proof of concept" experiments for isotope harvesting. In Chapter 2 a measurement will be presented that was useful for the development of separation strategies for the harvesting of ^{67}Cu and to measure the final purity of ^{55}Co productions. Chapter 3 will address the design of an end station for use at the end of a beam line at the NSCL to collect isotopes in water. This end station was tested and validated using a purified ^{24}Na beam. Chapter 4 presents the collection of a mostly pure ^{67}Cu beam and its subsequent separation and use for antibody labelling. Chapter 5 expands on Chapter 4 by testing the separation strategy using a no wedge beam (this means that the beam was not subjected to the majority of the magnetic separation in the A1900) thus it contained many contaminants. This

chapter also presents the separation, purification and the radiolabelling of an antibody with ^{67}Cu followed by injection into tumor-bearing mice, and the resulting 5-day biodistribution. Chapter 6 consists of a side project, the production of ^{55}Co via the $^{58}Ni(p,\alpha)^{55}Co$ reaction, looking at free $^{55}CoCl_2$ (not chelated) in tumor bearing mice and the resulting biodistribution at 24 and 48 hrs, along with labeling DOTA or NOTA conjugated peptides in order to determine the stability of ^{55}Co in DOTA and NOTA complexes in vivo. Conclusions and thoughts on future work are presented in Chapter 7.

References

1 Pantaleo, M. A. *et al.* Conventional and novel PET tracers for imaging in oncology in the era of molecular therapy. *Cancer Treat Rev* **34**, 103-121, doi:DOI 10.1016/j.ctrv.2007.10.001 (2008).

2 Chen, K. & Conti, P. S. Target-specific delivery of peptide-based probes for PET imaging. *Adv Drug Deliver Rev* **62**, 1005-1022, doi:DOI 10.1016/j.addr.2010.09.004 (2010).

3 Gomes, C. M., Abrunhosa, A. J., Ramos, P. & Pauwels, E. K. J. Molecular imaging with SPECT as a tool for drug development. *Adv Drug Deliver Rev* **63**, 547-554, doi:DOI 10.1016/j.addr.2010.09.015 (2011).

4 *National Nuclear Data Center*, <http://www.nndc.bnl.gov/> (1994).

5 Dictionary, A. H. S. (Houghton Mifflin Company, 2002).

6 *Facility for Rare Isotope Beams*, <http://www.frib.msu.edu/about> (

7 Hamoudeh, M., Kamleh, M. A., Diab, R. & Fessi, H. Radionuclides delivery systems for nuclear imaging and radiotherapy of cancer. *Adv Drug Deliver Rev* **60**, 1329-1346, doi:DOI 10.1016/j.addr.2008.04.013 (2008).

8 Dash, A., Knapp, F. F. & Pillai, M. R. Targeted radionuclide therapy--an overview. *Current radiopharmaceuticals* **6**, 152-180 (2013).

9 Bollen, G. *University hosts premier rare-isotope facility*, <http://cerncourier.com/cws/article/cern/28717> (2002).

10 Friedlander, G., Kennedy, J. W., Macias, E. S. & Miller, J. M. *Nuclear and Radiochemistry* 3edn, (John Wiley & Sons, 1981).

11 Ehmann, W. D. & Vance, D. E. *Radiochemistry and Nuclear Methods of Analysis*. Vol. 116 (John Wiley and Sons, 1991).

12 Rahmim, A. & Zaidi, H. PET versus SPECT: strengths, limitations and challenges. *Nucl Med Commun* **29**, 193-207 (2008).

13 Coleman, R. E. Single Photon-Emission Computed-Tomography and Positron Emission Tomography in Cancer Imaging. *Cancer* **67**, 1261-1270 (1991).

14 Kelloff, G. *et al.* Progress and promise of FDG-PET imaging for cancer patient management and oncologic drug development. *Clinical Cancer Research* **11**, 2785-2808, doi:Doi 10.1158/1078-0432.Ccr-04-2626 (2005).

15 Hoh, C. K. Clinical use of FDG PET. *Nuclear Medicine and Biology* **34**, 737-742, doi:DOI 10.1016/j.nucmedbio.2007.07.001 (2007).

16 Taylor, A., Schuster, D. M. & Alazraki, N. *A Clinician's Guide to Nuclear Medicine*. (Society of Nuclear Medicine, 2003).

17 Kume, M. *et al.* A semi-automated system for the routine production of copper-64. *Applied Radiation and Isotopes* **70**, 1803-1806, doi:DOI 10.1016/j.apradiso.2012.03.009 (2012).

18 Pen, A. *et al.* Design and construction of a water target system for harvesting radioisotopes at the National Superconducting Cyclotron Laboratory. *Nucl Instrum Meth A* **747**, 62-68, doi:DOI 10.1016/j.nima.2014.02.010 (2014).

19 McCann, J. W. *et al.* Radiation Emission from Patients Treated with Selective Hepatic Radioembolization Using Yttrium-90 Microspheres: Are Contact Restrictions Necessary? *J Vasc Interv Radiol* **23**, 661-667, doi:DOI 10.1016/j.jvir.2012.01.070 (2012).

20 Nucleonica Decay Engine.

21 Pillay, V., Gan, H. K. & Scott, A. M. Antibodies in oncology. *New Biotechnol* **28**, 518-529, doi:DOI 10.1016/j.nbt.2011.03.021 (2011).

22 Boswell, C. A. & Brechbiel, M. W. Development of radioimmunotherapeutic and diagnostic antibodies: an inside-out view. *Nuclear Medicine and Biology* **34**, 757-778, doi:DOI 10.1016/j.nucmedbio.2007.04.001 (2007).

23 Buchsbaum, D. J. Imaging and therapy of tumors induced to express somatostatin receptor by gene transfer using radiolabeled peptides and single chain antibody constructs. *Semin Nucl Med* **34**, 32-46, doi:DOI 10.1053/j.semnuclmed.2003.09.005 (2004).

24 Iagaru, A., Goris, M. L. & Gambhir, S. S. Perspectives of molecular imaging and radioimmunotherapy in lymphoma. *Radiol Clin N Am* **46**, 243-252, doi:DOI 10.1016/j.rcl.2008.03.007 (2008).

25 Dearling, J. L. J. *et al.* Imaging cancer using PET - the effect of the bifunctional chelator on the biodistribution of a Cu-64-labeled antibody. *Nuclear Medicine and Biology* **38**, 29-38, doi:DOI 10.1016/j.nucmedbio.2010.07.003 (2011).

26 Zhang, Y. *et al.* Positron Emission Tomography Imaging of CD105 Expression with a Cu-64-Labeled Monoclonal Antibody: NOTA Is Superior to DOTA. *Plos One* **6**, doi:ARTN e28005 DOI 10.1371/journal.pone.0028005 (2011).

27 Morrissey, D. J., Sherrill, B. M., Steiner, M., Stolz, A. & Wiedenhoever, I. Commissioning the A1900 projectile fragment separator. *Nucl Instrum Meth B* **204**, 90-96, doi:Doi 10.1016/S0168-583x(02)01895-5 (2003).

28 O. Tarasov, D. B. LISE++: Radioactive beam production with in-flight separators. *Nuclear Instruments and Methods in Physics Research Section B: Beam Interactions with Materials and Atoms* **266**, 4657-4664 (2008).

29 Morrissey, D. Status of the FRIB project with a new fragment separator. *Journal of Physics: Conference Series* **267**, 012001, doi:10.1088/1742-6596/267/1/012001 (2011).

30 Ronningen, R. Isotope Inventories in Cooling Loop. *2nd Workshop on Isotope Harvesting at FRIB* (2012).

31 Loveland, W. D., Morrissey, D. J. & Seaborg, G. T. *Modern Nuclear Chemistry*. (John Wiley & Sons, 2006).

32 Phelps, M. E. *PET: Molecular Imaging and Its Biological Applications*. (Springer-Verlag, 2004).

Chapter 2

Specific Activity Measurement of ^{64}Cu: A Comparison of Methods

[This work has been published previously as Tara Mastren, James Guthrie, Paul Eisenbeis, Tom Voller, Efrem Mebrahtu, J. David Robertson, and Suzanne E. Lapi, *Applied Radiation and Isotopes*. **2014**, *90*, 117-121]

Introduction

Specific activity is a measurement of the purity of a radioisotope. Effective specific activity (ESA) is the amount of radioactivity per unit mass of competing metal for a certain chemical or biological reaction. True specific activity is the amount of radioactivity per μmol of atoms of the same element (for example amount of ^{64}Cu per μmol total copper). Theoretical maximum specific activity is the amount of radioactivity per μmol of the radioactive species (for example radioactivity of ^{64}Cu per μmol ^{64}Cu). The theoretical maximum specific activity for ^{64}Cu, a common radiometal used in preclinical and clinical research, is 2.47×10^5 mCi/μmol.

The specific activity of a given radionuclide is important in developing the chemistry for labelling compounds. Typically it is desired to have as close to the theoretical maximum specific activity as is reasonably achievable. In radiometal productions many efforts are in place to reduce the amount of contaminating metals present. Trace metal grade chemicals are used in various cleaning and manufacturing steps and all glassware and materials that come into contact with the radioactivity are washed in a nitric bath for 24 hours to remove surface metal contaminants. Additionally, separation chemistries to isolate the radiometal of interest from the target material are optimized to improve the final purity.

There is a growing demand for ^{64}Cu for use in Positron Emission Tomography (PET) research. A review of the literature shows that the number of publications involving ^{64}Cu has more than tripled since 2000. The 12.7 hr half-life and the low beta energy of ^{64}Cu (E_{avg} = 0.278 MeV) makes it an optimal PET isotope for imaging up to 48 hours after administration (**Figure 2-1**). Similarly these properties of ^{64}Cu make it an ideal candidate for labeling peptides and antibodies as the time required for these tracers to accumulate in the target organs (a few to several hours) requires labels with commensurate half-lives.[1-7]

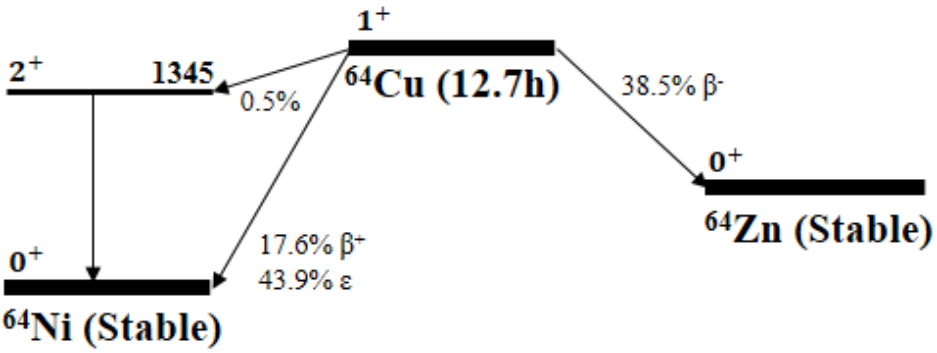

Figure 2-1. The decay scheme for ^{64}Cu showing decay by β^+, β^-, and ε.

Measurement of the effective specific activity (ESA) of ^{64}Cu is important to the application of ^{64}Cu because metal impurities present in the sample can have a negative impact on radiolabelling.[8] The current and most common method for measuring the effective specific activity (ESA) of ^{64}Cu productions is by titration with a suitable chelator such as 1,4,8,11-tetraazacyclotetradecane-1,4,8,11-tetraacetic acid (TETA).[9,10] This approach measures the ESA relative to the metal's affinity for the TETA molecule but does not distinguish between the different types of metals present in the sample. Other methods that have been developed to measure ESA of ^{64}Cu include voltammetry, liquid chromatography-mass spectrometry (LC-MS), and inductively coupled plasma mass spectrometry (ICP-MS). Voltammetry measures the amount of cold (non-radioactive) copper contamination but not the amount of the other contaminating metals.[11] The recently reported LC-MS method measures the concentration of metal contaminants present that bind to a particular chelator, however it is a relatively expensive and complex method that may also require additional method development for new chelators.[8] While ICP-MS is a sensitive multi-element analysis technique that can simultaneously determine the concentration of all the metal contaminants in the sample, it is also an expensive technique and not readily available at all institutions for radioactive samples. For this reason, a method is

desired that is robust and will identify and measure trace amounts of metal impurities in samples of ^{64}Cu.

In this chapter a high-performance liquid-chromatography (HPLC) ion-chromatography method that measures trace amounts of metals (ppb) was used to measure the transition metal contaminants in twenty different ^{64}Cu lots produced at Washington University School of Medicine. This method was validated by comparing the data to the current TETA titration method and ICP-MS. Ion chromatography is simple, fast (<25min), and practical for routine measurement of the cold metal contaminants in a radioactive sample of ^{64}Cu. Due to the high sensitivity of this technique, ion chromatography was instrumental in determining separation strategies for isotope harvesting experiments where radioactive tracers could not be employed.

Materials and Methods

TETA Titrations: Trace metal grade reagents including ammonium acetate, ammonium hydroxide, and hydrochloric acid were obtained from Sigma Aldrich (St. Louis, MO). 1,4,8,11-tetraazacyclotetradecane-1,4,8,11-tetraacetic acid was obtained from Macrocyclics (Dallas,TX). ^{64}Cu was produced in house at Washington University using an automated module.[12] 2 mL microcentrifuge tubes were acid washed in 50% nitric acid bath overnight before use. TLC plates (silica gel 60F-254 glass 5x10cm 0.25mm precoat) were obtained from Millipore (Billerica, MA).

Ion Chromatography: PDCA (1.4 mM pyridine-2,6-dicarboxylate / 13.2 mM Potassium hydroxide / 1.12 mM Potassium sulfate / 14.8 mM Formic acid) PAR (4-(2-pyridylazo)resorcinol), and PAR dilutent (1.0 M 2-dimethylaminoethanol/0.50 M Ammonium hydroxide/0.30 M Sodium bicarbonate) were obtained from Dionex. TraceSELECT Ultra, ACS

reagent for ultratrace analysis water and nickel, copper, cobalt, iron, and zinc and TraceCERT atomic absorption standards 1000 mg/L were obtained from Sigma (St Louis, MO).

Mass Spectrometry: A PerkinElmer NexION 300X ICP-MS was used for all ICP-MS measurements. Linearity standards were prepared from commercial multi-element and single-element solutions (High Purity Standards). The diluent for samples and standards was a solution of 3% w/w HNO_3 that was prepared from Optima grade nitric acid (Fisher Scientific) and fresh 18.2 MΩ-cm water (EMD Millipore)

TETA Titration

The TETA titration method was based on that reported previously.[8] 7.4 MBq (20 µL) of ^{64}Cu was added to eight different concentrations of TETA in ammonium acetate pH 5.5 ranging from 4.3×10^{-4} nmol to 6.3×10^{-1} nmol. Final volume was brought to 100 µL using 0.5 M ammonium acetate buffer pH 5.5. The solutions were placed in an agitating incubator at 80 ºC for 20 min. Solutions were cooled to room temperature and then centrifuged. A 1µL sample from each TETA concentration along with 1 µL unbound ^{64}Cu was analyzed for percent ^{64}Cu incorporation determined by Thin Layer Chromatography (TLC) using silica plates and 1:1 mixture of 10% ammonium acetate and methanol as an eluent. Plates were analyzed using a Radio TLC Plate Reader (Bioscan, Washington DC). Data was plotted as molar concentration of TETA vs. % ^{64}Cu incorporation. The curve was fit using a sigmoid plot fit program in Prism (Graphpad, California). The EC50 value, concentration of TETA that bound to 50% of the ^{64}Cu, was determined from this fit. The ESA was set equal to two times the EC50 value.

Ion Chromatography

Twenty completely decayed ^{64}Cu lots of varying activity at end of bombardment were measured at two concentrations in triplicate. Each sample was originally brought to 1mL by adding TraceSELECT Ultra water (Sigma), then samples were diluted to 74 kBq/µL (back calculated activity to end of bombardment for the sample) with TraceSELECT Ultra water 0.740 kBq and 18.5 MBq from this dilution were brought to a final volume of 3 mL with TraceSELECT Ultra water. The concentrations were adjusted depending on the amount of metal contamination present. The lower concentration was typically used to measure contaminating nickel at 1-10 µg/L and the higher concentration solution was used to measure the copper, iron and zinc contaminants at 1-10µg/L. A metal-free HPLC system equipped with a GP-50 pump, AD20 detector, and a PC10 post column delivery system was used with a Dionex CS5A 2-mm Transition Metal Column. 1mL of each sample was injected into the metal free ion chromatography system. The eluent (1.4 mM pyridine-2,6-dicarboxylate / 13.2 mM Potassium hydroxide / 1.12 mM Potassium sulfate / 14.8 mM Formic acid) was passed through the column at 0.30 mL/min. As the metals elute from the column they pass through a mixing loop with 1.0 M 2-dimethylaminoethanol/0.50 M Ammonium hydroxide/0.30 M Sodium bicarbonate containing 0.06g/L 4-(2-pyridylazo) resorcinol (PAR) at 0.15 mL/min. This post column reagent flow is controlled by the PC-10 post column delivery system using pressurized helium. During this time the metals complex with the PAR dye prior to UV analysis at 530 nm. Calibration curves that ranged from 1 µg/L to 10 µg/L were made for copper, nickel, zinc, cobalt, and iron using TraceCERT atomic absorption standards, 1000 mg/L in nitric acid.

ICP Mass Spectrometry

Linearity standards were prepared in 3% HNO_3 from a commercial high purity standards multielement solution containing all elements of interest. Individual single-element standards of Zn and Ni were also prepared in order to measure and normalize for mass fractionation among Ni isotopes. The internal standards Sc, Ga, and In were added to all samples and linearity standards in order to compensate for matrix effects and instrument sensitivity drift.

Samples were analyzed using a PerkinElmer NexION 300X ICP-MS operated in KED (Kinetic Energy Discrimination) mode. All isotopes were analyzed twice, once at a helium flow of 2.5 mL/min (low flow) and 4.5 mL/min (high flow). High-flow results are reported all elements measured.

Results

TETA Titrations

ESA as measured by TETA titration over the twenty lots varied between 49.6 and 973.1 GBq/µmol.

Ion Chromatography

Calibration curves for five different metals including iron, copper, nickel, zinc, and cobalt were linear at concentrations ranging from 1µg/L to 10µg/L with R^2 values of 0.95 or greater (**Figure 2-2**). Standard error of the estimate for the five curves were calculated to be 2.01 µg/L for iron, 0.56 µg/L for copper, 0.48µg/L for nickel, 0.42µg/L for zinc, and 0.05µg/L for cobalt. The lower limit of detection was 1µg/L for copper and cobalt, 2µg/L for nickel and iron, and 3µg/L for zinc. **Figure 2-3** shows an overlay of the 5µg/L calibration sample with a blank. The

absorbance of the five different metal-PAR complexes at 530 nm are different when measuring the same concentration. This can be seen in **Figure 2-3** and is responsible for the different slopes shown in **Figure 2-2**.

Ion chromatography yielded the concentration (mg/L) of cold copper, nickel, zinc, and iron that were present in the ^{64}Cu samples diluted to 1mL, cobalt was not detected as a contaminant. **Figure 2-4** shows the amount in mg/L of nickel, copper, iron, and zinc measured by IC compared to ICP-MS of each of the twenty samples measured with the exception of zinc which only shows IC measurement.

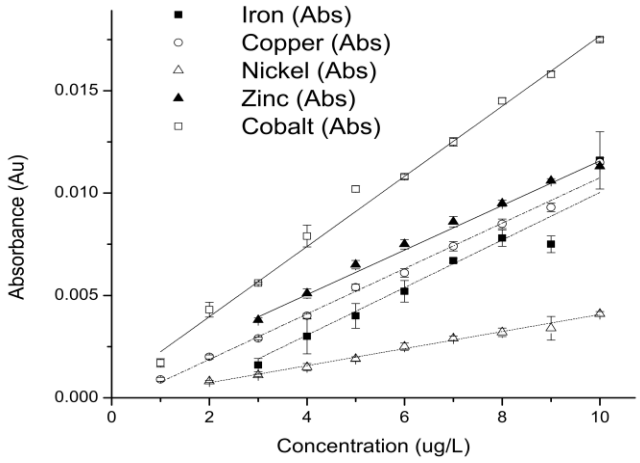

Figure 2-2. Calibration curves for assessment of metal contamination using ion chromatography. Five calibration curves were made for iron, copper, nickel, zinc, and cobalt. R^2 values for these curves were > 0.95. The lower limit of detection that resulted in a linear curve for copper and cobalt is 1 ug/L, iron and nickel is 2 ug/L, and zinc is 3 ug/L. All samples were brought between the lower limits and 10 ug/L for analysis.

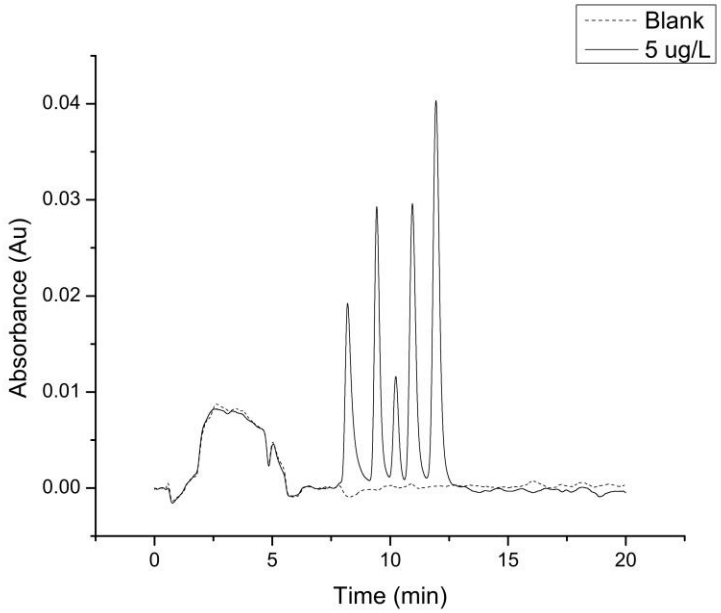

Figure 2-3. Ion Chromatography of the 5µg/L calibration standard. From left to right peaks represent iron, copper, nickel, zinc, and cobalt. The absorbance at 530nm was measured.

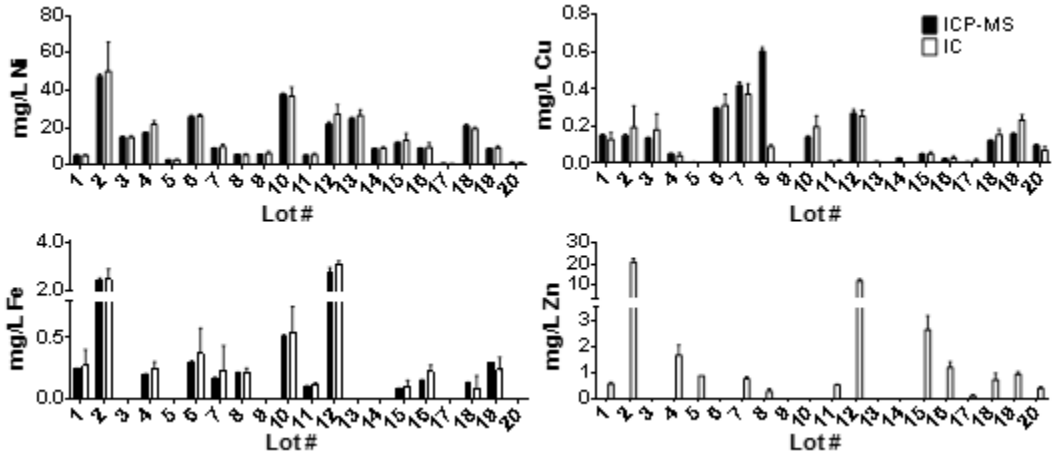

Figure 2-4. Ion Chromatography vs ICP-MS. The amount in mg/L of nickel, copper, iron, and zinc measured by IC compared to ICP-MS of each of the twenty samples measured with the exception of zinc which only shows IC measurement.

When constructing the calibration curves zinc contamination was an issue. All glassware and vials must be acid washed for at least 24 hrs in 50% HNO_3 to minimize contamination. Zinc was a perpetual contaminant in the autosampler vials so manual injections using 5.0 mL syringes (Thermo Scientific SUN-SRi™ Luer-Slip Syringes) were used and found to be free of zinc contamination. Additionally TraceSELECT Ultra water (Sigma, St Louis) had to be used for all dilutions as the in-house milli-Q water contained as much as 3 ppb zinc. Storage of the sample in 2.0 mL acid washed microfuge tubes for a significant amount of time (weeks or more) will lead to zinc leaching out from the plastic, therefore it was best to make all dilutions immediately prior to analysis in order to minimize this contamination.

Mass Spectrometry

ICP-Mass Spectrometry was used as the "gold standard" method to validate ion chromatography for determining amounts of metal impurities. The Bland-Altman method[13] was used to compare the ion chromatography measurements with those from ICP- Mass Spectrometry and the results are graphically shown in **Figure 2-5**. Iron had a bias of -33.2µg/L with a 95% confidence interval of -126µg/L to 60.2µg/L and copper, with the exception of lot #8 which was omitted due to high variation, had a bias of -11.1µg/L with a 95% confidence window of -78.7µg/L to 56.6µg/L. Nickel was separated into two calculations, for lots under 20mg/L the bias was -0.241mg/L and had a 95% confidence window from -1.11mg/L to 0.602mg/L and at all concentrations ranging up to 50mg/L the bias was -0.755mg/L with a 95% confidence window of -4.1mg/L to 2.6mg/L.

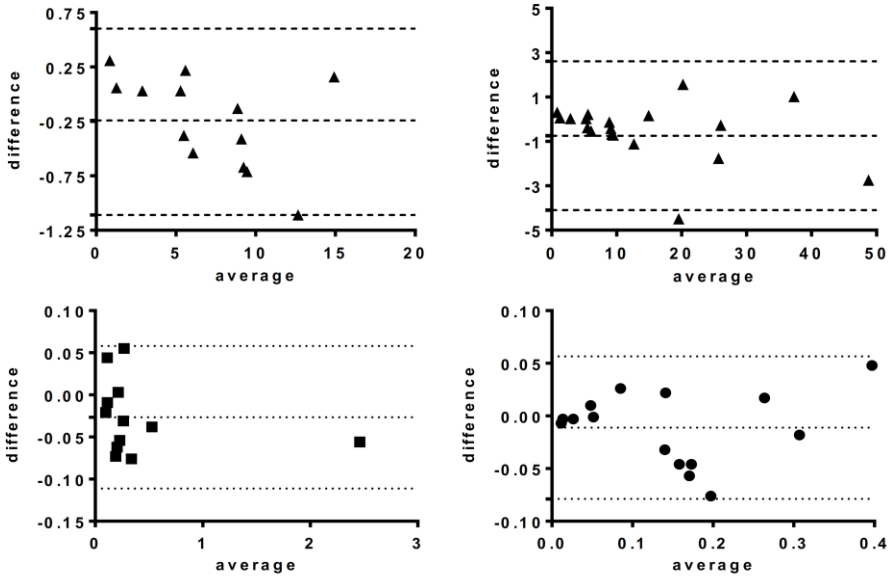

Figure 2-5. Bland-Altman plots comparing ion chromatography to ICP-mass spectrometry. Iron (squares), copper (circles), and nickel (triangles) < 20mg/mL top left all concentrations top right.

The difference in zinc measurements was quite large and it is likely that the samples were contaminated with zinc between the two measurements, likely caused by zinc leaching from the plastic microfuge tubes used to transport the samples to the ICP-MS lab, and therefore the results are not shown. ICP-MS did show very small concentrations of cobalt (0.34-12 μg/L) which was much lower than the detection limit of the Ion Chromatography method and considered negligible compared to the other metal contaminations.

Discussion

TETA titration, ion chromatography, and ICP mass spectrometry data were compared in order to analyze large variances in ESA. TETA values in seventeen lots were graphed against true specific activity (^{64}Cu radioactivity per µmol copper) in **Figure 2-6**, two lots were left out due to variation from the trend likely a result of TETA titration error. A link between cold copper contamination and effective specific activity is observed which was expected. The ESA values were lower than the true specific activity values. This difference is likely due to the contribution of other metals such as nickel and iron binding to the TETA molecule thus affecting the measurement. The log K values for copper, nickel, and iron for TETA are 21.7, 19.91, and 13.1 respectively and the moles of TETA remaining compared to the moles of nickel and iron available for binding are quite small and thus both are believed to have some effect on overall specific activity.

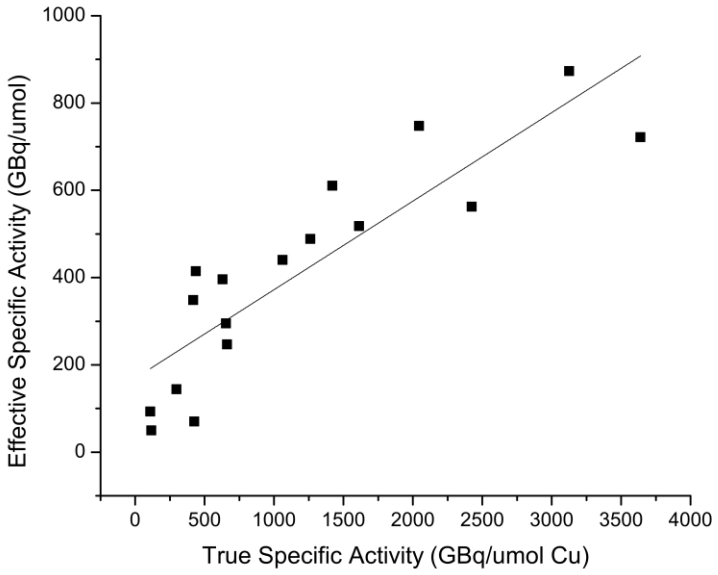

Figure 2-6. Effective vs True Specific Activity. The graph of effective specific activity (TETA) vs. true specific activity (ICP-MS) illustrates the relationship between copper contamination and TETA specific activity.

Sources of copper contamination are currently being explored. One potential source is the raw ^{64}Ni material. Other potential sources are the reagents used in the purification chemistry or contamination during the electroplating process.

For routine analysis the TETA and ion chromatography method are useful in determining impurities and ESA of different lots of ^{64}Cu. Ion chromatography is useful as a troubleshooting method as it can show which metals are contaminating a sample and help to determine the source of the contamination. ICP mass spectrometry is useful for looking at all the impurities that could be present and also to confirm routine measurements.

Conclusions

Ion chromatography is a good method for routinely analyzing trace amounts of transition metals in radioactive samples. This method can measure in the parts per billion range and therefore large amounts of radioactivity do not have to be injected in order to get an accurate measurement. The main drawback for measuring metal contaminants in ^{64}Cu productions is determining the dilution factor that brings the low levels of copper and iron to the 1-10 µg/L range required for detection. More work will be done to determine the source of the cold metal contaminants, steps that can be done to minimize or eliminate them, and at what concentration these impurities have the largest effect.

References

1 Anderson, C. J. & Welch, M. J. Radiometal labeled agents (non-technetium) for diagnostic imaging. *Chem Rev* **99**, 2219-2234, doi:Doi 10.1021/Cr980451q (1999).

2 Smith, S. V. Molecular imaging with copper-64. *Journal of inorganic biochemistry* **98**, 1874-1901, doi:10.1016/j.jinorgbio.2004.06.009 (2004).

3 Anderson, C. J., Wadas, T. J., Wong, E. H. & Weisman, G. R. Cross-bridged macrocyclic chelators for stable complexation of copper radionuclides for PET imaging. *Q J Nucl Med Mol Im* **52**, 185-192 (2008).

4 Wadas, T. J., Wong, E. H., Weisman, G. R. & Anderson, C. J. Copper chelation chemistry and its role in copper radiopharmaceuticals. *Current pharmaceutical design* **13**, 3-16 (2007).

5 Anderson, C. J. & Ferdani, R. Copper-64 Radiopharmaceuticals for PET Imaging of Cancer: Advances in Preclinical and Clinical Research. *Cancer Biother Radio* **24**, 379-393, doi:DOI 10.1089/cbr.2009.0674 (2009).

6 Shokeen, M. & Anderson, C. J. Molecular imaging of cancer with copper-64 radiopharmaceuticals and positron emission tomography (PET). *Accounts of chemical research* **42**, 832-841, doi:10.1021/ar800255q (2009).

7 Marquez, B. V., Ikotun, O., Meares, C. F. & Lapi, S. E. Development of a Radiolabeled Irreversible Peptide (RIP) as a PET Imaging Agent for Vascular Endothelial Growth Factor. *J Labelled Compd Rad* **56**, S86-S86 (2013).

8 Zeng, D. & Anderson, C. J. Rapid and sensitive LC-MS approach to quantify non-radioactive transition metal impurities in metal radionuclides. *Chem Commun (Camb)* **49**, 2697-2699, doi:10.1039/c3cc39071c (2013).

9 McCarthy, D. W. *et al.* Efficient production of high specific activity 64Cu using a biomedical cyclotron. *Nucl Med Biol* **24**, 35-43 (1997).

10 Avila-Rodriguez, M. A., Nye, J. A. & Nickles, R. J. Simultaneous production of high specific activity Cu-64 and (CO)-C-61 with 11.4 MeV protons on enriched Ni-64 nuclei. *Applied Radiation and Isotopes* **65**, 1115-1120, doi:DOI 10.1016/j.apradiso.2007.05.012 (2007).

11 Van Elteren, J. T., Kroon, K. J., Woroniecka, U. D. & De Goeij, J. J. M. Voltammetry detection of copper in high specific activity Cu-64. *Applied Radiation and Isotopes* **51**, 15-19, doi:Doi 10.1016/S0969-8043(98)00186-9 (1999).

12 Kume, M. *et al.* A semi-automated system for the routine production of copper-64. *Applied radiation and isotopes : including data, instrumentation and methods for use in agriculture, industry and medicine* **70**, 1803-1806, doi:10.1016/j.apradiso.2012.03.009 (2012).

13 Bland, J. M. & Altman, D. G. Statistical Methods for Assessing Agreement between Two Methods of Clinical Measurement. *Lancet* **1**, 307-310 (1986).

Chapter 3

Design and construction of a water target system for harvesting radioisotopes at the National Superconducting Cyclotron Laboratory

[This work has been published previously as Aranh Pen, Tara Mastren, Graham F. Peaslee, Kelly Petrasky, Paul A. DeYoung, David J. Morrissey, Suzanne E. Lapi, *Nucl Instrum Meth A*. **2014**, *747*, 62-68]

Introduction

FRIB is currently scheduled for completion in 2022 and will have the capacity to accelerate uranium up to energies of 200 MeV/nucleon, and lighter ions to slightly higher energies, with a beam power as high as 400 kW to produce a broad range of rare radioisotopes through fragmentation. FRIB will provide these high-power beams at intensities several orders of magnitude higher than are currently obtainable, which will provide the most intense secondary ion beams of these rare isotopes in the world.[1] The unused radioisotopes will be stopped in the cooling water in FRIB's primary beam dump, a spinning titanium container with cooling water circulating at ~300 gallons per minute to dissipate the large heat load and provide a vehicle for the storage and disposal of unused radioisotopes. The technology to pass large volumes of cooling water through ion-exchange columns to remove radioisotopes has been well-developed in the nuclear power industry,[2] and the ability to conduct radiochemical separation and harvesting of certain long-lived radioisotopes from the cooling water of the primary beam dump has been designed into FRIB.[3] Developing aqueous extraction and separation methods for the ancillary harvesting of specific radioisotopes from FRIB's beam dump would be beneficial to many isotope users without interfering with the primary users' experiments.

Radioisotope harvesting of ^{13}N has been conducted in the past from the interaction of a fast ^{14}N primary beam with water,[4] but harvesting experiments with heavier beams had not been conducted before this work. In the study just cited only a few radioactive products could be produced in the water and ^{13}N was found to be the predominant activity. Experiments were needed, where collection of the secondary beam and fragmentation products is achieved, in order to determine the viability of "harvesting" isotopes of interest from an aqueous beam stop.

In order to collect the secondary beam an end station was designed that could stop the ions in an aqueous target. In this chapter this end-station design and construction is discussed in detail and results of testing using an analyzed high-energy beam of ^{24}Na are presented. The ^{24}Na collected in the water was isolated in order to obtain an extraction efficiency. Using this end station, the efficiency with which this isotope, and other isotopes of interest, would be extracted from water could be measured, optimized and compared to the direct measurement of the production rate in the A1900 separator (see below). This efficiency could then be used to estimate the activity of isotopes of interest that would potentially be extracted from the FRIB beam dump.[5,6] The development of a water-based target system for harvesting radioisotopes at the NSCL was the initial step for the proof-of-principle experiments to harvest useful radioisotopes from FRIB.

Materials and Methods

End Station Design

In order to collect and isolate specific radioisotopes of interest from a cocktail of other isotopes produced at the NSCL, a complete, remote-controlled, water target system was designed, constructed and tested with a radioactive beam. The following features were included in the final system:

The system had to be completely automated, remote-controlled and operated from outside the experimental vault during beam irradiation for radiation safety reasons.

This system had to be capable of performing several remote water collection/storage cycles before being recharged in order to conduct systematic studies with various beam conditions (six in the present case). For example, the purity or intensity of the analyzed beam

could be changed and deposited into separate water volumes. Thus, a water manifold system to move volumes of water to/from the target cell into separate collection vessels was necessary.

During the previous light-ion extraction experiments,[4] radiolytic production of radioactive gases was observed, thus the target water cell was designed to include a gas manifold system to capture off-gases and to purge the target water with helium to remove dissolved gases before irradiation. In addition, the target system was designed to be physically isolated from the accelerator vacuum system by passing the high-energy beam through an air gap before reaching the water target.

These features were realized in a stand-alone unit with a main enclosure housing the hardware and plumbing and a second enclosure housing the electronics, all controlled remotely over ethernet. There are three main components to the stand-alone unit: first, a water-holding reservoir in which aliquots of purified water were held in individual commercially-available HDPE (high density polyethylene) containers. There are six 175 mL conical HDPE bottles (Nalgene, 3143-0175) in the water reservoir system, each filled with 100 mL of distilled water (Sigma-Aldrich, 7732-18-5) prior to beam collection. The water in each reservoir was sparged with helium for ~30 minutes prior to irradiation. A flow sensor (Omron Electronics Inc – EMC Div, D6F-P001A1) was used to ensure that the helium, regulated by an electronic valve (SMC, ITV1010-21N1BS4), was properly flowing during sparging and when pushing the water though the manifold system to/from the target cell. A pressure sensor (Honeywell Sensing and Control, SSCSANN001BGAA5) was used to monitor the irradiation cell for gases produced during beam collection. Second, a custom irradiation cell was built, into which water was transferred from the holding reservoir, for stopping and collection of the beam particles. The target cell had a thin entrance window (8 μm Kapton) and was constructed from PTFE (polytetrafluoroethylene). The

internal volume of the irradiation cell took the shape of a truncated cone for containing any divergence of the stopping secondary beam, see **Figure 3-1**. Third, a movable carousel of commercially available PTFE bottles was included for the transfer and temporary storage of the irradiated water samples. After irradiation, the water was transferred to a collection bottle via a tube supported on a pneumatic linear actuator (SMC, CDJ2KB16-45-B) that extended into the bottle to capture any spraying during liquid transfer operations. The actuator was retracted before movement of the carousel to the next collection bottle. Two magnetic sensors (Cherry, MP201802) on the linear actuator were used to confirm that the actuator rod was in the up position before rotating the carousel or that it was the down position and the tubing was in the bottle, ready for dispensing water from the target cell. There were ten PTFE collection/storage bottles (Cole-Palmer, 015.150.2) in the 35.6 cm diameter carousel for post-irradiation retrieval of the water. A stepper motor (Lin Engineering, 85BYGH450A-08), controlled by a stepper motor drive (Lin Engineering, CW250), was used to rotate the carousel and position the collection bottles as necessary. Four photo sensors (Sharp, GP1A57HRJ00F) viewed notches cut into the carousel plate to identify each of the ten bottle positions. A fifth photo sensor was used to center each bottle prior to reading the position identification and a capacitive sensor (Carlo Gavazzi, CD50CNF06NO) was used to determine if the collection bottle contained water thus ensuring that a new sample would not be delivered to a filled bottle. All components of the system that could come into contact with water were metal-free (or Teflon-coated) to reduce metal contamination and the loss of aqueous radioisotopes by plating onto metal surfaces. The end station incorporated metal-free, air-operated, normally closed, two-way valves (SMC, LVQ20-Z07N) controlled by low-voltage (5V) solenoids (SMC, SY3A00-5U1, manifold: SS5Y3-10F2-12BS-N7D0). FEP (Fluoroethylpropylene) fittings (SMC, LQ3 Series) and Teflon tubing (SMC,

TIHA07N-33) were used if they came in contact with water. A Measurement Computing I/O device (Measurement Computing, USB-1208LS, USB-SSR24, SSR-ODC-05) was used to communicate with the sensors and to control the stepper motor and electronic valve regulators (for both the helium used for sparging the water and the air for operating the metal-free valves. The entire end station was remotely operated using LabVIEW software (National Instruments, 776670-35).

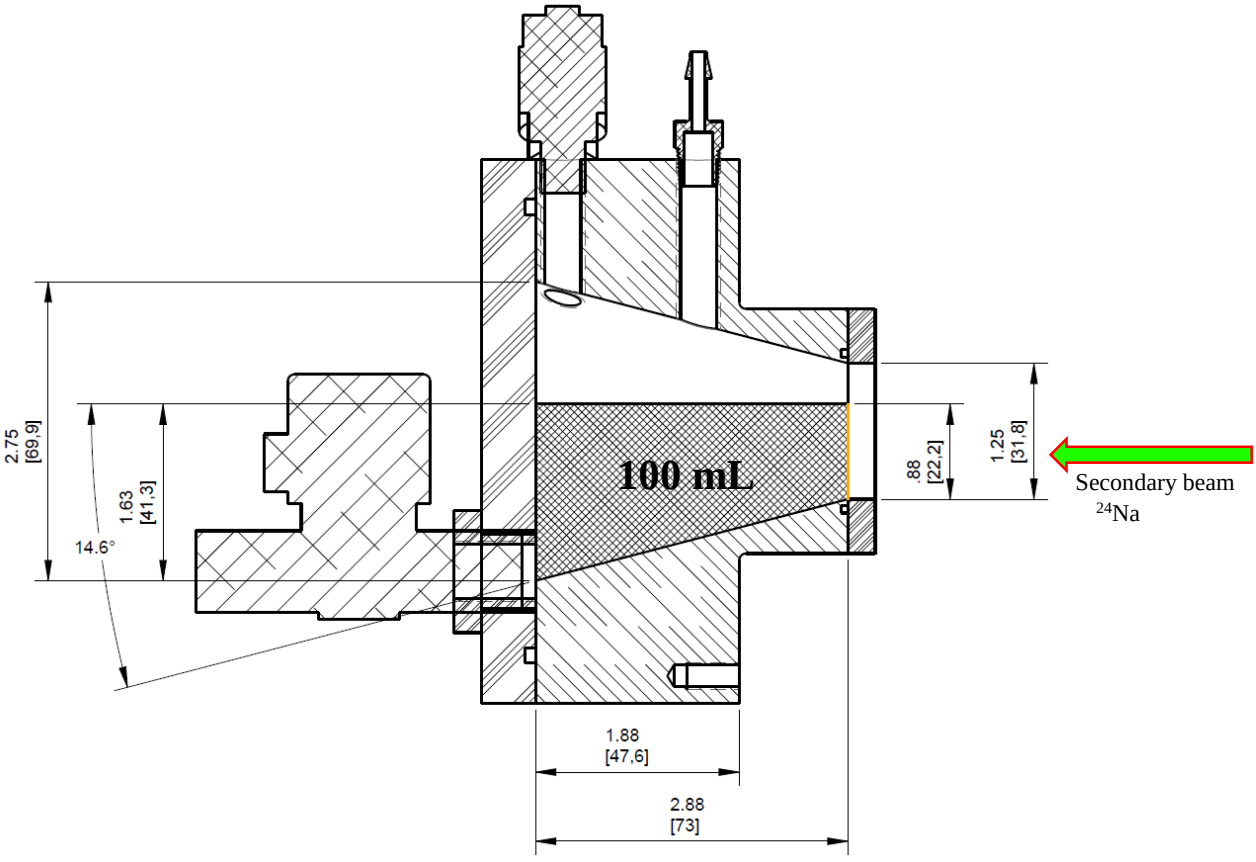

Figure 3-1. Schematic design of the PTFE water target cell containing 100 mL of water. Dimensions are in inches [mm], angles in degrees.

A concern during operation was the possible over-pressurization of the irradiation cell due to localized heat production and radiolysis of water, producing radioactive and other gases. This concern was addressed by programming the LabVIEW system to open the helium exit valve on the top of the cell and venting the cell into a 152 m (500 ft) length of 6.35 mm (¼ inch) tubing if the target cell pressure exceeded 0.14 atm above gauge (2 psig) as determined by the pressure sensor installed to monitor the irradiation cell. This length of tubing was calculated to exceed the distance traversed by the diffusion of $^{11}CO_2$ at atmospheric pressure through the tube within 10 half-lives of ^{11}C.

In addition to the safety checks built into the LabVIEW control program, two webcams and LED lighting strips were added to allow visual monitoring of the end-station. Remote desktop connections were used to control the LabVIEW programs running in two laptop computers physically wired to the end-station electronics in the vault. A radiation monitoring system was also incorporated into the end-station to qualitatively measure the presence of activity in the proper locations. The radiation detector system consisted of eight CsF detectors each with a photomultiplier tube, a fast discriminator and a scaler. These detectors were placed at different locations within and outside the target assembly to monitor the flow of radioactive solutions into different collection vessels during the experiments to ensure the radioactivity was moving only to the desired location. A schematic diagram of end station is shown in **Figure 3-2**, and photos of the completed system are shown in **Figure 3-3**. The end-station was fabricated at Hope College and then installed in the S1 vault at the NSCL.

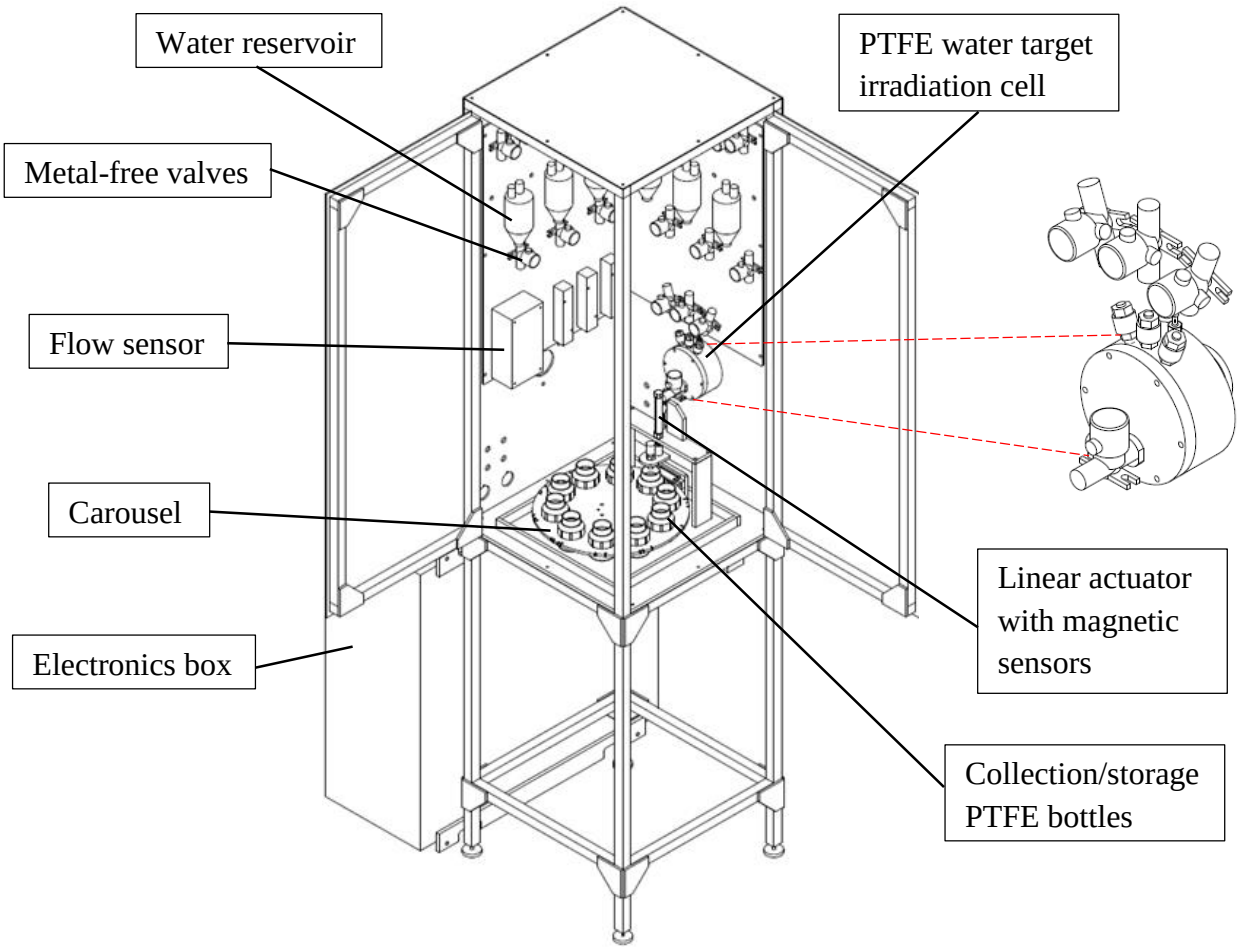

Figure 3-2. Schematic diagram of the complete end-station. The doors to the end-station are shown in the open position, and the reservoirs at the top and the carousel at the bottom are apparent. The electronics control box is in the background at floor level.

Figure 3-3. Photographs of the water cell collection end-station. (Left) Installation in the vault where the beam enters from the left, **A** is the side of the isolation box that holds the target cell and associated plumbing (see Fig. 3-2). **B** houses the electronic controls and **C** is a laptop that controls the system. (Center) Side view of the target end-station that shows **D**: the water reservoir system, **E**: the PTFE target cell and **F**: the rotating collection bottle system, (Right) Close up of the end of the beam line and **G**: water cell window, **H**: a removable scintillator in front of the target assembly, **I**: beam collimator.

Simulation Results

As part of the planning process, modeling of the radioisotopes delivered to the water cell by the A1900 and their decay products was carried out using the LISE++ code[5] with the EPAX3 cross sections[6] and the Nucleonica© decay engine,[7] respectively. The information from these programs was only used to estimate the amount of radioactivity in the solutions collected and to identify potential contaminants in the secondary beam prior to the measurements. These first tests of the production and collection focused on ^{24}Na because of its convenient 14.997-hour half-life and its characteristic high-energy gamma-ray emission which allowed identification and quantization by offline gamma-ray spectroscopy. It was decided to produce the ^{24}Na from a ^{40}Ar primary beam based on the high availability of the argon beam and the relatively efficient delivery of ^{24}Na by the separator. Calculations using the LISE++ code indicated that significant

amounts of other radioisotopes would not be present in the analyzed ^{24}Na beam, therefore neither extraction nor separation was necessary post irradiation, allowing the focus to remain on determining the overall collection efficiency.

The LISE++ calculation (version 9.4.15) for an ^{40}Ar primary beam (140 MeV/u) at the maximum intensity available at the NSCL of 75 pnA,[8] using an 1151 mg/cm^2 thick beryllium production target and a 289 mg/cm^2 aluminum wedge with a 1 percent momentum acceptance at the Image-2 position[9] predicted a 70% pure beam at the collection station that would result in ~1.7 ×10^{10} ^{24}Na particles at (~88 MeV/u at the A1900 focal plane) 85 MeV/u after the water target window after the minimum collection time of one hour (see below). **Table 3-1** provides a list of the isotopes in the separated secondary beam that have a production rate greater than 1 s^{-1} (note that the predicted production rate of ^{24}Na under these conditions is 4.62×10^6 s^{-1}). The next most abundant isotope was stable ^{25}Mg at 28% of the total rate while the remaining 2% consisted of a few nuclides that do not contribute to the radioactivity levels after a five minute cooling period. If all the kinetic energy of the incident secondary beam was absorbed in the water there would be a negligible temperature increase of <0.05 K in the 100 mL of water in the irradiation cell. This value was calculated for the total collection time, the production rate and kinetic energy of each nuclide. **Table 3-1** shows that the only significant activity delivered to the water was ^{24}Na,

Table 3-1. Predicted production rates of isotopes greater than 1s^{-1}

Nuclide	Half-life	Focal Plane Rate (s^{-1})	Activity (Bq, 5m EOB)
^{26}Al	717 ky	8.97E+01	~0
^{25}Mg	Stable	1.84E+06	0
^{24}Na	14.997 h	4.62E+06	2.1E+05
^{23}Ne	37.2 s	1.37E+05	~0
^{21}F	4.16s	5.63E+01	0
^{20}O	13.51 s	4.30E +03	~0
^{17}C	193 ms	2.43E+01	0
Total	**6.60E+06**		

however, the fast beam will react with the hydrogen and oxygen nuclei in the water to produce some ^{18}F, ^{15}O and ^{11}C. This production is more difficult to model so the samples were held for about 8-24 hours prior to shipping to allow these intermediate half-life isotopes to decay.

^{24}Na Beam Collection

The water target system was used to collect four separate samples during a 24 hour period. As in the simulations described above, the $^{40}Ar^{18+}$ primary beam at 140 MeV/u was fragmented in a beryllium target to produce ^{24}Na. The ^{24}Na ions were separated in the A1900 projectile fragment separator[9] and arrived at the focal plane with an energy of ~88 MeV/u. The primary beam intensity was attenuated by a factor of ~10 for the first two sample collections, then delivered at the full intensity of ~75 pnA for two additional sample collections. The exact experimental parameters are listed in **Table 3-2**. The primary beam was incident on an 1151 mg/cm^2 beryllium target, the A1900 separator was set for maximum production of the ^{24}Na fragment with momentum acceptance slits adjusted to a 1% momentum full acceptance using a 289 mg/cm^2 aluminum wedge in the center of the A1900 separator, and the focal plane (FP) mass-selection aperture was 10 mm. The beam intensity and purity were measured using the common delta-E/Time-of-Flight technique with the standard A1900 focal plane silicon-PIN diode and cyclotron RF signal prior to delivery of the beam to the experimental end station. The ^{24}Na production rate at the focal plane was ~1.04(0.02)x10^5 pps ^{24}Na per pnA of primary beam and the exact composition of the secondary beam during the sample collections, i.e., 72(2)% ^{24}Na was in good agreement with the simulation. In addition, the "FP plastic scintillator" made of 150 μm BC-400 (CRAD06) was positioned in the path of the beam for beam normalization

(calibration) runs and removed when collecting the ^{24}Na secondary beam in the water. The scintillator was used to directly measure the beam intensities at rates below ~10^6 pps. During the sample collection runs the beam exited the vacuum system through a 75 μm zirconium exit window, followed by a 89 mm air gap, entered the water cell through a 8 μm Kapton window, and had a calculated range of ~11 mm in the distilled and degassed H_2O (73 mm thick). The primary and secondary beam intensities were recorded by various intercepting and

Table 3-2. A1900 fragment separator and beam line settings for ^{24}Na production.

Block	**Description**	**Value**	
Primary Beam Target	Beryllium	1151	mg/cm^2
D1 Bρ	Dipole Magnet	3.16650	Tm
D2 Bρ	Dipole Magnet	3.16650	Tm
I2 Slits	1% Momentum Acceptance (dp/p)	60	mm
I2 Wedge	Aluminum	289	mg/cm^2
D3 Bρ	Dipole Magnet	3.01230	Tm
D4 Bρ	Dipole Magnet	3.01230	Tm
CRAD06	BC-400 Scintillator (removable)	150	μm
D5 Bρ	Dipole Steering Magnet	3.01230	Tm
D6 Bρ	Dipole Steering Magnet	3.01230	Tm
Exit Window	Zirconium	75	μm
Air Gap	Air	88.9	mm
Collimator	Aluminum, 3.175 cm diameter	6.35	mm
CRAD02	BC-400 Scintillator (removable)	150	μm
Water Target Window	Kapton	8	μm
Water Target	Liquid water	73	mm

non-intercepting detectors during different phases of the experiment (**Figure 3-4**). A 6.35mm thick aluminum collimator was placed in front of the exit window scintillator (at the end-station) to ensure only the particles that entered the water cell were counted.

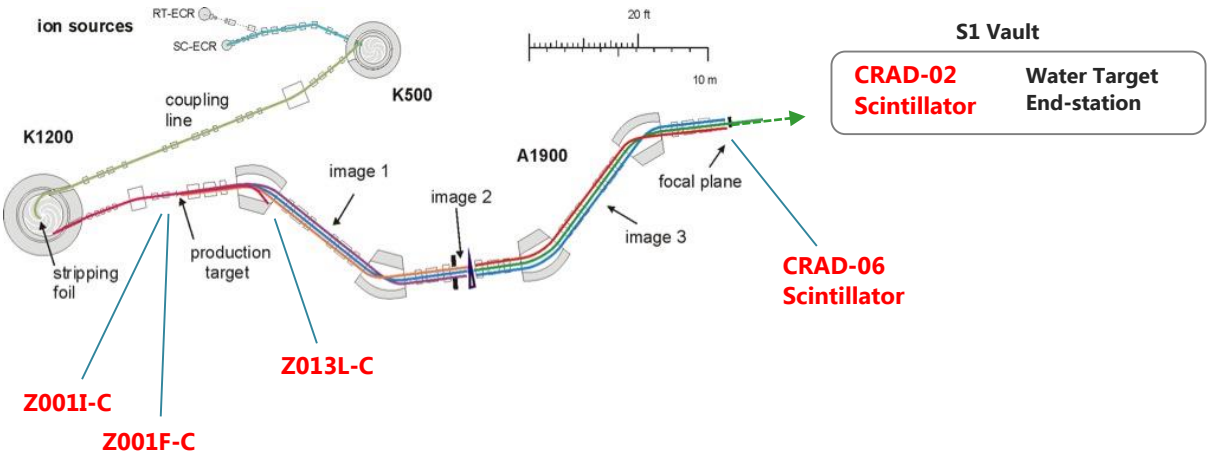

Figure 3-4. Schematic diagram of NSCL indicating approximate locations of intercepting and non-intercepting detectors (Z001I-C, Z001F-C, Z013L-C, CRAD-06 and CRAD-02).

The FP scintillator could only be used to monitor the secondary beam at lower intensities (with saturation occurring around 10^6 pps). In order to collect the maximum amount of ^{24}Na and not be limited by the scintillator, a non-intercepting beam monitor was necessary that: 1) could measure high-intensity primary beam directly or indirectly, 2) could continuously monitor the beam, and 3) had a linear relationship to the counting rates observed in the scintillators at lower beam intensities. The secondary beam rate was indirectly determined using two different methods. In the first method the ^{24}Na rate at the end station was calculated from the FP scintillator by constructing a calibration curve obtained from measurements of the beam at various intensities using a series of Faraday cups that intercept the primary beam, the Z001I-C and Z013L-C non-intercepting primary beam monitors, and the FP scintillator in the secondary beam path. The Z001I-C is a non-intercepting beam monitor just before the A1900 production

target that provides a signal proportional to the primary beam intensity. The Z013L-C non-intercepting beam monitor in the first dipole of the A1900 also provides a signal proportional to the primary beam intensity. During the sample collection runs, when the scintillator was removed from the beam, data from the Z001I-C and Z013L-C non-intercepting beam monitors were used to determine the secondary beam intensity. The calibration curve obtained for the Z013L-C beam monitor is shown in **Figure 3-5**. The second method relied on using the ^{24}Na production rate measured at the A1900 focal plane prior to the collection runs, as indicated above, combined with an estimate of the primary beam intensity. The data from non-intercepting Z001I-C beam monitor was used to infer the primary beam current during the run using a calibration established with a Faraday cup that intercepted the primary beam at the A1900 target position (Z001F-C).

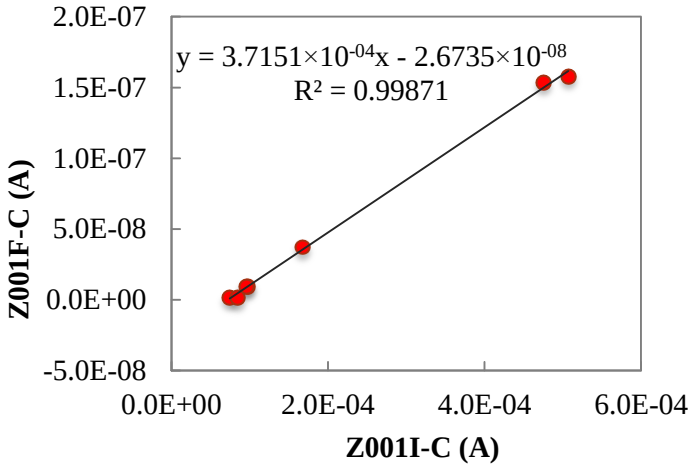

Figure 3-5. Calibration curve for the non-intercepting primary beam monitor Z001I-C versus the intercepting Z00lF-C Faraday cup signal intensity.

After the isotope collections were complete, the samples were transported approximately one day later to Hope College for preparation and analysis. The 100 mL samples of water were reduced to ~15 mL via gentle evaporation and quantitatively transferred to an x-ray fluorescence (XRF) cup with minimal air gaps, which was then capped with an 8 μm Kapton window for offline gamma spectrometry. Each sample was measured repeatedly for at least 20 minutes over a 5-day period in a low-background radiometric detection facility at Hope College. The three low-background systems at this facility consist of three Ortec 20% high-purity germanium detectors with resolutions of 1.2, 2.5, and 4.1 keV at 1369 keV, shielded by layers of aluminum (0.5”), copper (0.5”) and lead (4”). Gamma ray spectra were recorded and peak integrations and background subtractions were performed using a linear function background fit to each peak for the 1369 keV gamma ray of ^{24}Na. Besides the 511 keV peak, there were no other radionuclides greater than 0.5% of the 1369 keV peak detected in the samples. These detectors were calibrated with known sources for energy calibration and absolute counting efficiency. The number of ions implanted in the water were then calculated and used to determine the collection efficiency.

Experimental Results

The primary beam intensity was calculated using the Z001F-C vs Z001I-C calibration curve (**Figure 3-5**) and the integrated data for Z001I-C obtained during each run. As the relationship between Z001F-C and ^{24}Na was $1.04(0.02)\times10^{5}$ ^{24}Na/pnA (where pnA is the intensity of the ^{40}Ar primary beam measured by the Z001F-C detector), obtained from the beam analysis conducted by the A1900 group, the ^{24}Na rate at the focal plane could be calculated. **Table 3-3** contains a summary of the numerical results obtained for the sample collection runs. The gamma-ray spectroscopy of the samples yielded results having a precision of ~1%. This

value is the relative experimental precision of multiple measurements of the same aliquot. The calculated extraction efficiencies, taken as the ratio of the number of particles at the A1900 focal plane and the number of particles observed in the water was 20 ± 1%. This modest collection efficiency is believed to be due, in part, to beam losses between the focal plane and the end-station. The estimated losses during the handling of the aqueous ^{24}Na solutions were less than 10%. Thus, we observed approximately 70% loss in beam transmission between the focal plane and the target. The typical transmission from the A1900 to end-stations at the NSCL is approximately 80 to 90% and thus the observed losses are surprisingly large. Since the goal of the experiment was not to obtain maximum yield of the ^{24}Na particles, but rather to demonstrate isotope collection and subsequent harvesting, the beam line transmission was not optimized.

Table 3-3. Summary of the ^{24}Na collection efficiencies.

^{24}Na particles				
	Run 1	**Run 2**	**Run 3**	**Run 4**
γ-spectroscopy	5.84E+08 ± 4E+06	7.19E+08 ± 5E+06	1.90E+10 ± 1E+08	1.85E+10 ± 1E+08
Focal Plane Particles Calculated by FC (Z001I-C)	2.83E+09 ± 9E+07	3.8E+09 ± 1E+08	9.5E+10 ± 3E+09	8.8E+10 ± 3E+09
Extraction efficiency	0.21 ± 0.01	0.19 ± 0.01	0.20 ± 0.01	0.21 ± 0.01
Focal Plane Particles Calculated by scintillator (CRAD06)	2.8E+09 ± 1E+08	3.6E+09 ± 1E+08	9.0E+10 ± 4E+09	8.4E+10 ± 3E+09
Extraction efficiency	0.21 ± 0.01	0.20 ± 0.01	0.21 ± 0.01	0.22± 0.01

Conclusions

A water filled collection system was constructed and has been successfully used to stop a beam of ~85 MeV/u ^{24}Na produced at the NSCL. The end station operated flawlessly during irradiation and multiple samples were collected remotely at particle intensities of ~2x10^6 pps.

The samples were transported and characterized off-line in a remote location by gamma spectroscopy using HPGe detectors. Two independent methods of calculating the secondary beam intensity agreed within ~1% providing confidence that the total beam intensity was well-known. There were no observed release of radiolytic gases from the system nor any spills or loss of radioactive liquids. This work compromises the first step in providing the viability of isotope harvesting from heavy-ion beam facilities using a water activity accumulation cell.

References

1 Morrissey, D. Status of the FRIB project with a new fragment separator. *Journal of Physics: Conference Series* **267**, 012001, doi:10.1088/1742-6596/267/1/012001 (2011).

2 W.E. Prout, E. R. R., H.J. Groh. Ion exchange absorbtion of cesium by potassium hexacyanocobalt (II) ferrate (II). *Journal of Inorganic and Nuclear Chemistry* **27**, 473-479 (1965).

3 M. Hausmann, A. A., A. Amthor, M. Avilov, L. Bandura, R. Bennett, G. Bollen, T. Burgess, S. Chouhan, V. Graves. Design of the Advanced Rare Isotope Separator ARIS at FRIB. *Nuclear Instruments and Methods in Physics Research Section B: Beam Interactions with Materials and Atoms* **317**, 349-353, doi: 10.1016/j.nimb.2013.06.042 (2013).

4 Morrissey, D. J., Nolen, J. A. & Tiedje, J. M. Radiotracers from Heavy-Ion Fragmentation. *Nucl Instrum Meth B* **10-1**, 963-966, doi:Doi 10.1016/0168-583x(85)90149-1 (1985).

5 Tarasov, O. B. & Bazin, D. LISE plus plus : Radioactive beam production with in-flight separators. *Nucl Instrum Meth B* **266**, 4657-4664, doi:DOI 10.1016/j.nimb.2008.05.110 (2008).

6 Summerer, K. Improved empirical parametrization of fragmentation cross sections. *Physical Review C* **86**, doi:Artn 014601 Doi 10.1103/Physrevc.86.014601 (2012).

7 Nucleonica Decay Engine. http://www.nucleonica.net/RadioactiveDecay.aspx

8 Stolz, A. *et al.* New developments and capabilities at the coupled cyclotron facility at Michigan State University. *Proceedings of the Cyclotrons 2013 Conference, Vancouver* (2013).

9 Morrissey, D. J., Sherrill, B. M., Steiner, M., Stolz, A. & Wiedenhoever, I. Commissioning the A1900 projectile fragment separator. *Nucl Instrum Meth B* **204**, 90-96, doi:Doi 10.1016/S0168-583x(02)01895-5 (2003).

Chapter 4

Feasibility of Isotope Harvesting at a Projectile Fragmentation Facility: ^{67}Cu

[This work has been published previously as Tara Mastren, Aranh Pen, Graham F. Peaslee, Nick Wozniak, Shaun Loveless, Scott Essenmacher, Lee G. Sobotka, David J. Morrissey, and Suzanne E. Lapi, *Scientific Reports*. **2014**]

Introduction

With the successful construction and validation of the end station discussed in chapter 2, we are now ready to move onto one of the isotopes of interest listed in **Table 1-2**. The isotope we chose to start with, which can be used in medicine as a therapeutic isotope, is ^{67}Cu.[2-4] Its relatively long 2.58 day half-life is ideal for labeling antibodies that typically have several-day biological half-lives and its maximum β^- energy of 562 keV makes it a good candidate for radiotherapy.

Obtaining therapeutic doses that are typically on the order of hundreds of mCi/patient[5] has proved to be quite difficult due to inconsistent production and no reliable supply.[5-8] ^{67}Cu can be made via several nuclear reactions: ^{68}Zn(p,2p)^{67}Cu, ^{70}Zn(p,α)^{67}Cu, ^{67}Zn(n,p)^{67}Cu, and ^{68}Zn(γ,p)^{67}Cu; however each reaction has practical drawbacks. For example, ^{68}Zn(p,2p)^{67}Cu has a small but broad (in energy) cross section (**Figure 4-1**) and in order to efficiently produce the

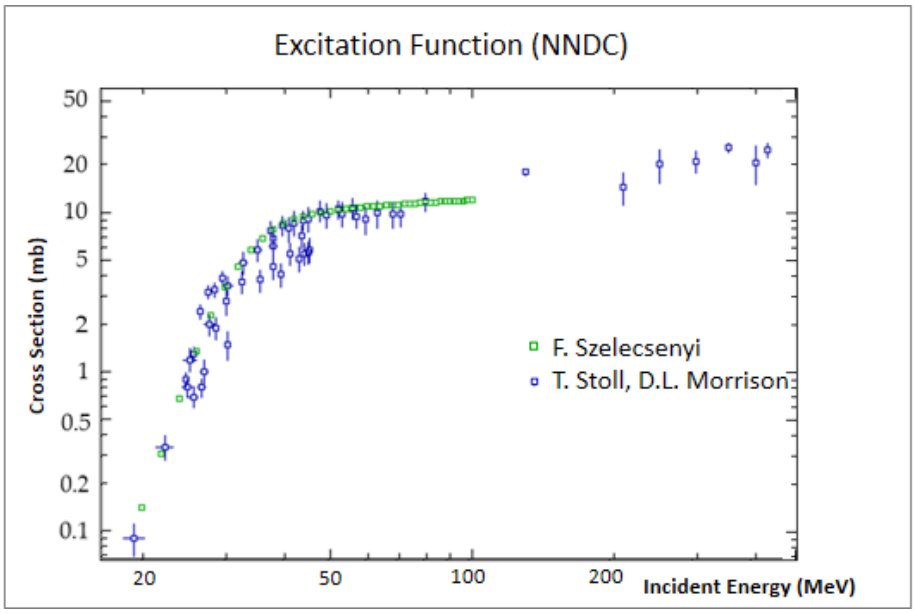

Figure 4-1. ^{68}Zn(p,2p)^{67}Cu excitation function showing low but broad (in energy) cross section.[1]

large quantities needed for therapeutic doses thick targets and high-energy proton accelerators, such as those at Brookhaven[9,10] or Los Alamos National Laboratories,[11] need to be employed. These facilities have missions that make routine production of ^{67}Cu problematic.[5] Studies at several facilities of the ^{70}Zn(p,α)^{67}Cu reaction have obtained varying yields and the production of the large quantities needed for therapeutic studies are challenging with this method.[12-14] Production via the ^{67}Zn(n,p)^{67}Cu and ^{68}Zn(γ,p)^{67}Cu reactions have undesirable side reactions and concerns about waste products create challenges for their large scale use.[5] It is estimated that FRIB will be able to produce a saturated activity of ^{67}Cu as high as ~2 Ci depending on the primary beam[15] so that harvesting of ^{67}Cu could provide a consistent supply of this isotope.

Figure 4-2 shows the decay schemes for isotopes at the bottom of the A=67 mass parabola. It is important to note that good separation from gallium must be achieved due to the similar half-life, emitted gamma rays, and likely significant production rate of ^{67}Ga.[15] Additionally the production of ^{67}Ni ($t_{1/2}$ = 50s) will contribute to the overall ^{67}Cu production rate (as the former decays to the latter) resulting a net production of ^{67}Cu greater than its primary production. Reported here are the results of these studies and the observation of relatively high chemical extraction efficiency.

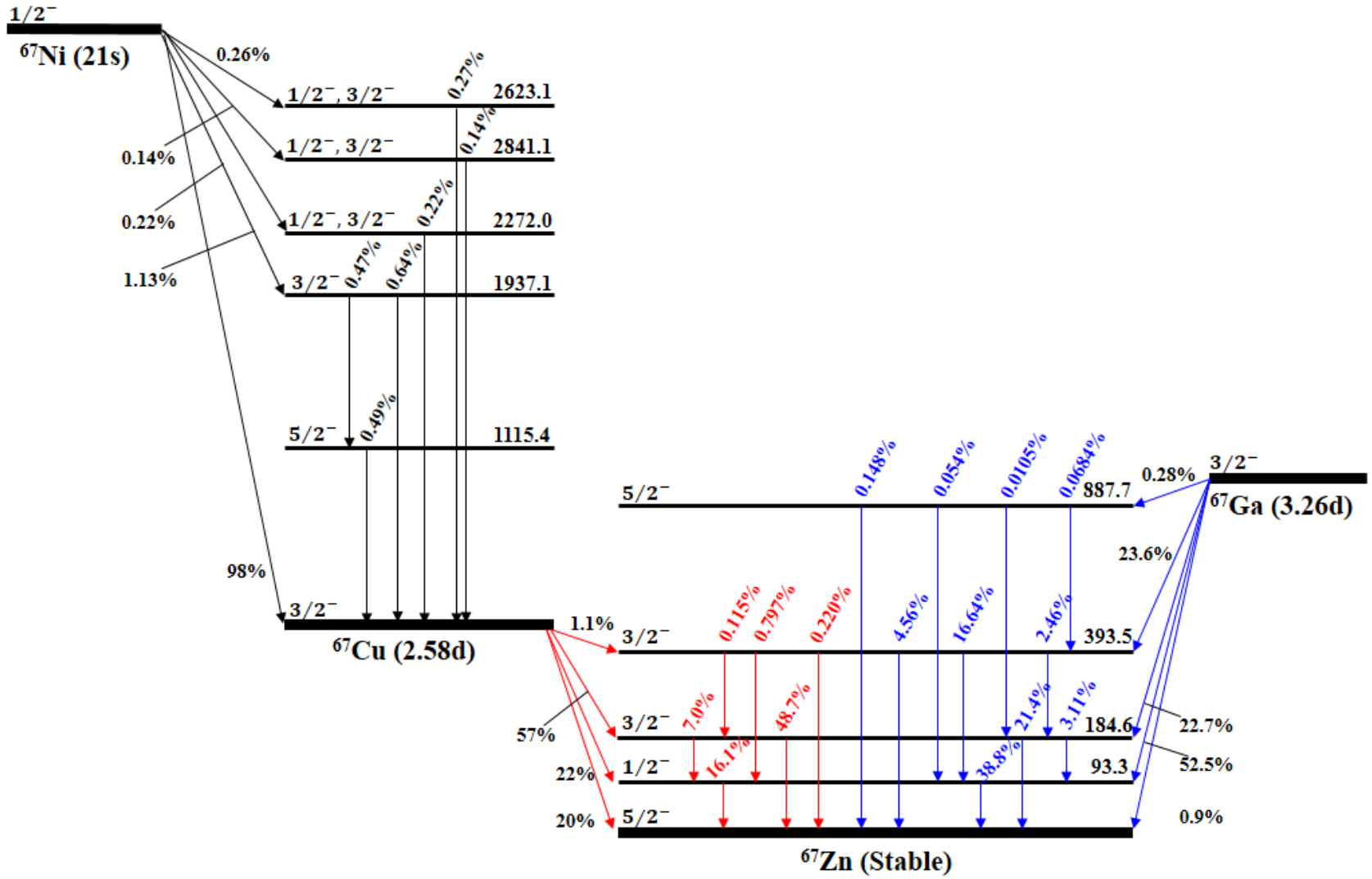

Figure 4-2. Decay schemes for isotopes at the bottom of the A=67 mass parabola.

Methods

Beam Collection and Calibration

A 25 particle-nA 130 MeV/u ^{76}Ge beam was fragmented using a 510.8 mg/cm^2 thick beryllium production target in the A1900 projectile-fragment separator.[16] After fragmentation of the primary beam, ^{67}Cu was selected using the A1900 with a 236.7 mg/cm^2 aluminum wedge in the center, the focal plane (FP) mass-selection aperture set to 10 mm, and the momentum acceptance slits open to 2% (full momentum acceptance). **Table 4-1** lists the exact experimental parameters used in the separator and beam line. The beam intensity and purity were measured using the standard delta-E/Time-of-Flight technique with a silicon-PIN diode in the A1900 focal plane and cyclotron RF signal prior to delivery of the beam to the experimental end station.[16] The secondary beam was collected for four hours in the liquid water target system before being transferred to a collection vessel. Four additional collections, each lasting four hours, were made before shipping samples to Washington University and Hope College for chemical separation and analysis.

Table 4-1. Experimental parameters for the ^{67}Cu secondary beam at the NSCL.

Block	Description	Value
Primary Beam Target	Beryllium	510.797 mg/cm^2
D1 Bρ	Dipole magnet	3.2822 Tm
I1 Slits	Momentum acceptance (dρ/ρ)	2.03%
D2 Bρ	Dipole magnet	3.2822 Tm
I2 Slits	Momentum acceptance (dρ/ρ)	2%
I2 Wedge	Aluminum	236.685 mg/cm^2
D3 Bρ	Dipole magnet	2.9147 Tm
D4 Bρ	Dipole magnet	2.9147 Tm
CRAD06	BC-400 scintillator (removable)	155 µm
D5 Bρ	Dipole steering magnet	2.9027 Tm
D6 Bρ	Dipole steering magnet	2.9027 Tm
Exit Window	Zirconium	75 µm
Air Gap	Air	89 mm
Water Target Window	Kapton	8 µm
Water Target	H_2O	73 mm

At the NSCL there are several non-intercepting beam monitors, Faraday cups, and a BC-400 plastic scintillator that can be used to measure beam current. The Faraday cups and scintillator can be used to determine particles per second, however, only the non-intercepting beam monitors can be used to measure the beam at full intensity during the sample collections. Calibration curves had to be established comparing the non-intercepting beam monitors with the Faraday cups and scintillators in order to calculate particles per second delivered to the water target station. Two calibrations of the beam monitors were performed during which the beam was attenuated by 10^{-1} to 10^{-3} times the full beam intensity. The currents from Faraday-cups, non-intercepting beam monitors, and the count rates from the scintillators were recorded and used to construct linear calibration curves. An aliquot from each of the five water samples was analyzed with an HPGe detector to determine the amount of ^{67}Cu present in the sample and decay corrected to the end-of-bombardment in order to determine the beam transport efficiency.

Separations Involving Chelating Disk

All separations using the high-performance extraction disk (3M Empore, MN) were carried out with 100mL 1.25M ammonium acetate (trace metals grade) and pH adjusted to 5 by adding acetic acid (trace metals grade). The high-performance extraction disk is functionalized with iminodiacetic acid groups and at pH 5 the carboxylate groups are negatively charged and will bind to metal cations. The solution was then drawn through a 25mm diameter extraction disk in a glass microanalysis vacuum filter holder (Millipore, MA) with vacuum, after the disk was pretreated by rinsing with 20mL milli-Q water, 20mL 3M nitric acid (trace metals grade), 2-50mL milli-Q water, 50mL 0.1M ammonium acetate, followed by two additional rinses of 25mL milli-Q water, allowing the disk to dry between each rinse. When passing the 100mL sample

through the extraction disk, a new vacuum flask was used to save the eluent so that it could be analyzed by HPGe detector for radioactivity that did not bind to the extraction disk.

Germanium Separation Validation

Several concentrations of aqueous germanium ranging from 0.04-0.5 ppm in 1.25 M ammonium acetate were passed through the extraction disk using the method described above. The chelation disk was analyzed using particle-induced x-ray emission (PIXE) by irradiating the chelation disk with 3.4 MeV protons for five minutes at beam intensities between 2.25-2.80 nA. A Si(Li) detector was used to measure the resulting x-rays. The characteristic K_α x-rays for germanium were analyzed to determine the amount of germanium bound to the chelation disk.

^{68}Ga and ^{64}Cu Separation Validation

200µCi of ^{68}Ga obtained from a ^{68}Ge/^{68}Ga generator and 200µCi of ^{64}Cu produced at Washington University in St. Louis were added to 100mL of 1.25M ammonium acetate and passed through the extraction disk using the method given above. The extraction disk was surveyed by HPGe for ^{68}Ga and ^{64}Cu using the characteristic gamma rays, 1077.3keV (3.22%) for ^{68}Ga and 1345.8keV (0.475%) for ^{64}Cu. The extraction disk was returned to the filter holder and 10mL of 6M hydrochloric acid (trace metals grade) was added to remove ^{64}Cu from the extraction disk. Both the extraction disk and the filtrate were analyzed by HPGe to measure amounts of ^{68}Ga and ^{64}Cu present in each.

Copper, Nickel, and Zinc Separation Validation

Aqueous solutions containing 100µg of copper, nickel and zinc (1000mg/L AAS Standards, Sigma Aldrich, USA) were added to 100mL 0.1M ammonium acetate solution at pH 5.5 and passed through the chelation disk as described above. 10mL of 6M hydrochloric acid (trace metals grade) was then added to remove the nickel, copper, and zinc that were bound to the chelation disk. This solution was then passed through an anion-exchange column containing 2.5g AG1-8X resin (Bio-Rad, USA) and washed with an additional 10mL of 6M HCl to remove the nickel followed by 10mL of 0.5M HCl to remove the copper. Each 10mL fraction was brought to dryness by evaporation through overnight heating at 80ºC and reconstituted in 1mL Ultratrace water (Sigma Aldrich, USA) and analyzed by an HPLC trace metal ion chromatography method.[17]

^{67}Cu Separation

First, each 100mL sample was adjusted to 1.25M solution of NH_4OAc by adding 9.6g trace metals grade ammonium acetate and pH adjusted to 5 by adding trace metals grade acetic acid. The ~100mL solution was then passed through the chelation disk as described above. The filter holder was transferred to a clean vacuum flask and 10mL of 6M trace metal grade hydrochloric acid was passed through to remove the ^{67}Cu along with the nickel and zinc contaminants. The 6M HCl elution was then transferred to an anion-exchange column with AG1-X8 resin, the 10mL eluate was collected and then an additional 10mL of 6M hydrochloric acid was passed through the column and collected. Finally 10mL 0.5M hydrochloric acid was added to the resin and 1mL fractions of the eluate were collected. All eluates were analyzed for radiochemical purity by observing the characteristic gamma rays in an HPGe detector.

^{67}Cu-NOTA-Trastuzumab Labelling

A 10mg/mL stock of NOTA-NCS was made by dissolving 3.66mg NOTA-NCS (Macrocyclics, USA) in 366uL Dimethyl sulfoxide. 50uL of 21ug/uL Trastuzumab (Genentech, USA) was added to 4uL NOTA-NCS stock solution and 96uL 0.1M sodium carbonate pH 9.0 and incubated for 1hr at 37C on a shaking incubator. A Zeba spin desalting column (40kDa cutoff, 0.5mL) was used to buffer exchange the conjugate into 0.1M ammonium acetate buffer at pH 5.5. Concentration of the NOTA-Bz-NCS-Trastuzumab was measured using the bicinchoninic acid (BCA) assay.

The two 1mL 0.5M hydrochloric acid samples with the largest amounts of ^{67}Cu were brought to dryness and reconstituted using 50uL of 0.1M ammonium acetate at pH 5.5. 5uL was transferred to a new tube and 5uL 50mmol EDTA was added. The remaining 45uL was added to a microfuge tube along with 2uL NOTA-Bz-NCS-Trastuzumab and brought to 50uL by adding 0.1M ammonium acetate at pH5.5. Tubes were placed in a shaking incubator at 37ºC for twenty minutes. This method was adapted from one previously reported by Ferreira et al.[18] The solution containing ^{67}Cu-NOTA-Bz-NCS-Trastuzumab was then challenged with 1µL 50mmol EDTA. 1uL from each tube was spotted on ITLC paper (Agilent,) at 2cm from the bottom of the paper and placed in 1cm running buffer (1:1 10% ammonium acetate and methanol) and ran until the eluent was 5cm past the starting point (7cm total). The paper was then analyzed by radio TLC scanner.

^{7}Be Cross Section Analysis

After allowing the short-lived isotopes to decay, the 100mL eluent from the chelation disk was analyzed for presence of ^{7}Be using HPGe analysis of the 477 keV gamma ray (10.44%)

present in spectra collected for 12 and 24 hours. The counts were decay corrected back to the end of each collection run.

Results

Beam Calibration and Collection

A 76 MeV/A ^{67}Cu secondary beam of 77% purity was selected from a fragmented ^{76}Ge primary beam using the A1900 fragment separator[16] and delivered to the S1 vault where the water target station was set up to collect the incoming beam. In order to quantify the amount of ^{67}Cu delivered to the target, calibration curves were developed to convert the signals from the non-intercepting beam monitors that were continuously operating during beam collections and the fully-intercepting Faraday-cups or scintillators that could not be in place during the sample collections.

Two separate calibration methods were used to determine the number of beam particles delivered to the water target station during two calibration runs performed approximately 12 hours apart. One calibration run was *prior* to most of the collections and the other was *post* most of the collections. In the first method a calibration curve was established to normalize the proportional data from the non-intercepting beam monitors (Monitors A and B in **Figure 4-3**) to the direct measurements of the primary beam current (in nA) with a Faraday cup. The proportional rates from A and B were integrated over the course of each run and then multiplied by the conversion factor of $4.1 \pm 0.2 \times 10^5$ ^{67}Cu ions per second per particle-nA of primary beam (determined by the A1900 operations group) to give the rate of ^{67}Cu atoms delivered. The second method established calibration curves of two non-intercepting beam monitors A and B with the focal-plane plastic scintillator that was used to measure the rate of secondary beam

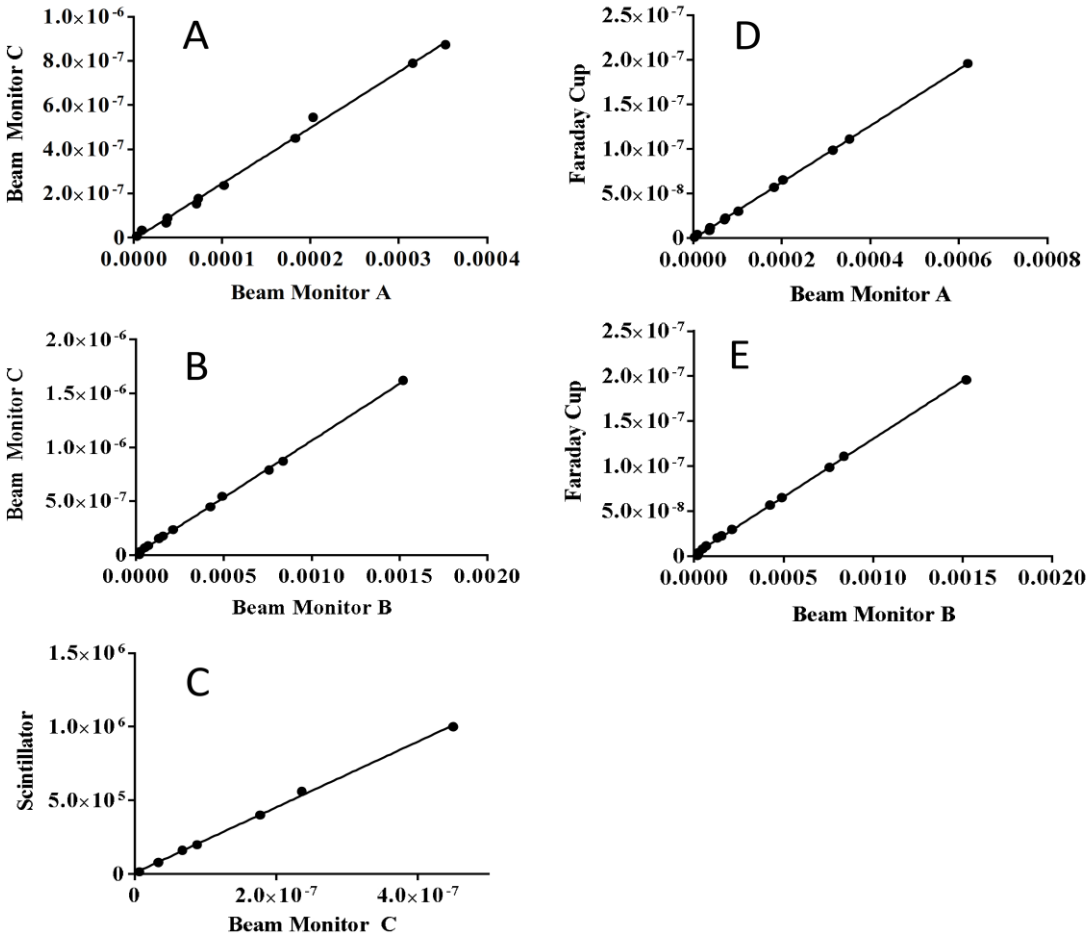

Figure 4-3: The results of the calibration performed with Method 2 are shown in panels: (A) Beam Monitor A vs Beam Monitor C, (B) Beam Monitor B vs Beam Monitor C, and (C) Beam Monitor C vs Scintillator. The results of the calibration performed with Method 1 are shown in panels: (D) Beam Monitor A vs Faraday-Cup and (E) Beam Monitor B vs Faraday-Cup.

arriving at the A1900 focal plane in particles per second, and these values were integrated over the course of each run and multiplied by the purity factor of 77% to obtain the total atoms of ^{67}Cu delivered to the beam stop. Due to the different working ranges of the detectors used to measure the beam current, two separate calibration curves had to be used. The first curve converted the high-intensity beam measured with the non-intercepting beam monitors A and B to

a medium intensity non-intercepting beam monitor C and the second curve converted the medium intensity non-intercepting beam monitor C to the low intensity focal-plane scintillator values in particles per second. The data for both methods for the second calibration run carried out post-collection are shown in **Figure 4-3**. Linear functions were found to provide excellent descriptions of all of the data.

Five collections were performed, each lasting approximately four hours, and the water from each run was collected as an individual sample for each run. The numbers of ^{67}Cu ions delivered to the liquid water target system in each run, calculated using the two methods, along with the values obtained by measuring the gamma-ray activity for aliquots taken from the samples using an HPGe detector are listed in **Table 4-2**. The values obtained from the two calibration curves were averaged for beam monitor A and B in both methods. The average transport efficiency of the ^{67}Cu secondary beam into the liquid water target system from the A1900 separator to the water target system was found to be 84 ± 5 %. The modest intensity reduction occurred between the focal plane and the end station or on the collimator immediately in front of the water target station entrance window.

Table 4-2: Beam delivered to the water target station calculated using beam monitor A or B averaging the data from the prior and post collection calibration curves compared to the amount measured in the water using an HPGe detector.

Method	Run 1(kBq)	Run 2(kBq)	Run 3(kBq)	Run 4(kBq)	Run 5(kBq)
1 A	552 (31)	551 (31)	521 (30)	512 (29)	524 (30)
1 B	527 (31)	527 (31)	503 (29)	493 (28)	500 (29)
2 A	524 (24)	523 (24)	494 (22)	485 (22)	497 (23)
2 B	501 (29)	501 (29)	478 (28)	469 (28)	476 (28)
Average	526 (29)	525 (29)	499 (27)	490 (27)	499 (28)
HPGe	460 (9)	452 (9)	425 (8)	403 (8)	397 (8)
Transport efficiency	87 (5)	86 (5)	85 (5)	82 (5)	80 (4)

Chemistry

To plan the chemical separation procedure, modeling of the radioisotopes delivered to the water cell and their decay products was carried out using the LISE++ code with the EPAX3 cross sections and the Nucleonica© decay engine, respectively, as was carried out for the previous ^{24}Na work.[8] The theoretical beam components with half-lives greater than one minute predicted by the LISE++ code to enter the target water are given in **Table 4-3**. Note that the projectile fragment separator tends to deliver more isotonic (same number of neutrons) than isotopic (same number of protons) contaminants and the primary beam is completely removed.

Table 4-3. Predicted secondary beam components with half-lives greater than one minute.

Nuclide	Half-life	Particles/s
^{67}Cu	2.58d	7.33E6 (79.3%)
^{66}Ni	2.28d	2.93E5 (3.2%)
^{65}Ni	2.52h	1.42E5 (1.5%)
^{69}Zn	56m	1.25E6 (13.5%)
^{70}Ga	21.14m	1.01E3 (0.1%)
^{68}Zn	Stable	2.30E5 (2.5%)

All of the different metals were effectively separated from the ^{67}Cu collections using the methods described below. The chemical separation relied on absorption of the positively charged cations to a metal-chelation disk, elution, and separation by anion-exchange chromatography. All methods were validated prior to the ^{67}Cu separations using either non-radioactive species or radioactive surrogate species as tracers. An experiment measuring the efficiency of removing germanium (primary beam) contamination that would be present in the primary beam dump in future work at FRIB was determined using PIXE (Particle Induced X-ray Emission) analysis of 0.04-0.5 ppm germanium that was passed through the chelating disk. The results showed average germanium retention of only 2.7 ± 0.9 %. This is likely due to the formation of the neutral compound $Ge(OH)_4$ at pH 5[19] that did not bind to the negatively charged

carboxylate groups. In order to test the separation strategy for copper and gallium, ^{68}Ga ($t_{1/2}$=68 min) obtained from a ^{68}Ge/^{68}Ga generator (Eckert and Ziegler, Germany) and ^{64}Cu ($t_{1/2}$=12.7 h) produced at Washington University in St. Louis[20] were used as radioactive tracers. Passage of ^{68}Ga and ^{64}Cu solutions through the chelation disk found that both metals remained bound within the disk with greater than 99% efficiency; however, 10 mL of 6 M HCl was able to elute, 98 ± 1 % of ^{64}Cu from the disk, while 97 ± 2 % of ^{68}Ga remained fixed to the disk. This is due to Ga^{3+} having a greater affinity for the chelation disk than Cu^{2+} and thus Ga^{3+} would require a higher chloride concentration to elute. Subsequent separation of copper from zinc and nickel was obtained using anion-exchange chromatography and verified by ion chromatography.[17] The percent of the initial nickel and zinc concentrations were found to be 4 ± 2 % and 6 ± 4 %, respectively in the 0.5M HCl fraction. The average copper recovery from this method was shown to be 86 ± 4%. The resulting separation process is shown schematically in **Figure 4-4**.

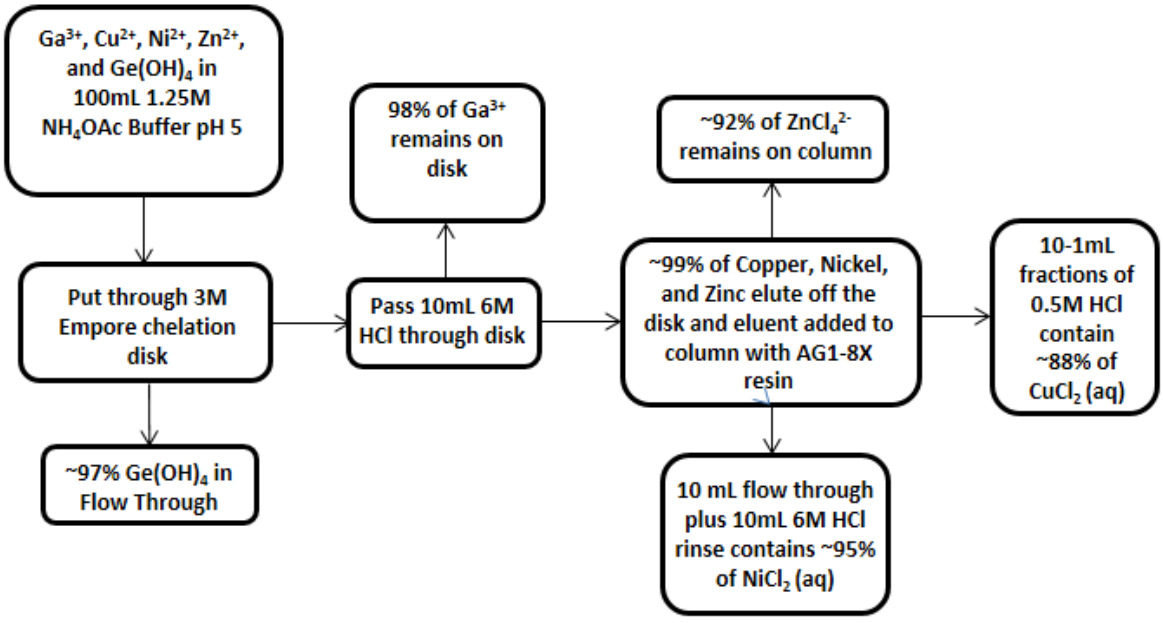

Figure 4-4: Flow chart indicating the separation strategy to recover ^{67}Cu from the aqueous samples containing ^{67}Cu projectile fragments collected at the NSCL.

Four of the ^{67}Cu samples were shipped to Washington University in St. Louis and processed as described above. **Table 4-4** contains the values for the recovery of ^{67}Cu from the aqueous solutions containing the projectile fragments from the NSCL. The average recovery of ^{67}Cu was found to be 88 ± 3 %, a value in excellent agreement with the tracer studies. The separated (final) ^{67}Cu fractions were analyzed using an HPGe detector (Canberra, USA) calibrated using a 2mL mixed source (Eckert and Ziegler, Germany) and no radioactive impurities were observed. The gallium species had completely decayed from the sample before processing due to its short half-life and the decontamination factors for nickel and zinc were 20 and 12.5 respectively.

Table 4-4. Chemical recovery of ^{67}Cu from the aqueous solutions produced at the NSCL.

	Run2(kBq)	Run3(kBq)	Run4(kBq)
Starting Activity	452 (9)	425 (8)	403 (8)
Recovered Activity	388 (8)	380 (8)	353 (7)
Percent Recovery	86 (2)	89 (3)	88 (2)

Test labeling of an antibody, Trastuzumab, was performed to demonstrate that ^{67}Cu separated from the water beam dump would be chemically active. Bicinchoninic acid (BCA) assay showed the final concentration of the conjugated NOTA-Bz-NCS-Trastuzumab to be 7.9mg/mL. The radiochemical yield of ^{67}Cu-NOTA-Bz-NCS-Trastuzumab of 0.5μCi/ug was found to be greater than 95% by radio instant thin-layer chromatography (ITLC). **Figure 4-5** shows the results of fast-protein liquid chromatography of NOTA-Bz-NCS-Trastuzumab, radio ITLC of ^{67}Cu-NOTA-Bz-NCS-Trastuzumab, radio ITLC of ^{67}Cu-EDTA along with an illustration of the NOTA chelate bound to Trastuzumab.

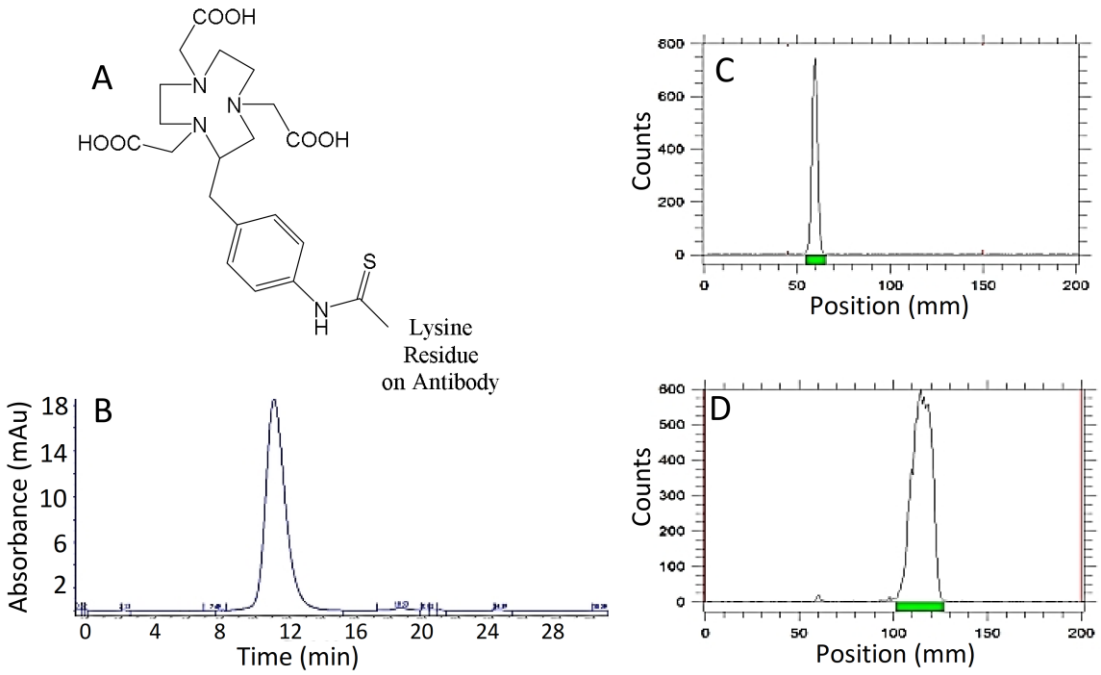

Figure 4-5: (A) Structure of the NOTA-Bz-NCS conjugated to lysine residues on Trastuzumab. (B) Fast Protein Liquid Chromatography of NOTA-Bz-NCS-Trastuzumab indicating an intact conjugated antibody. (C) Radio instant thin layer chromatography of ^{67}Cu-NOTA-Bz-NCS-Trastuzumab challenged with EDTA. The sharp peak at 60mm and the absence of a later peak signifies a fully labeled antibody. (D) Radio instant thin layer chromatography of ^{67}Cu-EDTA which serves as a negative control.

The production of ^{7}Be from reactions of beam on water

One concern with using an aqueous beam dump to collect high-energy fragments is the buildup of long-lived radioactivity from nuclear reactions with the water. ^{7}Be ($t_{1/2}$=53.3 d) is produced in reactions between essentially all fast ion beams and water. While ^{7}Be can be easily separated from the ^{67}Cu in this experiment, there may be instances where this contaminant could interfere with the harvesting process. The predicted production rate of ^{7}Be with an incident medium mass beam (A≈67) is 6.4 x 10^{-4}/incident ion.[15] The ^{7}Be concentrations in the present samples were measured using HPGe spectroscopy and showed that the production of ^{7}Be per incident ion on water was 5 ± 2 x 10^{-4}.

In addition to ^{7}Be, ^{11}C and ^{13}N were observed byproducts of the interaction of the secondary beam on water. Due to the short half-life of these isotopes, they were not observed on the HPGe detector, however their decay was observed using a CsF detector that monitored the collection vials upon completion of a four-hour collection. Future experiments will be designed in order to quantify the amount of these short-lived byproducts that are produced.

Discussion

A liquid water target station previously designed to collect fast, secondary beams from the National Superconducting Cyclotron Laboratory was used to collect five samples of ^{67}Cu. The five collections lasted for four hours each, and the samples were then shipped to Hope College and Washington University in St. Louis for further analysis and chemical separation. ^{67}Cu was effectively separated from the beam contaminants with an average recovery of 88 ± 3 %. The resulting ^{67}Cu was then bound to NOTA-Bz-NCS-Trastuzumab with a radiochemical yield of >95%. These results demonstrate the feasibility of harvesting useful radioisotopes from

the aqueous beam dump at the Facility for Rare Isotope Beams (FRIB) now under construction at Michigan State University. Future experiments will be performed to collect and separate ^{67}Cu from an unanalyzed, i.e., mixed secondary beam to better mimic the conditions that would be present in the actual FRIB beam dump.

The overall production of ^{67}Cu at the NSCL was estimated to be 7.33 x 10^6 pps for the ^{76}Ge beam and experimental conditions reported here[16]. An observed rate of 1.13 x 10^7 pps of ^{67}Cu was measured during this experiment which closely matches the predicted yield for the NSCL. Since the same codes are used to estimate yields at FRIB, this bodes well for an expected production rate of ~2Ci of ^{67}Cu in the primary beam dump at saturation during regular operations. Similarly the production of ^{7}Be was also measured to be 5.7 x 10^3 pps, which also compare favorably with the predicted production rate of 4.7 x 10^3 pps.

While this proof-of-principle experiment made use of a water target cell to collect the beam in a small volume of non-circulating water, in the future at the Facility for Rare Isotope Beams there will be ion exchangers present which could act as potential sources for isotope harvesting. Additional research will be needed in order to determine how much ^{67}Cu (and other isotopes of interest) can be extracted from the resin for the purposes of isotope harvesting.

The most promising radionuclides for isotope harvesting from FRIB would be those which cannot be produced easily by other means, such as with a reactor or small medical cyclotron. Additionally, isotope availability may depend on the needs of the primary user, how pure the isotopes need to be and the frequency of production. While this is a very promising source of isotopes for many fields, it should be noted that isotopes obtained in this manner will not be available continuously due to an incompatibility with the primary beam requirements. Thus, due to the nature of this technique, it is likely that medium- to long-lived research isotopes,

like the one studied here, will be the most promising targets for isotope harvesting from heavy-ion fragmentation facilities.

References

1 Nucleonica Decay Engine.

2 O'Donnell, R. T. *et al.* A clinical trial of radioimmunotherapy with Cu-67-2IT-BAT-Lym-1 for non-Hodgkin's lymphoma. *Journal of Nuclear Medicine* **40**, 2014-2020 (1999).

3 Schwarzbach, R., Zimmermann, K., Blauenstein, P., Smith, A. & Schubiger, P. A. Development of a Simple and Selective Separation of Cu-67 from Irradiated Zinc for Use in Antibody Labeling - a Comparison of Methods. *Applied Radiation and Isotopes* **46**, 329-336, doi:Doi 10.1016/0969-8043(95)00010-B (1995).

4 Zimmermann, K. *et al.* Targeting of renal carcinoma with (CU)-C-67/64-labeled anti-L1-CAM antibody chCE7: selection of copper ligands and PET imaging. *Nuclear Medicine and Biology* **30**, 417-427, doi:Doi 10.1016/S0969-8051(03)00019-2 (2003).

5 Smith, N. A., Bowers, D. L. & Ehst, D. A. The production, separation, and use of Cu-67 for radioimmunotherapy: A review. *Applied Radiation and Isotopes* **70**, 2377-2383, doi:DOI 10.1016/j.apradiso.2012.07.009 (2012).

6 R.T. O'Donnell, G. L. D., D.L. Kukis, K.R. Lamborn, S. Shen, A. Yuan, D.S. Goldstein, C.E. Carr, G.R. Mirick, S.J. DeNardo. A Clinical Trial of Radioimmunotherapy with 67Cu-2IT-BAT-Lym-1 for Non-Hodgkin's Lymphoma. *Journal of Nuclear Medicine* **40**, 2014-2020 (1999).

7 Connett, J. M. *et al.* Radioimmunotherapy with a Cu-64-labeled monoclonal antibody: A comparison with Cu-67. *P Natl Acad Sci USA* **93**, 6814-6818, doi:DOI 10.1073/pnas.93.13.6814 (1996).

8 Novak-Hofer, I. & Schubiger, P. A. Copper-67 as a therapeutic nuclide for radioimmunotherapy. *Eur J Nucl Med Mol I* **29**, 821-830, doi:DOI 10.1007/s00259-001-0724-y (2002).

9 Dasgupta, A. K., Mausner, L. F. & Srivastava, S. C. A New Separation Procedure for Cu-67 from Proton Irradiated Zn. *Applied Radiation and Isotopes* **42**, 371-376 (1991).

10 Mausner, L. F., Kolsky, K. L., Joshi, V. & Srivastava, S. C. Radionuclide development at BNL for nuclear medicine therapy. *Applied Radiation and Isotopes* **49**, 285-294, doi:Doi 10.1016/S0969-8043(97)00040-7 (1998).

11 Norenberg, J., Staples, P., Atcher, R., Tribble, R., Faught, J., Riedinger, L,. . Workshop on the Nation's Needs for Isotopes: Present and Future *Co-sponsored by the US DOE Offices of Nuclear Physics and Nuclear Energy, Rockville, Maryland*, (2008).

12 Jamriska, D. J. *et al.* Activation Rates and Chemical Recovery of Cu-67 Produced with Low-Energy Proton Irradiation of Enriched Zn-70 Targets. *J Radioan Nucl Ch Ar* **195**, 263-270, doi:Doi 10.1007/Bf02035965 (1995).

13 Kastleiner, S., Coenen, H. H. & Qaim, S. M. Possibility of production of Cu-67 at a small-sized cyclotron via the (p,alpha)-reaction on enriched Zn-70. *Radiochim Acta* **84**, 107-110 (1999).

14 K. Hilgers, T. S., Y. Skakun, H.H. Coenen, S.M. Qaim. Cross-section measurements of the nuclear reactions natZn(d,x)64Cu, 66Zn(d,a)64Cu and 68Zn(p,an)64Cu for the production of 64Cu and technical developments for small-scale production of 67Cu via the 70Zn(p,a)67Cu process. *Applied Radiation and Isotopes* **59**, 343-351 (2003).

15 Ronningen, R. Isotope Inventories in Cooling Loop. *2nd Workshop on Isotope Harvesting at FRIB* (2012).

16 Morrissey, D. J., Sherrill, B. M., Steiner, M., Stolz, A. & Wiedenhoever, I. Commissioning the A1900 projectile fragment separator. *Nucl Instrum Meth B* **204**, 90-96, doi:Doi 10.1016/S0168-583x(02)01895-5 (2003).

17 Mastren, T. *et al.* Specific activity measurement of Cu: A comparison of methods. *Applied radiation and isotopes : including data, instrumentation and methods for use in agriculture, industry and medicine* **90C**, 117-121, doi:10.1016/j.apradiso.2014.03.016 (2014).

18 Ferreira, C. L. *et al.* Comparison of bifunctional chelates for Cu-64 antibody imaging. *Eur J Nucl Med Mol I* **37**, 2117-2126, doi:DOI 10.1007/s00259-010-1506-1 (2010).

19 Park, H. J. & Tavlarides, L. L. Germanium(IV) Adsorption from Aqueous Solution Using a Kelex-100 Functional Adsorbent. *Ind Eng Chem Res* **48**, 4014-4021, doi:Doi 10.1021/Ie801733d (2009).

20 Kume, M. *et al.* A semi-automated system for the routine production of copper-64. *Applied Radiation and Isotopes* **70**, 1803-1806, doi:DOI 10.1016/j.apradiso.2012.03.009 (2012).

Chapter 5

Harvesting ^{67}Cu from the Collection of an Unanalyzed Secondary Beam at the National Superconducting Cyclotron Laboratory

Introduction

The collection of the analyzed ^{67}Cu secondary beam at the NSCL, discussed in Chapter 4, was an idealized case. The separation from numerous beam contaminants must be performed to better address the feasibility of harvesting ^{67}Cu from an aqueous beam dump. The fragment separator at the FRIB facility[1,2] will operate similarly to the A1900 at the NSCL.[3] The fragmented primary beam will travel through a dipole magnet to remove the primary beam and the fragmented isotopes that differ in magnetic rigidity from the isotope of interest to the end user. At the FRIB facility the discarded isotopes will go into an aqueous beam dump. Because an aqueous beam dump does not currently exist at the NSCL the normal beam separation process must be manipulated to obtain an impure (unanalyzed) secondary beam.

The aluminum wedge in the A1900 (**Figure 5-1**)[3] is an important part of the beam purification process. Several different isotopes will have a similar magnetic rigidity to the one selected for the isotope of interest after the fragmentation process, however they will differ in charge. The energy of the ions is reduced as they transfer energy to the electrons in the medium

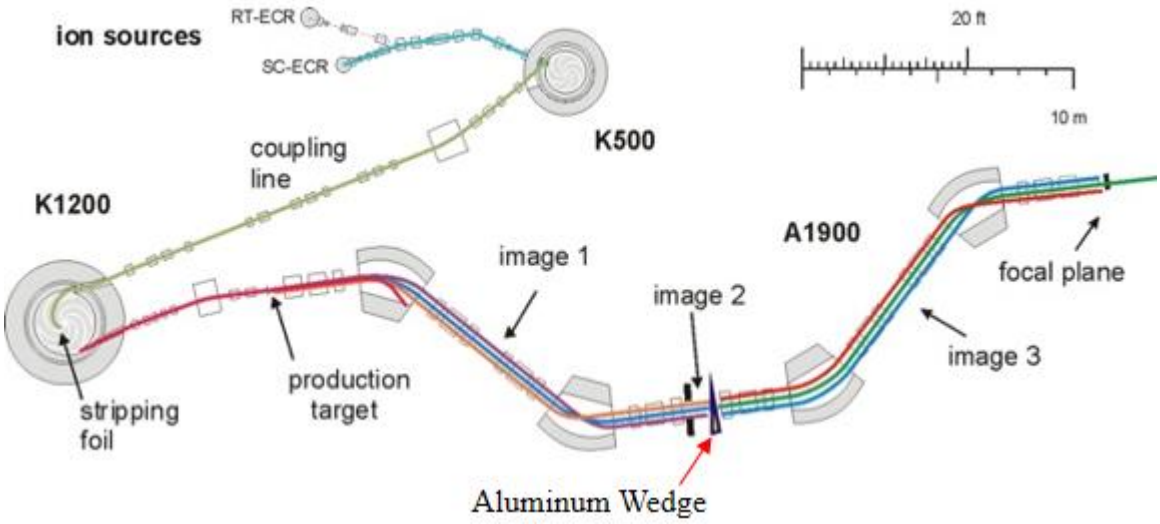

Figure 5-1. Schematic of the A1900 fragment separator at the NSCL.[3] The aluminum wedge is shown.

(this energy loss is well described by the Bethe-Bloch equation). This loss of energy changes each ion's momentum and its magnetic rigidity (the reduction in magnetic rigidity is proportional to the momentum change if the charge state is not changed). At the energies of the present work, the ions are fully stripped so the charge, Q, is equal to the atomic number, Z. The beam is usually purified by passing it through another set of dipoles set to pass the rigidity of the isotope of interest after it passes though the wedge absorber. An unanalyzed beam can be obtained by removing the aluminum wedge. Collection of this unanalyzed secondary beam using the water target station, discussed in Chapter 3, is a better representation of the conditions that would be present in the beam dump at FRIB.[4]

Previously, we were able to separate ^{67}Cu from nickel, zinc, germanium, and gallium collected from an analyzed secondary beam using a two-part chemical purification process. A more complicated procedure had to be developed for separation of ^{67}Cu from the unanalyzed beam, which consisted primarily of first-row transition metals. Most of the elements present in the secondary beam consisted of one or more radioactive isotopes. Characteristic gamma rays for each radioisotope were analyzed to monitor the separation of ^{67}Cu from the different elements, which ranged in atomic number from 19 to 34.

Three separate collections were obtained and shipped to Washington University in St. Louis for chemical separation and gamma analysis. ^{67}Cu was chemically separated from the beam contaminants with high radiochemical purity and used to radiolabel an anti-EGFR antibody (Panitumumab).[5] Biodistribution studies were conducted with this radiopharmaceutical using colon cancer xenografts to demonstrate proof of concept.

Materials and Methods

Beam Collection

In a similar manner to the method discussed in Chapter 4, a 25 particle-nA 130 MeV/u ^{76}Ge beam was fragmented using a 493 mg/cm^2 thick beryllium production target in the A1900 projectile-fragment separator.[3] The aluminum wedge was removed from the center of the A1900 to obtain an unanalyzed secondary beam. The focal plane (FP) mass-selection aperture was set to 10 mm and the momentum acceptance slits open to 2% (full momentum acceptance). The experimental parameters for the separator and beam line are listed in **Table 5-1**. Note that the two sets of dipoles D1-D2 and D3-D4 are set of the same rigidity. This arrangement passes 92.9 MeV/u $^{67}Cu^{29+}$, which corresponds to a momentum of 28.5 GeV/c, and other ions with different momenta but the same rigidity. The slits fix the range of momenta that are passed to ± 2% of value of each ion that corresponds to a Brho = 3.2822 Tm. The beam intensity and purity were measured using the standard delta-E/Time-of-Flight technique with a silicon-PIN diode in the A1900 focal plane and cyclotron RF signal prior to delivery of the beam to the experimental end station.[3]

Table 5-1. Experimental parameters for the ^{67}Cu secondary beam at the NSCL.

Block	Description	Value
Primary Beam Target	Beryllium	493 mg/cm^2
D1 Bρ	Dipole magnet	3.2822 Tm
I1 Slits	Momentum acceptance (dρ/ρ)	2.03%
D2 Bρ	Dipole magnet	3.2822 Tm
I2 Slits	Momentum acceptance (dρ/ρ)	2%
D3 Bρ	Dipole magnet	3.2822 Tm
D4 Bρ	Dipole magnet	3.2822 Tm
D5 Bρ	Dipole steering magnet	3.2822 Tm
D6 Bρ	Dipole steering magnet	3.2822 Tm
Exit Window	Zirconium	75 μm
Air Gap	Air	89 mm
Water Target Window	Tantalum	12.7 μm
Water Target	H_2O	73 mm

Three separate collections of the secondary beam were made using the water target system as described in Chapter 3 with two modifications. Due to the higher intensity of the beam compared to previous experiments, a 12.7 μm tantalum foil was used in place of the 8μm kapton film. Additionally, room temperature water was circulated through the water target cell at 100 mL/min via a Teflon tube, to keep the collection water below 30ºC.

Beam Current and Collection Efficiency

Several carbon disks (1.245" in diameter and 0.4" thick) were used to collect the incoming beam at various times throughout the experiment. A rotating wheel with 12 holes 1.25" in diameter, containing the carbon disks in alternating positions, was placed between the zirconium exit window and the entrance window to the water target station. The rotating wheel could be controlled remotely from outside of the experimental vault. A position consisting of an empty hole was used during aqueous beam collection. At various times during the experiment, the wheel was rotated so that one of the carbon disks was in line with the entrance window. The secondary beam was collected by the carbon disk for 2-5 minutes before returning the wheel to an empty position. The carbon disks were shipped to Hope College for gamma analysis using an HPGe detector to obtain a beam current (^{67}Cu atoms/second).

The beam current was measured by several non-intercepting beam monitors located throughout the A1900.[3] Because the non-intercepting beam monitors measured an intensity that was proportional to the beam current and not the actual beam current, a calibration factor had to be obtained to relate the two parameters. The intensity measured by the beam monitors was averaged for the time interval corresponding to the respective carbon disk irradiation. The calibration factor was obtained by dividing the measured ^{67}Cu atoms per second by the average

intensity measured by the beam monitors. To calculate the total amount of ^{67}Cu delivered to the water target station, the beam intensities measured throughout the experiment using the non-intercepting beam monitors were integrated over the total time of collection and multiplied by the calibration factor. The ^{67}Cu beam collection efficiency was calculated as the total number of ^{67}Cu atoms collected, as measured by HPGe, divided by the total number of ^{67}Cu atoms delivered.

Preliminary Separation Experiments

The first step in developing a separation strategy was to monitor where cobalt, iron, and manganese appeared in the separation strategy used in Chapter 4. 10 μg of Cu, Zn, Ni, Co, Fe, and Mn were added to 100 mL of 1.25 M NH_4OAc pH 5 and passed through a chelation disk as described previously. At pH 5 the carboxylate functional groups on the chelation disk are negatively charged, thus attracting positively charged ions. The metal ions in the above solution existed as 2^+ ions with the exception of manganese, which likely existed as both a 2^+ ion and as a MnO molecule. The addition of 10 mL 6 M HCl to the chelation disk extracted the 2^+ metals that were chelated by the disk without removing the 3^+ metals from the disk. Following passage through the chelation disk the 6M HCl fraction was added to an anion exchange column containing 2.5g of AG1-X8 resin (Bio-Rad, CA). The elution constants of these metals for quaternary amine functionalized resin vary with the concentration of hydrochloric acid.[6] Varying amounts of 6M, 4M, 2.5M and 0.5M HCl were used to elute the different metallic ions from the anion exchange resin. Each fraction collected was evaporated to dryness and reconstituted in 5 mL of 3% HNO_3 (the metallic ions existed as Cu^{2+}, Ni^{2+}, Zn^{2+}, Co^{2+}, Mn^{2+},

Fe^{2+}). An aliquot of each fraction was diluted by a factor of 500 and measured via Ion Chromatography[7] to monitor the separation of the different elements.

The separation of cobalt from copper was more difficult than with the other divalent metals because the elution constants of these two metals are similar.[6] Because the elution constant for cobalt rises at a steeper rate than that of copper between 6M and 3M hydrochloric acid, we varied the concentration of HCl in this range monitoring the copper-cobalt separation with the radiotracers ^{55}Co and ^{64}Cu. 3.7 MBq of ^{55}Co and ^{64}Cu in 10 mL of 6M HCl were added to an anion exchange column with 2.5g of AG1-X8 resin and the eluate was collected. Three additional fractions of 10 mL of 6M HCl were added to the resin and their eluate was collected. 10 mL of 4M HCl were added to the resin and the eluate was collected. Then, 10 mL of 2.5M HCl were added to the resin and the eluate was collected. Finally, 10 mL of 0.5M HCl were added to the resin and the eluate was collected. The eluate from each fraction was analyzed by an HPGe detector to detect the characteristic gamma rays of ^{64}Cu (1345 keV) and ^{55}Co (931, 477, and 1408 keV).

The chemistry of vanadium is much more complex than the metals described above and it is likely that vanadium deposited in the aqueous beam dump will exist in several different charge states. The ion chromatography method cannot be used to measure the concentration of vanadium, therefore another method had to be developed to monitor the separation of vanadium. Vanadium was oxidized to the +5 oxidation state by the addition of hydrogen peroxide. A UV-Vis spectrophotometer at 450nm was used to obtain an absorbance for this solution. Calibration curves for vanadium in 6M, 2.5M, and 0.5M hydrochloric acid were obtained for concentrations ranging from 2mg/L to 12mg/L using an atomic absorbance standard of vanadium. Linear calibration curves were achieved.

A 100 mL 1mg/L solution of vanadium in 1.25M NH_4OAc pH 5 was passed through a chelation disk. 10 mL of 6M HCl were then passed through the disk and collected. 20μL of H_2O_2 were added to a 1 mL aliquot of the eluate and its absorbance measured at 450nm. The remaining 9 mL of 6M HCl were added to a column containing 2.5g AG1-8X resin. Two additional 10 mL 6M HCl fractions followed by a 10 mL 2.5M fraction were eluted from the column and 20μL of H_2O_2 were added to 1mL aliquots from each fraction and their absorbance measured at 450nm the absorbance peak for V(V) complexes.

Titanium in an aqueous solution is readily oxidized to TiO_2, which is insoluble in water. However, the concentration of titanium will be very low in the beam dump, therefore it is expected that TiO_2 will be soluble at this concentration. As with vanadium, titanium concentration cannot be measured using ion chromatography. However in acidic medium and in the presence of hydrogen peroxide titanium exhibits a bright yellow color representative of its +4 oxidation state. Calibration curves were made in 6M, 2.5M, and 0.5M HCl for concentrations ranging from 2mg/L to 12mg/L. Linear curves were obtained as the plot of absorbance at 405nm vs concentration.

An atomic absorption standard of TiO_2 was used to make a 100mL 1mg/L solution of titanium in 1.25M NH_4OAc at pH 5. This was passed through a chelation disk followed by 10 mL 6M HCl. A 1mL aliquot of the 6M HCl eluate was collected and 20μL H_2O_2 were added. The absorbance was measured at 405nm. The remaining 9mL of 6M HCl were subjected to anion exchange chromatography in the same manner as described for vanadium. 20μL H_2O_2 were added to a 1mL aliquot from each fraction and their absorbance measured at 405nm the absorbance peak for Ti(IV) complexes.

^{67}Cu Separation

First, each 100mL collection was adjusted to 1.25M solution of NH_4OAc by adding 9.6g trace metals grade ammonium acetate and pH adjusted to 5 by adding ~3mL trace metals grade acetic acid. The ~100mL solution was then passed through the chelation disk as described in Chapter 4. The filter holder was transferred to a clean vacuum flask and 10mL of 6M trace metal grade hydrochloric acid were passed through to remove the ^{67}Cu and other 2^+ metal contaminants bound to the chelation disk. The 6M HCl elution was then transferred to an anion-exchange column with AG1-X8 resin, the 10mL eluate was collected and then two additional 10mL fractions of 6M hydrochloric acid were passed through the column and collected. Next 10mL 2.5M hydrochloric acid were added to the resin and the eluate was collected. Then 10mL 0.5M HCl were added to the resin and the eluate collected. All eluates were analyzed for radiochemical purity by observing the characteristic gamma rays in an HPGe detector.

Conjugation of NOTA-Bz-NCS to Panitumumab

A 10mg/mL stock solution of NOTA-Bz-NCS was made by dissolving 4.18mg NOTA-Bz-NCS (Macrocyclics, USA) in 418μL of 0.1M sodium carbonate buffer (pH9). 50μL of 20μg/μL Panitumumab (Genentech, USA) were added to 10μL NOTA-Bz-NCS stock solution followed by the addition of 50μL of 0.1M sodium carbonate buffer (pH 9.0) and incubated at 37ºC for 1 hr in a shaking incubator. A Zeba spin desalting column (40K MWCO, 0.5mL) was used to buffer exchange the conjugate into 0.1M ammonium acetate buffer (pH 5.5). The concentration of the NOTA-Bz-NCS-Panitumumab conjugate was measured using the Bradford assay.[8]

Evaluation of Immunoreactivity

The immunoreactivity of the conjugated NOTA-Bz-NCS-Panitumumab was measured to verify that the conjugation did not affect the antigen-binding properties of the antibody. This was done by incubating different concentrations of ^{64}Cu-NOTA-Bz-NCS-Panitumumab with a fixed number of antigens (cells). Method 3 as described by Konishi et al[9] was used to measure the immunoreactive fraction (IF) of the radiolabeled antibody. The final effective specific activity of ^{64}Cu-NOTA-Bz-Panitumumab was 185 kBq/μg. Radiolabeling was confirmed to be >99% by radio thin-layer chromatography as described in Chapter 4. The radiolabelled Panitumumab was brought to a final concentration of 4.18 μg/mL in 0.1M NH_4OAc pH 5.5. Serial dilutions were performed so that solutions ranging from 0.0625 μg/mL through 4.18 μg/mL were obtained. 50μL of each concentration was added to 500μL of 3 x 10^6 HCT-116 cells suspensions containing 0.1% bovine serum albumin in PBS, in triplicate. Cell solutions were placed on a shaker at room temperature and incubated for 2 hours. Cells were pelleted at 1,000 x g for 3 minutes and the supernatant was removed. Cells were then washed three times with 500μL of phosphate buffered saline, pelleting and removing the supernatant between each wash. Standards containing the initial activity of each concentration along with the cell pellets were counted on a gamma counter. The immunoreactive fraction was calculated using equation 8 (**Equation 5-1**) as described by Konishi et al[9] where B is bound antibody, T is total antibody, F_{max} is the maximum number of binding sites, r is the immunoreactive fraction, and K_a is the association constant. The ratio of bound vs. total antibody was graphed against the total antibody (pmol) in Prism 6 (Graphpad, California). F_{max}, r, and K_a were used as the fitting parameters in order to obtain a best fit curve.

$$\frac{B}{T} = \left[\frac{F_{max}+rT+\frac{1}{K_a}}{2} - \sqrt{\frac{1}{4}\left(F_{max} + rT + \frac{1}{K_a}\right)2 - F_{max}rT}\right] \div T \qquad \textbf{Equation 5-1}$$

Animal Models

All animal care was performed as stated in the Guide for Care and Use for Laboratory Animals by the National Institutes of Health under a protocol approved by the Animal Studies Committee at Washington University in St. Louis. Female Athymic *Nu/Nu* mice (National Cancer Institute, USA) aged 6-9 weeks were anesthetized with a ketamine/xylazine cocktail (VEDCO, USA). 100 µL of approximately 3 x 10^7 cell/mL HCT-116 colon cancer cells suspended in saline were subcutaneously injected into the shoulder. Tumors were allowed to grow for two weeks before biodistribution studies.

Radiolabeling and Biodistribution of ^{67}Cu-NOTA-Bz-Panitumumab

The 2.5M HCl fractions from the three separations were mixed together, brought to dryness, and reconstituted in 30µL of 0.1M HCl (^{67}Cu existed as $^{67}Cu^{2+}$). 25µL (451 kBq) of ^{67}Cu was added to 25µL of 0.5M NH_4OAc and the final solution had a pH of 5.5 (at pH 5.5 the carboxylate groups on NOTA are negatively charged allowing Cu^{2+} to be chelated). 111 µL 5.5mg/mL NOTA-Bz-Panitumumab was added to the mixture and incubated at 37ºC for 30 minutes. Radiolabeling was confirmed using radio thin-layer chromatography. The solution was brought to 400µL by the addition of saline and non-specifically bound ^{67}Cu was challenged with EDTA (final EDTA concentration of 1mM).

113 kBq of ^{67}Cu-NOTA-bz-Panitumumab was injected into three HCT-116 colon cancer xenografted mice via the tail vein. Biodistribution studies were performed at five days post injection. Organs and tumors were harvested and weighed. The radioactivity associated with each organ was assayed in a gamma counter, background and decay corrected, to determine the percentage of injected dose per gram of organ (%ID/g).

Results

Beam Collection

A 76 MeV/u unanalyzed ^{67}Cu secondary beam with a purity of 2.6% was selected from a fragmented ^{76}Ge primary beam and delivered to the S1 vault where the water target station was set up to collect the incoming beam. The average calibration factors measured for Beam Monitors A and B were $2.6 \pm 0.5 \times 10^{9}$ and $6 \pm 1 \times 10^{12}$ respectively. The data from each of the irradiated carbon disks is listed in **Table 5-2**.

Table 5-2. Beam Current data obtained from irradiation of the carbon disks.

Sample	Total ^{67}Cu Atoms	Collection Time (s)	^{67}Cu atoms/s	Beam Monitor A Calibration Factor	Beam Monitor B Calibration Factor
Disk 1	1.41 (0.03) x 10^{9}	300	4.7 (0.1) x 10^{6}	1.97E+09	4.78E+12
Disk 2	6.0 (0.1) x 10^{8}	120	5.0 (0.1) x 10^{6}	2.40E+09	5.54E+12
Disk 3	1.13 (0.02) x 10^{9}	120	9.4 (0.2) x 10^{6}	2.91E+09	7.2E+12
Disk 4	8.0 (0.2) x 10^{8}	120	6.6 (0.1) x 10^{6}	3.47E+09	8.94E+12
Disk 5	1.61 (0.03) x 10^{9}	300	5.4 (0.1) x 10^{6}	2.29E+09	5.5E+12
Disk 6	6.5 (0.1) x 10^{8}	120	5.4 (0.1) x 10^{6}	2.62E+09	6.09E+12

An aliquot of 1 mL from each of the collections was analyzed by an HPGe detector to measure total ^{67}Cu activity using the characteristic gamma rays (91.3, 93.3, 184.6, 300.2, and 393.5 keV). It is important to note that ^{67}Ga was present in the secondary beam. Because greater than 99% of the gallium remains bound to the disk and more than 99% of the copper

elutes from the disk upon the addition of 6M HCl, the contribution to the above characteristic gamma rays from ^{67}Ga could be calculated and used to correct the total ^{67}Cu activity. These results were compared to the amount of ^{67}Cu delivered to the water target station for each collection and are listed in **Table 5-3**. The average collection efficiency was found to be 115 ± 18 %.

Sample	Z001I-C (Mbq)	Z030F-C (MBq)	HPGe (MBq)	Collection Efficiency
Collection 1	1.1 (0.2)	1.2 (0.3)	1.16 (0.03)	101 (15)
Collection 2	0.8 (0.2)	0.8 (0.2)	0.881 (0.003)	112 (17)
Collection 3	0.6 (0.1)	0.6 (0.1)	0.799 (0.002)	133 (20)

Development of a Chemical Separation Strategy

The theoretical beam contaminants delivered to the water cell and their decay products were modeled using the LISE++ code with the EPAX3 cross sections and the Nucleonica© decay engine, respectively, as was carried out for the previous experiments in Chapters 3 and 4. The theoretical contaminants at three days post irradiation are listed in **Table 5-4**. The separation strategy consists of two parts. First passing the liquid through a chelation disk functionalized with iminodiacetic acid groups. At pH 5, the carboxylate groups are negatively charged, which results in the binding of positively charged metal ions. Neutral or negatively charged species will not bind to the chelation disk and therefore can be separated from the isotope of interest $^{67}Cu^{2+}$. The second part consists of using hydrochloric acid to remove the 2^+ metal ions from the chelation disk. This is followed by passing the eluent through a column containing quaternary amine functionalized anion exchange resin. At high chloride concentrations many metals form negatively charged metal chloride species such as MCl_3^- or MCl_4^{2-}. Varying the concentration of chloride allows for separation of the first row transition

metals, as each metal forms these negatively charged complexes at different chloride concentrations. As the chloride concentration is lowered, metals exist primarily as cationic species and are eluted from the resin. Preliminary experiments determined that > 99% of the titanium, vanadium and manganese would be separated from ^{67}Cu with the chelation disk and the first three 6M HCl fractions. This resulted from the formation of TiO_2, $H_2VO_4^-$, Mn^{2+}, and MnO_2[10-12] in aqueous solutions at pH 5. Iron, existing as Fe^{2+}, was found to elute from the column in the 0.5M HCl fraction. The best separation achieved for cobalt and copper was the use of three 6M HCl fractions, which removed ~80% of the cobalt. Arsenic, in aqueous solutions at pH 5, exists both as the neutral compound H_3AsO_3 and the negatively charged complex $H_2AsO_4^-$. These arsenic species were expected to pass through the chelation disk.[13] Therefore, the separation strategy developed for the separation of ^{67}Cu from the aqueous beam dump consisted of the use of the chelation disk, followed by anion exchange using three fractions of 6M HCl, a 2.5M HCl fraction, and a 0.5M HCl fraction.

Separation of ^{67}Cu from the Secondary Beam Collections

Separation of ^{67}Cu was performed as discussed in the methods above. **Figure 5-2** shows the separation profile of all the beam contaminants as measured using HPGe analysis of the characteristic gamma rays for one or more isotopes of each element. HPGe spectra were obtained immediately after separation. Additional HPGe spectra taken for longer time intervals were obtained after the short-lived isotopes decayed to measure the concentrations of long-lived isotopes. **Figure 5-3** shows the HPGe spectra taken for each part of the separation.

Each gamma ray was assigned to an isotope by using the Lawrence Berkeley National Laboratory Radiation Search database.[14] In the case where different isotopes had gamma rays

that could not be resolved, other gamma rays were used to calculate the activity in order to correct for the peak contribution from both radioisotopes. All radioisotopes measured were corrected for decay while counting and results were decay corrected to the end of bombardment. The identifying isotopes, theoretical amount of each element with respect to ^{67}Cu, and the final contamination to ^{67}Cu ratios are listed in **Table 5-4**. The success of the chemistry is measured by the ratio of the final contaminant concentration vs the initial contaminant concentration. There are many cases where this ratio, the decontamination factor, is so large that no residual activity can be measured. The worst case observed was for cobalt, where the final solution could only be decontaminated by a factor of 3.

74 ± 4% of the ^{67}Cu was obtained in the 2.5M fractions with a radiochemical purity of >99%. The other contaminants present in the ^{67}Cu fractions measured by HPGe for 12 hours and decay corrected to end of bombardment were ^{58}Co (0.07%), ^{48}Sc (0.06%), ^{47}Sc (0.06%), and ^{72}Ga (0.30%). No additional radioactive contamination was detected in the 2.5M HCl ^{67}Cu fractions. The ^{67}Cu fraction was brought to dryness by heating followed by reconstitution in 20μL 0.1M HCl.

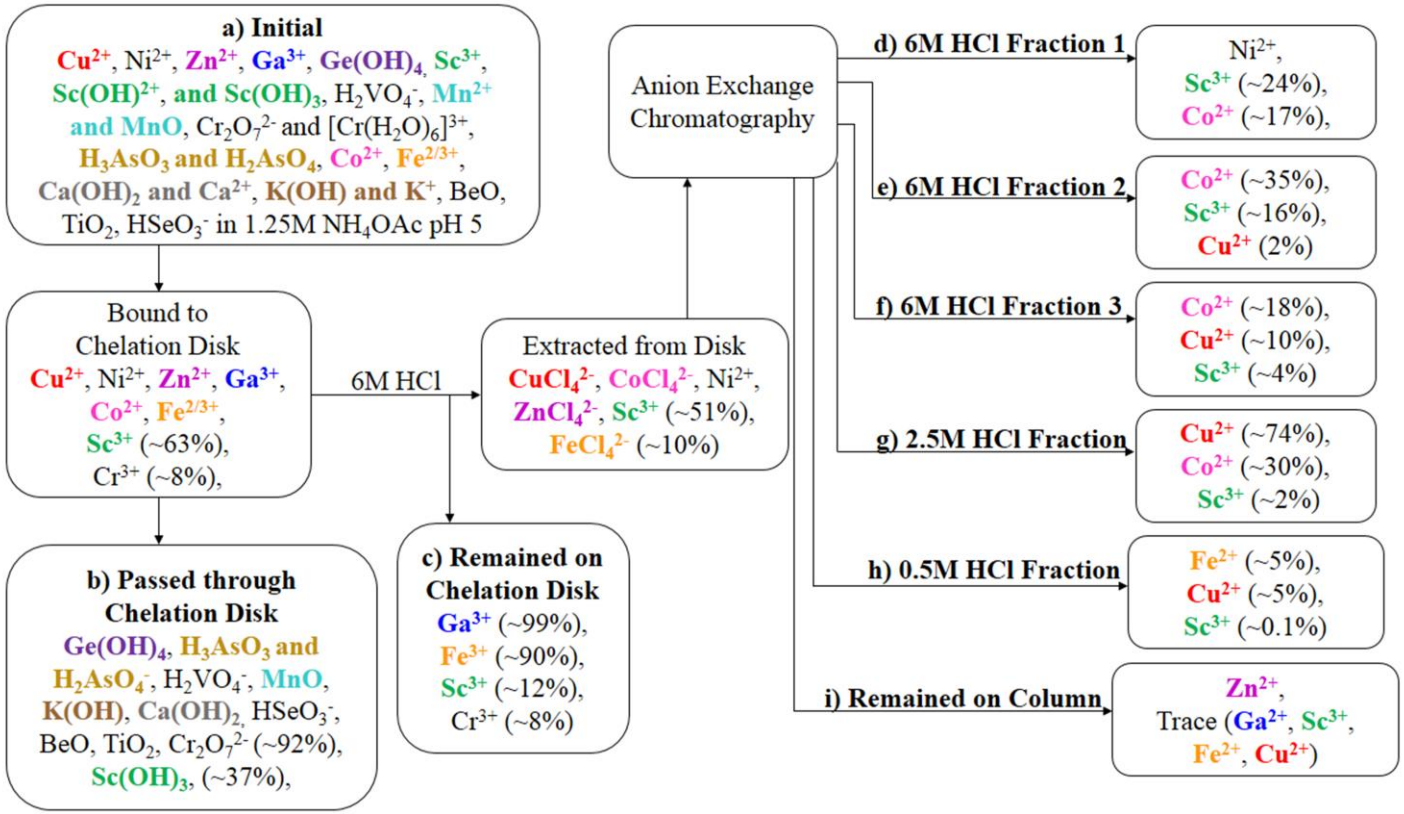

Figure 5-2. Flow chart showing the chemical separation of the isotopes present in each of the collections. Labels **a-i** correspond to the spectra shown in **Figure 5-3**.

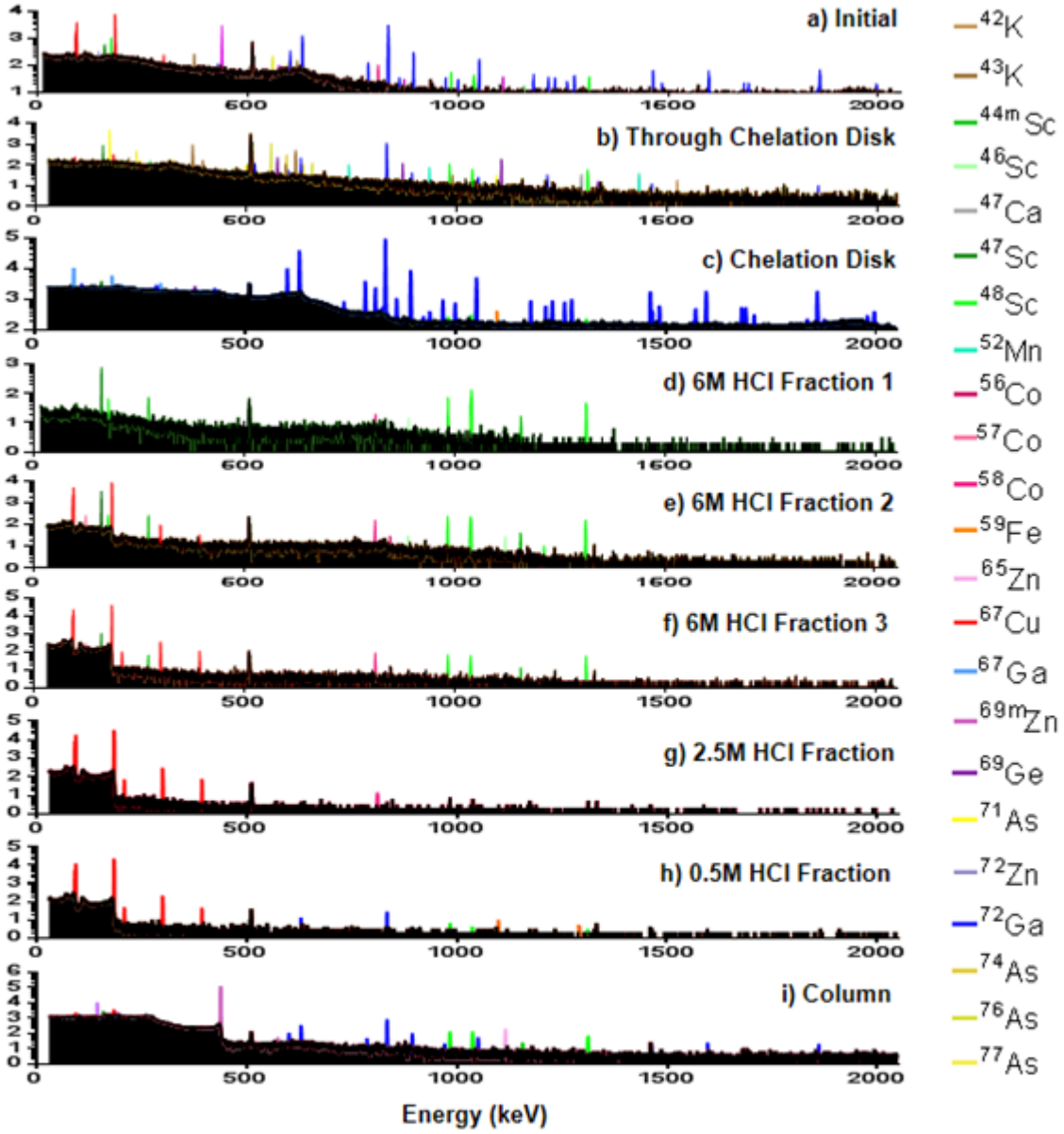

Figure 5-3. HPGe spectra for each part of the separation strategy. Panel's **a-i** correspond to the separation steps shown in **Figure 5-2**. The 2.5M HCl fraction (**g**) is where 74 ± 4% of the ^{67}Cu is eluted. The detector dead time for each measurement was kept below 5% to minimize the contribution of sum peaks.

Table 5-4. Contaminating elements present in the secondary beam collections at three days post bombardment, the isotopes used to follow the separation of each element, and the initial and final contaminant to ^{67}Cu ratios.

Contaminating Element	Identifying Isotopes	Initial Contaminant to ^{67}Cu Ratio	Final Contaminant to ^{67}Cu Ratio
Ge	^{69}Ge	30	Below Detection
As	^{74}As	24	Below Detection
Ga	^{72}Ga	5.48	0.1096
Zn	^{69M}Zn	5.48	Below Detection
Ni	^{57}Ni	3.55	Below Detection
Fe	^{59}Fe	2.58	Below Detection
Cu	^{67}Cu	1.87	1.87
Cr	^{51}Cr	1.13	Below Detection
K	^{43}K	0.81	Below Detection
Ca	^{47}Ca	0.81	Below Detection
V	^{48}V	0.42	Below Detection
Sc	^{46}Sc, ^{47}Sc, ^{48}Sc	0.39	0.0078
Mn	^{52}Mn	0.32	Below Detection
Se	^{75}Se	0.13	Below Detection
Co	^{58}Co	0.06	0.018

^{67}Cu-NOTA-Bz-Panitumumab Labeling and Biodistribution Studies

The final concentration of the NOTA conjugated Panitumumab was measured via the Bradford assay to be 5.55mg/mL. The immunoreactivity (measurement of the retained functionality of the antibody after conjugating with NOTA) was measured to be 97 ± 2 % and the data used to obtain this value is shown graphically in **Figure 5-4**. NOTA-Bz-Panitumumab was radiolabeled with ^{67}Cu at a final specific activity of 740Bq/μg.

113 kBq of 740 Bq/μg ^{67}Cu-NOTA-Bz-Panitumumab was injected into three colon cancer xenografted mice. At 5 days post injection the mice were sacrificed and their organs assayed for % Injected Dose per gram of tissue. Biodistribution data for ^{67}Cu-NOTA-Bz-Panitumumab is shown in **Figure 5-5**. The %ID/g of the tumor was found to be 12.5 ± 0.7 %, which is in strong agreement with results reported by Chang et al.[5]

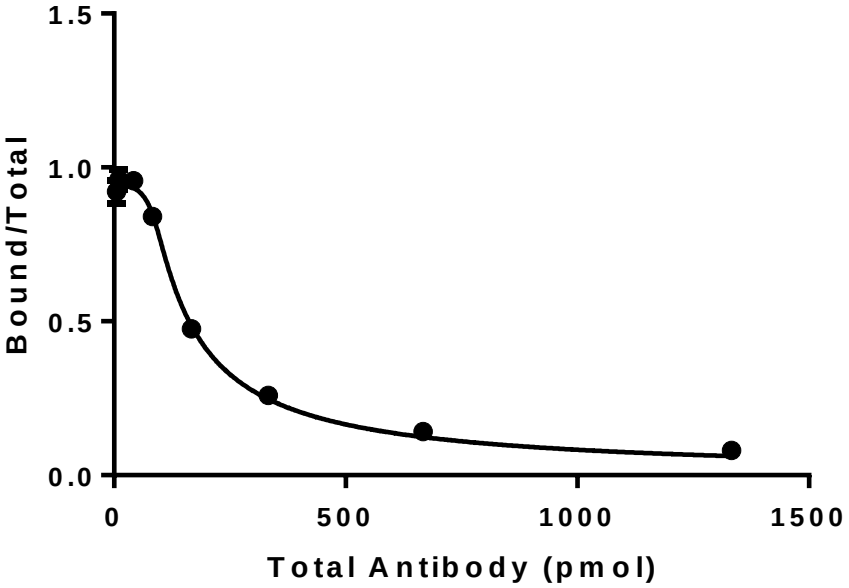

Figure 5-4. The ratio of bound vs total ^{64}Cu-NOTA-Bz-Panitumumab vs. the total amount of antibody (pmol). Immunoreactivity was calculated using method 3 as described by Konishi et al.[9]

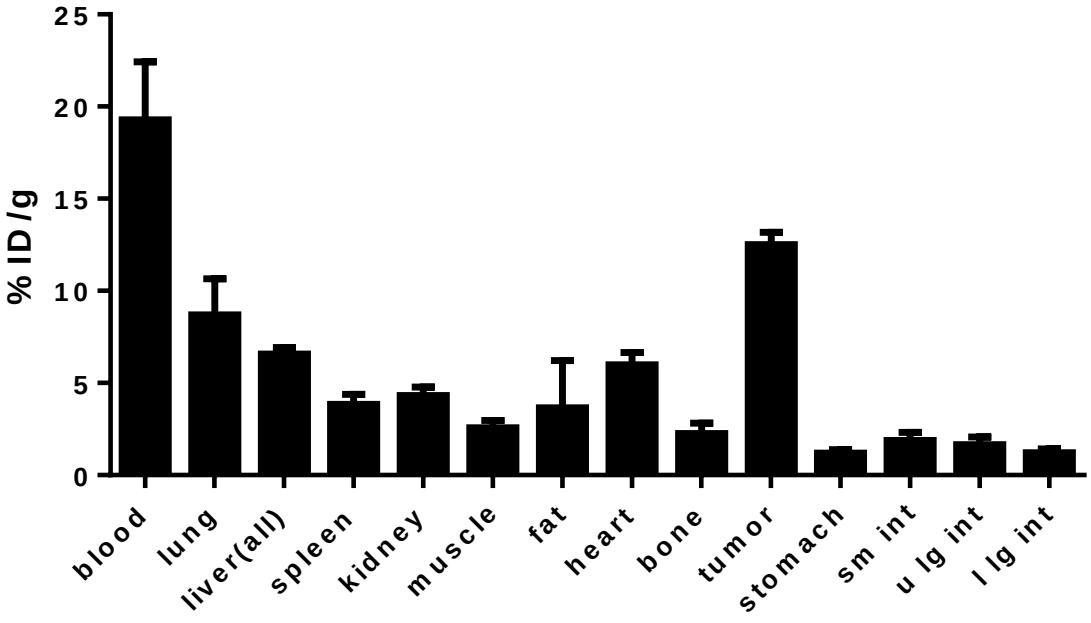

Figure 5-5. Biodistribution of ^{67}Cu-NOTA-Bz-Panitumumab in HCT-116 colon cancer xenografts. The %ID/g of the tumor was measured to be 12.5 ± 0.7 %.

Discussion

Our results show that ^{67}Cu was separable with high radiochemical purity from an aqueous beam dump containing many contaminants. An anti-EGFR antibody, Panitumumab, was successfully conjugated with NOTA-Bz-NCS without affecting its antigen binding properties. The purified ^{67}Cu was then used to radiolabel the Panitumumab conjugate to obtain a biodistribution profile for ^{67}Cu-NOTA-Bz-Panitumumab in HCT-116 colon cancer xenografted mice as a proof-of-concept.

The effective specific activity of ^{67}Cu-NOTA-Bz-Panitumumab was low (20nCi/μg). Since the elements in the secondary beam had one or more isotopes that could be used as a radiotracer, and the radiochemical purity of ^{67}Cu was measured to be greater than 99%, it is suspected that the lower specific activity did *not* result from poor separation of the secondary beam. One potential source of stable contamination is the tantalum foil that was used as the entrance window to the liquid water target cell. Other potential sources of contamination are from the glassware, vials, or chemicals used in the separation process. The final ^{67}Cu fraction has been shipped to Missouri University Research Reactor (MURR) for elemental analysis using inductively coupled plasma mass spectrometry.

One limitation of this study was the contaminants present in the beam as they only consisted of elements located in period four of the periodic table. It is estimated that ~60% of the primary beams supplied at FRIB will be uranium. Fragmentation of the uranium beam will create waste isotopes of all elements lower in mass than uranium. The additional contamination generated from uranium fragmentation will require additional separation steps and further loss of ^{67}Cu in the process. Future research should include the separation efficiency for ^{67}Cu from

fission fragments along with decontamination factors for elements between selenium and uranium in the periodic table.

Another limitation of this study was the exclusion of mixed bed resin as a first step in the separation strategy. At the FRIB facility the aqueous beam dump will be circulated through columns containing mixed bed resins as a way to remove the radioactivity from the water. Isotopes of interest for applications research will have to be eluted from this resin. Future experiments should be performed using the mixed bed resin that will be employed at FRIB.

In conclusion, ^{67}Cu was obtained with high radiochemical purity and the decontamination factors for elements from potassium through selenium were determined. ^{67}Cu was acquired in the proper chemical form to be used for radiolabeling molecular probes. These studies support the hypothesis that ^{67}Cu can be harvested from the aqueous beam dump at FRIB for use in pre-clinical research.

References

1 Morrissey, D. Status of the FRIB project with a new fragment separator. *Journal of Physics: Conference Series* **267**, 012001, doi:10.1088/1742-6596/267/1/012001 (2011).

2 M. Hausmann, A. A., A. Amthor, M. Avilov, L. Bandura, R. Bennett, G. Bollen, T. Burgess, S. Chouhan, V. Graves. Design of the Advanced Rare Isotope Separator ARIS at FRIB. *Nuclear Instruments and Methods in Physics Research Section B: Beam Interactions with Materials and Atoms* **317**, 349-353, doi: 10.1016/j.nimb.2013.06.042 (2013).

3 Morrissey, D. J., Sherrill, B. M., Steiner, M., Stolz, A. & Wiedenhoever, I. Commissioning the A1900 projectile fragment separator. *Nucl Instrum Meth B* **204**, 90-96, doi:Doi 10.1016/S0168-583x(02)01895-5 (2003).

4 Ronningen, R. Isotope Inventories in Cooling Loop. *2nd Workshop on Isotope Harvesting at FRIB* (2012).

5 Chang, A. J., Silva, R. A. D. & Lapi, S. E. Development and Characterization of 89Zr-Labeled Panitumumab for Immuno–Positron Emission Tomographic Imaging of the Epidermal Growth Factor Receptor. *Molecular Imaging* **0**, 1-11, doi:10.2310/7290.2012.00016 (2012).

6 Kraus, K. A. & Moore, G. E. Anion Exchange Studies. VI. The Divalent Transition Elements Manganese to Zinc in Hydrochloric Acid. *Journal of the American Chemical Society* **75**, 1460-1462, doi:10.1021/ja01102a054 (1953).

7 Mastren, T. *et al.* Specific activity measurement of (6)(4)Cu: a comparison of methods. *Applied radiation and isotopes : including data, instrumentation and methods for use in*

agriculture, industry and medicine **90**, 117-121, doi:10.1016/j.apradiso.2014.03.016 (2014).

8 Bradford, M. M. A rapid and sensitive method for the quantitation of microgram quantities of protein utilizing the principle of protein-dye binding. *Analytical biochemistry* **72**, 248-254 (1976).

9 Konishi, S. *et al.* Determination of immunoreactive fraction of radiolabeled monoclonal antibodies: What is an appropriate method? *Cancer Biother Radio* **19**, 706-715, doi:DOI 10.1089/cbr.2004.19.706 (2004).

10 Sakka, S. *Handbook of sol-gel science and technology : processing, characterization, and applications*. (Kluwer Academic Publishers, 2005).

11 Tufekci, N. & Celik, S. O. The Effects of Some Inorganic and Organic Species on Oxidation with Atmospheric Oxygen of Manganese in Natural Water. *Pol J Environ Stud* **20**, 201-207 (2011).

12 Tella, E. *et al.* The Mechanism of Retention of Vanadium Oxo-Species at the "Titanium Oxide/Aqueous Solution" Interface. *Global Nest J* **12**, 231-238 (2010).

13 Ngai, T. K. K. *ARSENIC SPECIATION AND EVALUATION OF AN ADSORPTION MEDIA IN RUPANDEHI AND NAWALPARASI DISTRICTS OF NEPAL* MASTER OF ENGINEERING IN CIVIL AND ENVIRONMENTAL ENGINEERING thesis, Massachusetts Institue of Technology, (2001).

14 Firestone, R. B. & Ekstrom, L. P. *Radiation Search*, <http://ie.lbl.gov/toi/radsearch.asp> (2004).

Chapter 6

Cyclotron production of high specific activity ^{55}Co and the evaluation of the stability of ^{55}Co metal-chelate-peptide complexes *in vivo*

Introduction

Recently interest in positron emitting metals has increased due to their longer half-lives when compared to traditional PET isotopes such as ^{18}F, ^{11}C, and ^{15}O. Currently the most common radiometals used in PET imaging are ^{64}Cu, ^{68}Ga, ^{89}Zr, and ^{86}Y with ^{64}Cu, ^{68}Ga, and ^{89}Zr being used in clinical trials. The chemistry of each metal is different and chelates need to be optimized for the radiometal of interest. Therefore when developing new positron-emitting radiometals for use in pre-clinical research it is important to establish chelators that provide stable metal-chelate complexes *in vivo*.

^{55}Co is an isotope also of interest for PET imaging. It has a half-life of 17.5 hr, a positron branching ratio of 77%, and an average positron energy of 570 keV (**Figure 6-1**) qualities that make it a candidate for labelling peptides, small molecules, and antibody fragments.[1-6] $^{55}CoCl_2$ has also been used clinically to image ischemia in stroke patients[7-10] and in late-onset epileptic seizures.[11] With the growing interest in ^{55}Co as a PET imaging agent, it is important to study the pre-clinical pharmacological properties of this isotope. Information on the biodistribution of free $^{55}CoCl_2$ along with the stability of ^{55}Co metal-chelate complexes *in vivo* is required to design imaging agents employing this isotope.

^{55}Co can be made via several nuclear reactions such as $^{58}Ni(p,\alpha)^{55}Co$, $^{56}Fe(p,2n)^{55}Co$, and $^{54}Fe(d,n)^{55}Co$.[12-19] The $^{54}Fe(d,n)^{55}Co$ has the highest measured cross section at low energies,[3,20] however ^{54}Fe has a low natural abundance and thus this target may be cost-prohibitive for routine production in most laboratories. The $^{56}Fe(p,2n)^{55}Co$ reaction also creates undesirable ^{56}Co via the $^{56}Fe(p,n)^{56}Co$ reaction. ^{56}Co is a positron emitting isotope with a half-life of 77d, many high energy photons, and chemically inseparable from ^{55}Co. The proton reaction on ^{58}Ni has a higher cross section at lower energies than the proton reaction on ^{56}Fe[16,18,19] making it more

desirable for low-energy (15 MeV) cyclotrons. This method also produces a small amount of a side product, ^{57}Co ($t_{1/2}$=271.8d). ^{57}Co decays 100% by electron capture and has a low-energy gamma ray of 122 keV. Therefore the nickel route is a better option for the production of ^{55}Co for applications in PET imaging.

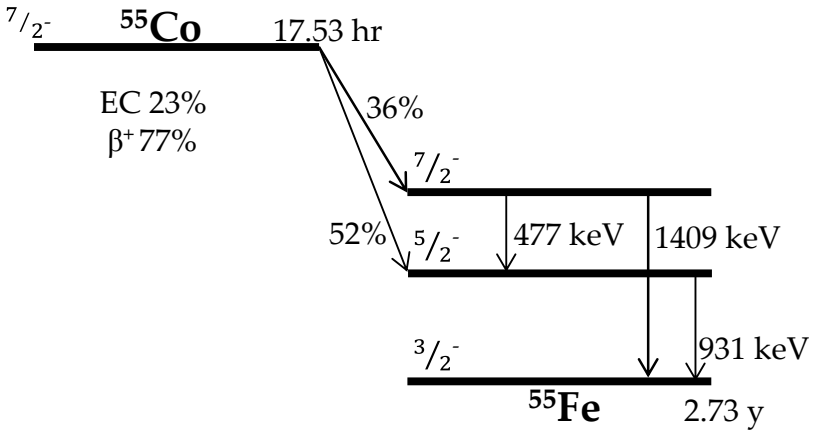

Figure 6-1. Simplified decay scheme for ^{55}Co.

The production of ^{55}Co using ^{nat}Ni and ^{58}Ni have been performed,[6,17] however only the radiochemical purity was reported and specific activity of the final product was not addressed. High effective specific activity (ESA) of radiometals is important as metal contaminants have negative impacts on radiolabelling,[21,22] For best radiolabelling results using ^{55}Co, ESA measurements must be performed and productions optimized so that high-specific activity material can be obtained.

In this work, the production of ^{55}Co via the ^{58}Ni(p,α)^{55}Co reaction is discussed along with ESA measurements performed using both DOTA titrations and Ion Chromatography.[21] An anti-VEGF peptide previously investigated by our group, L19K-FDNB, has been shown to have a long blood clearance time.[23] This property makes this peptide an optimal system for studying the

stability of different metal chelate complexes *in vivo* at time points up to 48 hrs. The biodistribution data for $^{55}CoCl_2$ and ^{55}Co-NO2A-L19K-FDNB and ^{55}Co-DO3A-L19K-FDNB were compared at 24 and 48 hrs post injection to establish the *in vivo* stability of ^{55}Co chelated with NO2A and DO3A in tumor-bearing mice.

Materials and Methods

Materials

Trace metals grade reagents were purchased from Sigma-Aldrich (USA) and used without purification and Milli-Q deionized water (18 MΩ cm^{-1}) was used for all dilutions unless stated otherwise. All glassware and vials were acid washed in 8M HNO_3 for 24 hrs prior to use. DOTA (1,4,7,10-tetraazacyclododecane-1,4,7,10-tetraacetic acid) was purchased from Macrocyclics (USA). Two versions of the peptide L19K were synthesized by CPC Scientific consisting of the sequence Chelate-PEG_4-GGNECDIARMWEWECFERK-$CONH_2$, with a Cys-Cys disulfide bridge and polyethylene glycol (PEG) as a spacer between peptide and chelator where the chelators were either NO2A or DO3A. ^{58}Ni was purchased from Isoflex (USA) with 99.48% isotopic enrichment.

Targetry and Irradiation

45-55 mg of ^{58}Ni in powder form was plated onto a gold disk by electrodeposition as previously described by McCarthy et al.[24] The electroplating cell was 9 cm in height with an inner diameter of 1.8 cm. The bottom of the cell consisted of a teflon base that connected to the gold disk exposing a 5 mm circle. A graphite rod was used as the cathode and stirred the solution slowly as a voltage of 2.5 V was applied for ~12 hrs. The current remained between 8-

20 mA throughout the process. Targets were irradiated on a 15 MeV cyclotron (CS-15) for 20-60 μAhrs. Targets were allowed to sit for two hours prior to processing to allow short-lived contaminants to decay.

Purification

For processing, targets were placed in 10 mL 9 M HCl and heated with reflux for approximately one hour in order to dissolve the nickel from the gold disk. Once the solution cooled it was placed in a 1 cm x 10 cm glass column (Biorad, USA) with 2.5 mg AG1-X8 resin (Biorad, USA). In order to determine separation conditions, the eluate along with 10-40 mL of 9 M HCl were collected followed by another 10 mL of 0.5 M HCl to elute the ^{55}Co. Fractions of 1 mL were collected and analyzed using an HPGe (High Purity Germanium) detector (Canberra, USA) and the final ^{55}Co fractions were evaporated to dryness and reconstituted with 20 μL Milli-Q water. ^{55}Co productions were analyzed using Ion Chromatography[21] for transition metal contaminations.

Effective Specific Activity

DOTA titrations were performed in order to determine the effective specific activity of ^{55}Co productions and the method was adapted from the TETA titration method reported previously by McCarthy et al.[24] 1.2 MBq (5 μL) of ^{55}Co was added to eight different concentrations of DOTA in ammonium acetate pH 5.5 ranging from 4.3×10^{-4} μmol to 6.3×10^{-2} μmol. Final volume was brought to 50 μL using 0.5 M ammonium acetate buffer pH 5.5. The solutions were placed in an agitating incubator at 37 ºC for 30 min. Solutions were cooled to room temperature and then centrifuged. A 1 μL sample from each DOTA concentration along

with 1 µL unbound ^{55}Co was analyzed for the percent ^{55}Co incorporated determined by Thin Layer Chromatography (TLC) using silica plates and 1:1 mixture of 10% ammonium acetate and methanol as an eluent. Plates were analyzed using a Radio TLC Plate Reader (Bioscan, Washington DC). Data was plotted as molar concentration of DOTA vs. % ^{55}Co incorporation. The curve was fit using a sigmoid plot fit program in Prism (Graphpad, USA). The EC50 value, concentration of ^{55}Co that bound to 50% of the DOTA molecules, was determined from this fit. The ESA was set equal to two times the EC50 value.

Animal Models

All animal care was performed as stated in the Guide for Care and Use for Laboratory Animals by the National Institutes of Health under a protocol approved by the Animal Studies Committee at Washington University in St. Louis. Female Athymic *Nu/Nu* mice (National Cancer Institute, USA) aged 6-9 weeks were anesthetized with a ketamine/xylazine cocktail (VEDCO, USA). 100 µL of approximately 2 x 10^7 cell/mL HCT-116 colon cancer cells suspended in saline were subcutaneously injected into the shoulder. Tumors were allowed to grow for two weeks before imaging and biodistribution studies.

Small-Animal PET/CT imaging

Prior to imaging, animals were anesthetized with 2% isoflurane. 100 µL of 74 kBq/µL $^{55}CoCl_2$ in 0.1 N saline was injected into HCT-116 tumor bearing mice (n=4) via tail vein injection and imaged using an Inveon MicroPET/CT scanner (Siemens, USA) at 2, 24, and 48 hrs post injection. Static PET images were acquired for 20 minutes. PET data was reconstructed

using standard methods with the maximum a posteriori probability (MAP) algorithm and co-registered with CT (computed tomography) using image display software (Inveon Research Workplace Workstation, Siemens, USA). Volumes of Interest (VOI) were drawn using CT anatomical guidelines.

Biodistributions

100 μL of 74 kBq/μL $^{55}CoCl_2$, 37 kBq/μL ^{55}Co-NO2A-FDNB, or 37 kBq/μL ^{55}Co-DO3A-FDNB in 0.1 N saline were injected into HCT-116 tumor bearing mice. ^{55}Co-NO2A-FDNB and ^{55}Co-DO3A-FDNB were prepared and labeled as the ^{64}Cu analogues described by Marquez et al.[23] and with a final specific activity of 3.7 MBq/ug. For each agent, (n=3) mice were sacrificed at 24 and 48 hrs post injection followed by removal of blood, lung, liver, spleen, kidney, muscle, fat, heart, brain, bone, tumor, stomach, small intestine (sm int), upper large intestine (u lg int), and lower large intestine (l lg int). Each organ was weighed and measured for radioactivity using a gamma counter. The radioactivity was background subtracted, decay corrected to time of injection and reported as % ID/g (percent injected dose/g tissue).

Statistical Analysis

All data were analyzed using Graphpad Prism version 6 (Graphpad, USA). *P* values were calculated using one-way ANOVA to compare more than two groups with one variable. *P* values with 95% confidence interval ($P < 0.05$) were considered significant.

Results

Production and Purification of High Specific Activity ^{55}Co

^{58}Ni was plated onto a gold disk with an average efficiency of 95 ± 3 % and thickness of ~300μm. Irradiations produced an average of 6 ± 1 MBq ^{55}Co/μAh which is consistent with yields predicted by Kaufman.[19] ^{57}Ni and ^{57}Co were coproduced at rates of 16 ± 2 kBq/μAh and 11 ± 2 kBq/μAh respectively.

Due to the coproduction of ^{57}Ni, separation could be analyzed by measuring the characteristic gamma rays of ^{57}Ni (E_1=1.378 MeV, I_1=81.7% and E_2=0.127 MeV, I_2=16.7%) and ^{55}Co (E_1=0.931 MeV, I_1=75%; E_2=0.477 MeV, I_2=20.2% and E_3=1.409 MeV, I_3=16.9%) in each fraction using an HPGe detector. Elution profiles for ^{57}Ni and ^{55}Co are shown in **Figure 6-2**. ^{57}Co contamination was determined by analyzing its characteristic gamma ray 0.122 MeV (85.6%) in each fraction. Washing the column with an additional 10-40 mL 9 M HCl removed nickel without significant loss of ^{55}Co. The average recovery of ^{55}Co with a 40 mL 9 M HCl column wash was 92 ± 3 %.

ESA measured via DOTA titration was found to be 259 MBq/μmol DOTA when washing the column with 10 mL 9 M HCl. Increasing the column wash to 40 mL resulted in an increased ESA of 1.96 GBq/μmol DOTA (**Figure 6-3**). Ion Chromatography measured nickel concentrations to be 3.5 μmol/μCi and 28 nmol/μCi for 10 mL and 40 mL column washes respectively. The only radioactive impurity found in the final ^{55}Co fraction was ^{57}Co at 0.2 % of the total ^{55}Co activity.

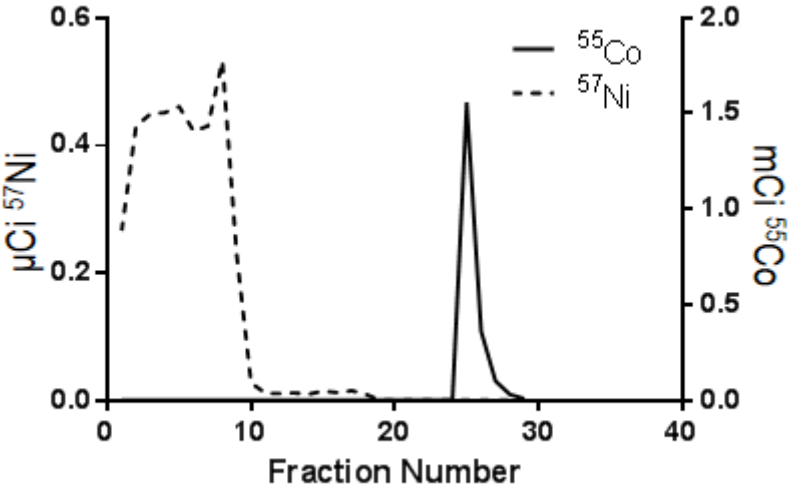

Figure 6-2. Concentration of ^{55}Co and ^{57}Ni in each fraction, as measured using HPGe detection of the characteristic gamma rays, showing good separation.

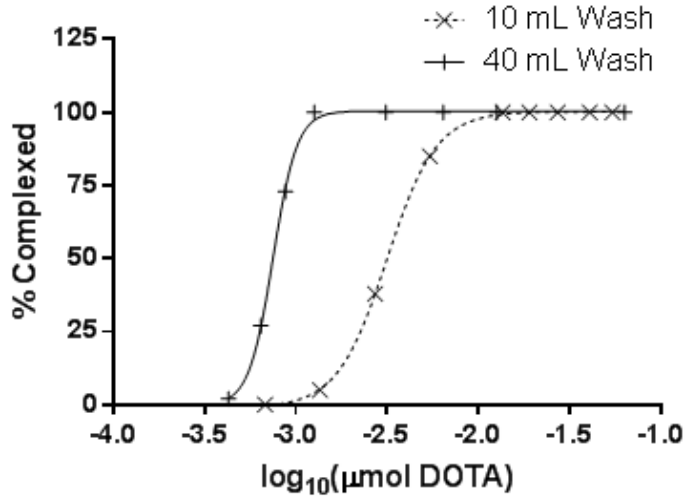

Figure 6-3. ^{55}Co-DOTA titration curves demonstrating a seven-fold increase in ESA (259 MBq/µmol to 1.96 GBq/µmol) when washing the column with an additional 40 mL 9 M HCl acid versus a 10 mL column wash.

$^{55}CoCl_2$ Small-Animal PET/CT Imaging and Biodistribution

As an emerging radioisotope, *in vivo* stability data of different ^{55}Co-chelate complexes had not been previously measured. In order to determine the *in vivo* stability of these chelates it is important to know where free ^{55}Co accumulates in tumor models. The distribution of free ^{55}Co had not been investigated in tumor xenograft models to our knowledge. HCT-116 tumor xenografts were imaged (**Figure 6-4A**) and post PET biodistributions (Table 1) were performed at 2, 24, and 48 hrs p. i. (post injection) to investigate the distribution of free ^{55}Co in this model. Interestingly, significant accretion of ^{55}Co occurred in the tumor at each of these time points. Tumor-to-blood ratios (**Figure 6-4B**) increased over time, likely due to clearance from the blood occurring at a higher rate than washout from the tumor implying that ^{55}Co is being retained in the tumor cells. Tumor-to-blood ratios at 2 and 48 hrs were 0.6 ± 0.1 and 1.9 ± 0.4 respectively exhibiting a 3-fold increase (P=0.006). High uptake in the heart could be due to the potential of Co^{2+} to mimic calcium influx.[7,10] Clearance of free ^{55}Co occurred through the liver and kidney as established by the high values listed in Table 1.

Table 1. $^{55}CoCl_2$ Biodistribution Data at 2, 24, and 48 hrs p. i.

Organ	2 hr (%ID/g)	24 hr (%ID/g)	48 hr (%ID/g)
Blood	4.5 ± 0.6	1.40 ± 0.04	0.46 ± 0.05
Lung	4.0 ± 0.3	1.9 ± 0.1	0.98 ± 0.09
Liver(all)	15.7 ± 0.4	6.2 ± 0.8	2.7 ± 0.7
Spleen	1.9 ± 0.4	0.82 ± 0.05	0.46 ± 0.04
Kidney	10.5 ± 1.4	4.4 ± 0.4	1.9 ± 0.2
Muscle	0.6 ± 0.1	0.37 ± 0.08	0.17 ± 0.03
Fat	1.5 ± 0.9	0.7 ± 0.4	0.23 ± 0.05
Heart	4.8 ± 0.4	2.8 ± 0.7	1.4 ± 0.2
Brain	0.31 ± 0.02	0.17 ± 0.03	0.11 ± 0.01
Bone	1.3 ± 0.2	0.8 ± 0.1	0.5 ± 0.1
Tumor	2.8 ± 0.6	1.6 ± 0.2	0.86 ± 0.08
Stomach	1.1 ± 0.1	1.0 ± 0.2	0.5 ± 0.1
Sm int	3.6 ± 0.6	1.1 ± 0.2	0.50 ± 0.04
U lg int	4.3 ± 0.8	1.5 ± 0.1	0.7 ± 0.1
L lg int	1.9 ± 1.0	2.2 ± 0.3	1.2 ± 0.2

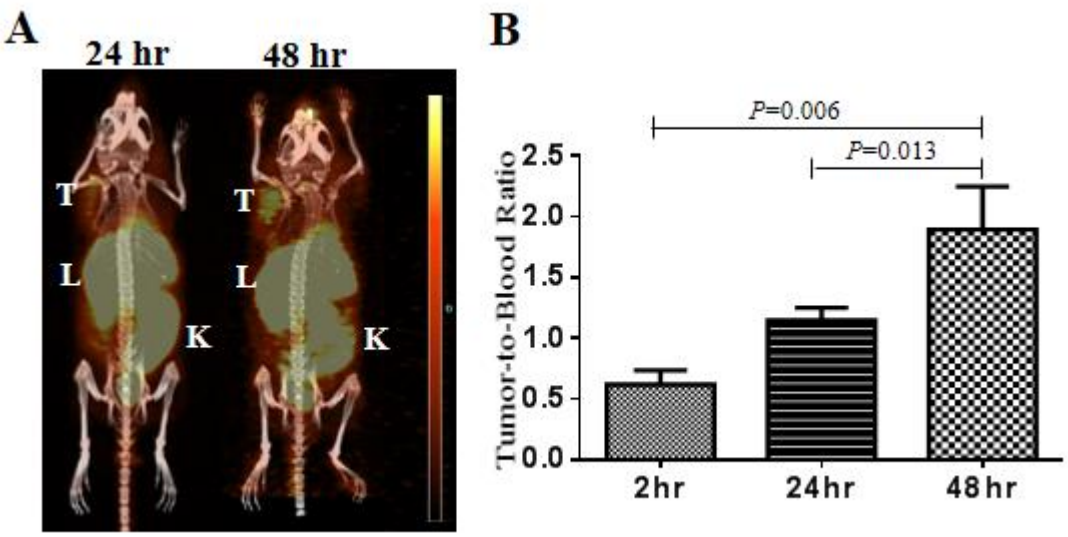

Figure 6-4. 24 and 48 hr PET images of $^{55}CoCl_2$ showing uptake in the tumor and clearance through the liver, kidney, and intestines (A). Tumor-to-blood ratio exhibits a 3-fold increase from 2-48 hrs (B).

Stability of ^{55}Co-Chelate Complexes

The stability of radiometal-chelate combinations is crucial when designing new PET imaging probes. Complexes that are not stable *in vivo* can lead to the radiometal decomplexing from the chelate and accumulating in different organs throughout the body increasing background signal and dose to non-target organs. It has previously been established that changing the radiometal on peptides can have a drastic effect on the affinity of the peptide to its receptor.[25] Using ^{55}Co to radiolabel L19K-FDNB dramatically decreased the affinity for VEGF when compared to labelling with ^{64}Cu.[23] This decreased affinity and long blood clearance time presents an optimal model to examine the *in vivo* stability of ^{55}Co-chelate complexes.

The 24 and 48 hr biodistributions of ^{55}Co-NO2A-L19K-FDNB and ^{55}Co-DO3A-L19K-FDNB were compared to the biodistribution of free ^{55}Co (**Figure 6-5**). These data show that

both NO2A and DO3A chelates radiolabeled with ^{55}Co exhibit good *in vivo* stability. This is ascertained by the low uptake of activity in the liver, lung, heart, bone, stomach, and small intestine when compared to high uptake of free ^{55}Co in these organs. The difference in uptake is most notable in the liver (6-fold decrease at 24 and 48 hrs) and the heart (4-fold decrease at 24 hrs and 7-fold decrease at 48 hrs).

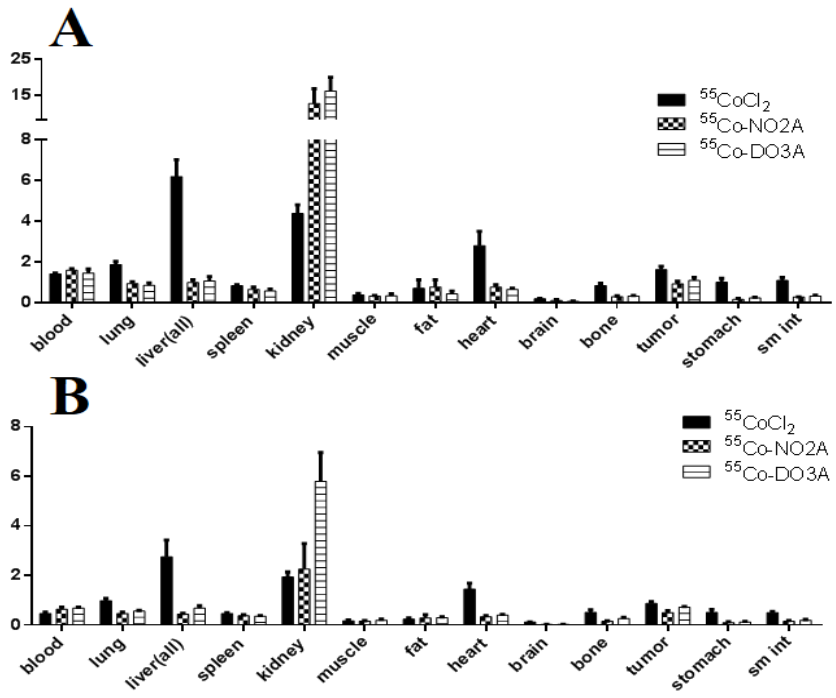

Figure 6-5. Comparison of the 24 hr (A) and 48 hr (B) biodistributions of $^{55}CoCl_2$ with ^{55}Co-NO2A-FDNB and ^{55}Co-DO3A-FDNB exhibiting the *in vivo* stability of ^{55}Co-NO2A and ^{55}Co-DO3A complexes.

Discussion

The $^{58}Ni(p,\alpha)^{55}Co$ reaction is an effective route for producing high specific activity ^{55}Co. Previously this method was reported using a copper disk[17] as opposed to gold, however using copper as the target backing material could have a negative effect on effective specific activity as copper has a high affinity to both NOTA and DOTA chelators and would compete with ^{55}Co for binding. The downside to this reaction is that it has a lower cross section when compared to other radiometals such as ^{64}Cu and ^{89}Zr, which may limit the availability of this isotope to facilities that have solid target cyclotron capabilities.

The biodistribution of $^{55}CoCl_2$ is comparable to those seen for $^{64}CuCl_2$.[26-30] The uptake in the tumor of ^{55}Co is of interest and should be evaluated further. It is possible that its uptake is due to the over expression of calcium ion channels often found in cancer cells. As discussed earlier several studies have shown uptake of $^{55}CoCl_2$ in ischemic cells and is believed to be due to ^{55}Co partially mirroring calcium influx.[7,10]

The *in vivo* stability of the NOTA and DOTA analogs, NO2A and NO3A, complexed with ^{55}Co provides the foundation for developing ^{55}Co labeled peptides, antibodies, nanoparticles and small molecules. ^{55}Co-NOTA and ^{55}Co-DOTA complexes demonstrate greater stability *in vivo* than ^{64}Cu-NOTA and ^{64}Cu-DOTA complexes which could be beneficial in cases where reduced background signal is desired i.e. liver metastases. Additionally the high positron branching ratio (4 times that of ^{64}Cu and 3 times that of ^{89}Zr) leads to similar images with a lower amount of radioactivity administered.

Since the affinity of some peptides is dependent on the attached radiometal it would be of interest to examine this effect on different peptide models. The anti-VEGF peptide used in this work exhibited lower affinity than previously measured with ^{64}Cu, however in work done by

Heppler et al.[2] ^{55}Co-DOTATOC showed the highest affinity for the somatostatin type two receptor than any other radiometal measured. Further research as to the structure activity relationship of these peptide-chelate-metal complexes would be significant for designing superior PET imaging probes.

Conclusions

^{55}Co can be made with high specific activity via the ^{58}Ni(p,α)^{55}Co reaction. The *in vivo* stability of ^{55}Co labeled NOTA and DOTA derivatives make this radioisotope a promising isotope for many different applications. Future work should compare the affinity of ^{55}Co labeled peptides with other radiometals to optimize the best metal-chelate-peptide combination for the application.

References

1 Mirzaii, M., Kakavand, T., Talebi, M. & Rajabifar, S. Electrodeposition iron target for the cyclotron production of Co-55 in labeling proteins. *J Radioanal Nucl Ch* **292**, 261-267, doi:DOI 10.1007/s10967-011-1399-x (2012).

2 Heppeler, A. *et al.* Metal-ion-dependent biological properties of a chelator-derived somatostatin analogue for tumour targeting. *Chem-Eur J* **14**, 3026-3034, doi:DOI 10.1002/chem.200701264 (2008).

3 Thisgaard, H., Olesen, M. L. & Dam, J. H. Radiosynthesis of Co-55- and Co-58m-labelled DOTATOC for positron emission tomography imaging and targeted radionuclide therapy. *J Labelled Compd Rad* **54**, 758-762, doi:Doi 10.1002/Jlcr.1919 (2011).

4 Goethals, P., Volkaert, A., Vandewielle, C., Dierckx, R. & Lameire, N. Co-55-EDTA for renal imaging using positron emission tomography (PET): A feasibility study. *Nuclear Medicine and Biology* **27**, 77-81, doi:Doi 10.1016/S0969-8051(99)00077-3 (2000).

5 Karanikas, G. *et al.* Examination of Co-complexes for radiolabeling of platelets in positron emission tomographic studies. *Thromb Res* **94**, 111-115, doi:Doi 10.1016/S0049-3848(98)00204-7 (1999).

6 Ferreira, C. L. *et al.* (55)Cobalt complexes with pendant carbohydrates as potential PET imaging agents. *Applied Radiation and Isotopes* **65**, 1303-1308, doi:DOI 10.1016/j.apradiso.2007.06.003 (2007).

7 De Reuck, J. *et al.* Cobalt-55 positron emission tomography in recurrent ischaemic stroke. *Clin Neurol Neurosur* **101**, 15-18, doi:Doi 10.1016/S0303-8467(98)00076-6 (1999).

8 Stevens, H. *et al.* (55)Cobalt (Co) as a PET-tracer in stroke, compared with blood flow, oxygen metabolism, blood volume and gadolinium-MRI. *J Neurol Sci* **171**, 11-18, doi:Doi 10.1016/S0022-510x(99)00229-4 (1999).

9 De Reuck, J., Santens, P., Strijckmans, K., Lemahieu, I. & Related, E. T. F. A. Cobalt-55 positron emission tomography in vascular dementia: significance of white matter changes. *J Neurol Sci* **193**, 1-6, doi:Doi 10.1016/S0022-510x(01)00606-2 (2001).

10 De Reuck, J. *et al.* The significance of cobalt-55 positron emission tomography in ischemic stroke. *Journal of stroke and cerebrovascular diseases : the official journal of National Stroke Association* **8**, 17-21 (1999).

11 De Reuck, J. *et al.* Cobalt-55 positron emission tomography in late-onset epileptic seizures after thrombo-embolic middle cerebral artery infarction. *J Neurol Sci* **181**, 13-18 (2000).

12 Al-Abyad, M., Comsan, M. N. & Qaim, S. M. Excitation functions of proton-induced reactions on natFe and enriched 57Fe with particular reference to the production of 57Co. *Applied radiation and isotopes : including data, instrumentation and methods for use in agriculture, industry and medicine* **67**, 122-128, doi:10.1016/j.apradiso.2008.07.006 (2009).

13 Sharma, H., Zweit, J., Smith, A. M. & Downey, S. Production of Cobalt-55, a Short-Lived, Positron Emitting Radiolabel for Bleomycin. *Applied Radiation and Isotopes* **37**, 105-109 (1986).

14 Brinkman, G. A., Helmer, J. & Lindner, L. Nickel and Copper Foils as Monitors for Cyclotron Beam Intensities. *Radiochem Radioa Let* **28**, 9-19 (1977).

15 Coetzee, P. P. & Peisach, M. Activation Cross-Sections for Dueteron-Induced Reactions on Some Elements of First Transition Series, up to 5,5mev. *Radiochim Acta* **17**, 1-& (1972).

16 Jenkins, I. L. & Wain, A. G. Excitation Functions for Bombardment of Fe-56 with Protons. *J Inorg Nucl Chem* **32**, 1419-&, doi:Doi 10.1016/0022-1902(70)80628-5 (1970).

17 Spellerberg, S., Reimer, P., Blessing, G., Coenen, H. H. & Qaim, S. M. Production of (55)Co and (57)Co via proton induced reactions on highly enriched (58)Ni. *Applied Radiation and Isotopes* **49**, 1519-1522, doi:Doi 10.1016/S0969-8043(97)10119-1 (1998).

18 Reimer, P. & Qaim, S. M. Excitation functions of proton induced reactions on highly enriched Ni-58 with special relevance to the production of Co-55 and Co-57. *Radiochim Acta* **80**, 113-120 (1998).

19 Kaufman, S. Reactions of Protons with 58-Nickel and 60-Nickel. *Physical Review* **117**, 1532-1538 (1960).

20 Zavorka, L., Simeckova, E., Honusek, M. & Katovsky, K. The Activation of Fe by Deuterons at Energies up to 20 MeV. *J Korean Phys Soc* **59**, 1961-1964, doi:Doi 10.3938/Jkps.59.1961 (2011).

21 Mastren, T. *et al.* Specific activity measurement of (6)(4)Cu: a comparison of methods. *Applied radiation and isotopes : including data, instrumentation and methods for use in agriculture, industry and medicine* **90**, 117-121, doi:10.1016/j.apradiso.2014.03.016 (2014).

22 Zeng, D. & Anderson, C. J. Rapid and sensitive LC-MS approach to quantify non-radioactive transition metal impurities in metal radionuclides. *Chem Commun (Camb)* **49**, 2697-2699, doi:10.1039/c3cc39071c (2013).

23 Marquez, B. V., Ikotun, O., Meares, C. F. & Lapi, S. E. Development of a Radiolabeled Irreversible Peptide (RIP) as a PET Imaging Agent for Vascular Endothelial Growth Factor. *J Labelled Compd Rad* **56**, S86-S86 (2013).

24 McCarthy, D. W. *et al.* Efficient production of high specific activity 64Cu using a biomedical cyclotron. *Nucl Med Biol* **24**, 35-43 (1997).

25 Ginj, M. & Maecke, H. R. in *Metal Ions in Biological Systems: Volume 42: Metal Complexes in Tumor Diagnosis and as Anticancer Agents* Vol. 42 (ed Helmut Sigel) Ch. 7, 600 (CRC Press, 2004).

26 Jorgensen, J. T., Persson, M., Madsen, J. & Kjaer, A. High tumor uptake of Cu-64: Implications for molecular imaging of tumor characteristics with copper-based PET tracers. *Nuclear Medicine and Biology* **40**, 345-350, doi:DOI 10.1016/j.nucmedbio.2013.01.002 (2013).

27 Zhang, H. Y., Cai, H. W., Lu, X., Muzik, O. & Peng, F. Y. Positron Emission Tomography of Human Hepatocellular Carcinoma Xenografts in Mice Using Copper (II)-64 Chloride as a Tracer. *Acad Radiol* **18**, 1561-1568, doi:DOI 10.1016/j.acra.2011.08.006 (2011).

28 Qin, C. X. *et al.* Theranostics of Malignant Melanoma with (CuCl2)-Cu-64. *Journal of Nuclear Medicine* **55**, 812-817, doi:DOI 10.2967/jnumed.113.133850 (2014).

29 Kim, K. I. *et al.* Detection of Increased 64Cu Uptake by Human Copper Transporter 1 Gene Overexpression Using PET with 64CuCl2 in Human Breast Cancer Xenograft Model. *Journal of nuclear medicine : official publication, Society of Nuclear Medicine* **55**, 1692-1698, doi:10.2967/jnumed.114.141127 (2014).

30 Peng, F. Y., Lutsenko, S., Sun, X. K. & Muzik, O. Positron Emission Tomography of Copper Metabolism in the Atp7b(-/-) Knock-out Mouse Model of Wilson's Disease. *Mol Imaging Biol* **14**, 70-78, doi:DOI 10.1007/s11307-011-0476-4 (2012).

Chapter 7

Conclusions

7.1 Radioisotopes in Medicine

Mother Nature provides us with several radioisotopes that are used for a broad range of disciplines. In addition to these naturally occurring radioisotopes, many radioisotopes are made synthetically using cyclotrons, linear accelerators, or nuclear reactors. Medical research employs almost exclusively synthetic radioisotopes for use in basic science research, imaging, and therapy.

From 2006 to 2010 the number of nuclear medicine procedures performed annually worldwide increased from 18 million to well over 30 million.[1,2] The growth of nuclear medicine has sparked an increase in the developments of advanced imaging and therapeutic agents and more radioisotopes are being used than ever before.[3] The desire for different chemistries is driving the increased demand for radioisotopes of elements not previously used for nuclear imaging and therapy. The distinctive chemistries and the broad range of nuclear properties of the many radioisotopes located near the line of beta-stability make for a large playing field of potential medical isotopes.

In **Figure 7-1** the current sources of medical radioisotopes are shown; however, some desired radioisotopes cannot easily be made by current methods. One such isotope is ^{67}Cu, a radioisotope of interest for cancer therapy.[4,5] To make usable quantities of ^{67}Cu a new method, isotope harvesting, is being investigated. The majority of the work in this thesis investigates the feasibility of harvesting ^{67}Cu from an aqueous beam dump at a new national facility.

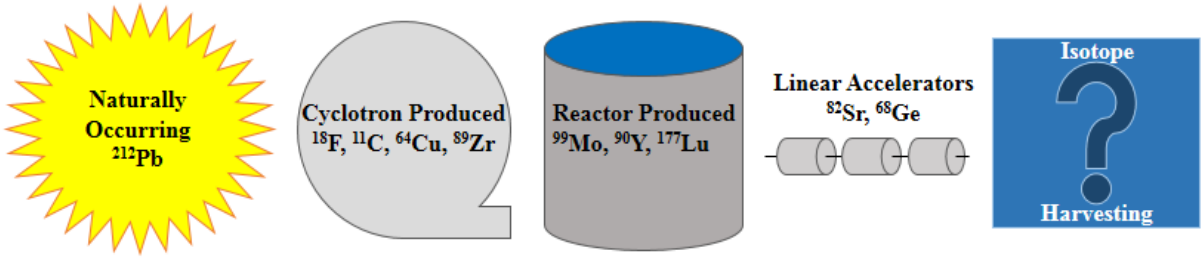

Figure 7-1. Examples of medical radioisotopes from different sources.

7.2 Isotope Harvesting Conclusions

The first step in determining the feasibility of isotope harvesting was the successful design and implementation of an end station that could serve as a mock beam dump. This end station was constructed and proved to be functional by several collections of ^{24}Na from the water exposed to an analyzed ^{24}Na beam. The end station proved to be very robust showing very little radioactive damage from the secondary ion beam.

With this first successful use of the end station, we moved on to an isotope of interest to medicine, ^{67}Cu. An analyzed ^{67}Cu secondary beam was collected in the water target cell and followed with the chemical separation of ^{67}Cu. Chemical separations gave an average recovery of 88 ± 3 % for ^{67}Cu which was in strong agreement with results obtained from preliminary separation experiments performed prior to the experiment. The final ^{67}Cu product was successfully used to radiolabel an anti-HER2 antibody Trastuzumab (Herceptin), which established that the ^{67}Cu obtained from the aqueous beam dump was both in the correct chemical form and appropriate effective specific activity.

The analyzed ^{67}Cu secondary beam was an idealized case. To better demonstrate the feasibility of isotope harvesting, collection and separation of ^{67}Cu from an unanalyzed (i.e. mixed) beam was performed. This collection contained many contaminants, both radioactive and stable. A separation strategy was designed and implemented and exhibited an average recovery of 74 ± 4 % for ^{67}Cu with a radiochemical purity of >99%. The resulting ^{67}Cu was used to radiolabel an anti-EGFR antibody, Panitumumab, and injected into colon cancer xenografted mice. The tumor uptake of the ^{67}Cu-NOTA-bz-Panitumumab was comparable to that observed previously by Chang et al.[6]

The final specific activity was 20 nCi/μg which is lower than normally observed with commonly available radioisotopes such as ^{89}Zr and ^{64}Cu. This low specific activity was likely due to stable metal contaminants as the final ^{67}Cu fraction had high radiochemical purity. The decontamination factors and the theoretical ratio of the different elements to ^{67}Cu present in the beam (**Table 5-4**) suggest that the low specific activity did not result from poor separation of the beam fragments. The stable metal contamination was most likely introduced to the ^{67}Cu fraction during the separation processes by some unknown source. Inductively coupled plasma mass spectrometry analysis of the final fraction will better determine the composition of the contamination and a method will be developed to eliminate this contamination in future experiments.

7.3 Future Work

Although we were able to separate ^{67}Cu from a fragmented ^{76}Ge beam with high radiochemical purity, there is still more work to be done before the true feasibility of harvesting this radioisotope can be determined. The first challenge to be addressed is the separation of ^{67}Cu from a fragmented uranium beam. It is estimated that 60% of the primary beams used at the Facility for Rare Isotope Beams will be uranium, which will require a more complicated chemical separation scheme to achieve good radiochemical purity and effective specific activity. The second challenge is the use of mixed bed resin. The aqueous beam dump at FRIB will constantly be circulated through a column of mixed bed resin. Experiments should be performed to observe the amount of ^{67}Cu that binds to this resin along with determining an elution protocol. Modifications are currently in progress to continuously circulate the water in the target cell through a column of mixed bed resin.

Experiments exploring the potential of harvesting other radioisotopes of interest would also be essential for the evaluation of the feasibility of isotope harvesting from FRIB. To make isotope harvesting a reality, examples of successful separations of several different radioisotopes of interest to a variety of fields should be provided. A proposal to collect secondary beams containing ^{48}V and ^{85}Kr at the NSCL has been accepted and the experiments are likely to start sometime next year. The harvesting of ^{67}Cu from the aqueous beam dump, as described herein, can serve as a scaffold from which separation strategies for the above radioisotopes in addition to those listed in **Table 1-2** can be built.

In conclusion, the work presented here provides a strong foundation for the harvesting of ^{67}Cu from a heavy-ion fragmentation facility. Radioisotope users from different fields would benefit from isotope harvesting at the future FRIB facility. While much more work still needs to be performed for ^{67}Cu and each radioisotope will present its own challenges, isotope harvesting appears to be a promising pathway to radioisotopes that are not currently available in usable quantities by conventional methods.

References

1 *Consultancy Meeting on Conversion Planning for Mo-99 Production Facilities from HEU to LEU* (Vienna, Austria, 2010).

2 Mettler, F. A., Jr. *et al.* Radiologic and nuclear medicine studies in the United States and worldwide: frequency, radiation dose, and comparison with other radiation sources--1950-2007. *Radiology* **253**, 520-531, doi:10.1148/radiol.2532082010 (2009).

3 Schelbert, H. R. Nuclear medicine at a crossroads. *Journal of nuclear medicine : official publication, Society of Nuclear Medicine* **52 Suppl 2**, 10S-15S, doi:10.2967/jnumed.110.085639 (2011).

4 O'Donnell, R. T. *et al.* A clinical trial of radioimmunotherapy with Cu-67-2IT-BAT-Lym-1 for non-Hodgkin's lymphoma. *Journal of Nuclear Medicine* **40**, 2014-2020 (1999).

5 Smith, N. A., Bowers, D. L. & Ehst, D. A. The production, separation, and use of Cu-67 for radioimmunotherapy: A review. *Applied Radiation and Isotopes* **70**, 2377-2383, doi:DOI 10.1016/j.apradiso.2012.07.009 (2012).

6 Chang, A. J., Silva, R. A. D. & Lapi, S. E. Development and Characterization of 89Zr-Labeled Panitumumab for Immuno–Positron Emission Tomographic Imaging of the Epidermal Growth Factor Receptor. *Molecular Imaging* **0**, 1-11, doi:10.2310/7290.2012.00016 (2012).

Glossary of Terms

Antibody: An antibody is a protein produced by the body's immune system against an antigens.

Antigen: A foreign substance that, when introduced into the body, is capable of stimulating an immune response.

Becquerel (Bq): Unit to measure radioactivity. 1Bq = 1disintegration/second

Catabolism: The set of metabolic pathways that breaks down molecules into smaller units to release energy.

Curie (Ci): Unit to measure radioactivity. 1Ci = 3.7x1010Bq (d/s)

DOTA: 1,4,7,10-tetraazacyclododecane-1,4,7,10-tetraacetic acid

EC50: The concentration of a drug that gives half-maximal response.

Effective Specific Activity: The amount of radioactivity per unit mass of competing metal for a certain chemical or biological reaction.

High-Performance Liquid Chromatography (HPLC): A high pressure system which employs a column and solvents to separate components of a solution.

Immunoreactivity: Measurement of the retained functionality of the antibody after conjugating with a chelator.

Inductively-Coupled Plasma Mass Spectrometry (ICP-MS): A mass spectrometer that is commonly used in elemental analysis.

Ion Chromatography (IC): An high-performance liquid chromatography method to separate several different first-row transition metals.

Magnetic Rigidity: The momentum per unit charge of a particle (p/q). The units of magnetic rigidity are Tm (tesla meters).

NOTA: 1,4,7-triazacyclononane-N,N',N''-triacetic acid

Particle nanoamps (pnA): Number of particles per nanoamp of beam (pnA is equal to nA for H+ or H- beams)

PIXE: Particle Induced X-ray Emmission, a method used in elemental analysis.

TETA: 1,4,8,11-tetraazacyclotetradecane-1,4,8,11-tetraacetic acid

Theoretical (Maximum) Specific Activity: The amount of radioactivity per μmol of the radioactive species (e.g. activity of 64Cu per μmol 64Cu).

True Specific Activity: The amount of radioactivity per μmol of atoms of the same element (e.g. activity of 64Cu per μmol copper).

Xenografts: Cells from one species transplanted into an organism of another species (i.e. human cells into mice).